

## DIAMante TESS AutoRegressive Planet Search (DTARPS): II. Hundreds of New TESS Candidate Exoplanets

ELIZABETH J. MELTON,<sup>1,2,3</sup> ERIC D. FEIGELSON,<sup>1,2,4</sup> MARCO MONTALTO,<sup>5</sup> GABRIEL A. CACERES,<sup>6</sup>  
ANDREW W. ROSENSWIE,<sup>1,7,8</sup> AND CULLEN S. ABELSON<sup>1,9</sup>

<sup>1</sup>*Department of Astronomy & Astrophysics, Pennsylvania State University, University Park, PA 16802, USA*

<sup>2</sup>*Center for Exoplanets and Habitable Worlds, Pennsylvania State University, University Park, PA 16802, USA*

<sup>3</sup>*Department of Physics and Optical Engineering, Rose-Hulman Institute of Technology, 5500 Wabash Avenue, Terre Haute, IN 47803, USA*

<sup>4</sup>*Center for Astrostatistics, Pennsylvania State University, University Park, PA 16802, USA*

<sup>5</sup>*INAF - Osservatorio Astrofisico di Catania, Via S. Sofia 78, I-95123 Catania, Italy*

<sup>6</sup>*Teachers Pay Teachers, 111 E 18th St, New York NY 10003*

<sup>7</sup>*Institut für Physik und Astronomie, Universität Potsdam, D-14476 Potsdam, Germany*

<sup>8</sup>*Leibniz-Institut für Astrophysik Potsdam (AIP), An der Sternwarte 16, D-14482 Potsdam, Germany*

<sup>9</sup>*Department of Physics and Astronomy, University of Pittsburgh, 100 Allen Hall, 3941 O'Hara St., Pittsburgh, PA 15260, USA*

(Received Submitted to AAS Journals, February 13 2023)

### ABSTRACT

The DIAMante TESS AutoRegressive Planet Search (DTARPS) project seeks to identify photometric transiting planets from 976,814 southern hemisphere stars observed in Year 1 of the TESS mission. This paper follows the methodology developed by [Melton et al. \(2022a, Paper I\)](#) using light curves extracted and pre-processed by the DIAMante project ([Montalto et al. 2020](#)). Paper I emerged with a list of 7,377 light curves with statistical properties characteristic of transiting planets but dominated by False Alarms and False Positives. Here a multistage vetting procedure is applied including: centroid motion and crowding metrics, False Alarm and False Positive reduction, photometric binary elimination, and ephemeris match removal. The vetting produces a catalog of 462 DTARPS Candidates across the southern ecliptic hemisphere and 310 objects in a spatially incomplete Galactic Plane list. Fifty-eight percent were not previously identified as transiting systems. Candidates are flagged for possible blending from nearby stars based on Zwicky Transient Facility data and for possible radial velocity variations based on *Gaia* satellite data. Orbital periods and planetary radii are refined using astrophysical modeling; the resulting parameters closely match published values for Confirmed Planets. Their properties are discussed in Paper III.

*Keywords:* exoplanet catalogs – exoplanet detection methods – light curve classification – period search – time domain astronomy – transits

### 1. INTRODUCTION

The search for transiting exoplanets from wide-field space-based surveys like the *Kepler* and TESS missions faces a variety of methodological challenges. Some are statistical in nature. The light curves must be extracted from images, detrended to reduce stellar and instrumental variations, and searched for periodic variations resembling planetary transits. Methods often involve spline fits or wavelet filtering followed by construction of a specially designed periodogram. A machine learning classifier trained on confirmed or simulated transits is then applied. This is typically a Random Forest classifier based on decision trees or a deep neural network.

In [Melton et al. \(2022a, , Paper I\)](#), we develop such a procedure and apply it to  $\sim 0.9$  million light curves from the DIAMante project's study of the TESS Year 1 southern sky survey [Montalto et al. \(2020\)](#). Our methods are based on [Caceres et al. \(2019a\)](#) who successfully applied them to the *Kepler* 4-year light curves ([Caceres et al. 2019b](#)). The statistical procedures are unusual for exoplanetary discovery: differencing operation for trend reduction, low-dimensional autoregressive modeling to remove remaining autocorrelation, a novel Transit Comb Filter periodogram,

and a carefully tuned Random Forest classifier applied to 37 scalar properties of each star. This project is called the DIAMante TESS AutoRegressive Planet Search (DTARPS); in Paper I we emerge with a DTARPS Analysis List of 7,377 possible exoplanets.

But the lists of potential exoplanets are quite unreliable at this stage. Efforts to detect small planets also allow False Alarms with unconvincing periodic behaviors. Astronomical False Positives are common, sometimes overwhelming, at this stage particularly due to blended background eclipsing binaries from stars in the vicinity of the target.

A multifaceted vetting procedure by skilled humans, sometimes assisted by a machine learning automated procedure, is needed to produce a catalog of candidate planets with sufficient reliability for spectroscopic followup observations and science analysis. Exoplanet candidate lists from large-scale efforts of transit detection and vetting include the *Kepler* Objects of Interest (Jenkins et al. 2010, 2020; Batalha et al. 2010; McCauliff et al. 2015; Coughlin et al. 2014), NGTS Armstrong et al. (2018), AstroNet (Yu et al. 2019), TESS Objects of Interest (TOIs, Guerrero et al. 2021), and DIAMante TESS candidates (Montalto et al. 2020). Additional recent vetting efforts include Zink et al. (2021), Dvash et al. (2022), Ofman et al. (2022), Kunimoto et al. (2022), Kostov et al. (2022), Caciapuoti et al. (2022), Mantovan et al. (2022), and Magliano et al. (2023).

McCauliff et al. (2015); Coughlin et al. (2016) and *autovet* for ground-based NGTS data by Armstrong et al. (2018). A neural network method is described by Shallue & Vanderburg (2018)

Here we describe the vetting process applied to the DTARPS Analysis List produced in Paper I. The goal is to refine the list by removing, as much as feasible, False Alarms (FAs) and False Positives (FPs). The sample of 7,377 light curves in the DTARPS Analysis List has many contaminants: the classifier has an FP rate of 0.37% with respect to the training sample, predicting  $\sim 3,900$  FPs. But there will also be FPs with behaviors that were not put in the injected training sample, and FAs where the periodic signal itself is spurious or unconvincing. A strong vetting effort is thus needed to produce a catalog of candidate planets that sacrifices recall rate but enhances the reliability.

This vetting is mostly based on astronomical rather than statistical considerations, and requires subjective judgments by the vetters. We have chosen here to have very strict criteria. The vetting reduces the sample size and therefore sensitivity (recall or True Positive rate) but also decreases the False Positive rate of the resulting sample.

We emerge here with a sample of 462 light curves that satisfy all of our vetting tests, and an additional 310 light curves from Galactic Plane targets that satisfy most of the vetting tests. We report the 462 stars as the *DTARPS Candidate Catalog* and the 310 stars as the *DTARPS Galactic Plane list*. Of these 777 stars, 457 have not been reported previously as possible host for transiting exoplanets. These stars are ready for spectroscopic followup for astronomical characterization. Melton et al. (2022b) (Paper III) proceeds with astronomical analysis of these samples including results on the Neptune desert, ultra-short period planets, and planet occurrence rates.

The present paper is organized as follows. Section 2 describes the vetting process applied to the DTARPS Analysis List obtained in Paper I. The main results are given in Section 3 with electronic tables for the DTARPS Candidates Catalog and DTARPS Galactic Plane List with a Figure Set providing graphical displays of light curve properties from the ARPS analysis. Candidate properties such as planet radius are refined and other catalog improvements are described in §4-5. The DTARPS Galactic Plane list is discussed further in §6. Four Appendices give notes on individual planet candidates (Appendices A-B), comparison between the DTARPS results and other surveys (Appendices C).

## 2. VETTING PROCEDURES

The DTARPS vetting process applied to the 7,377 objects in the DTARPS Analysis List (Paper I) contains five steps for vetting the candidates above the RF threshold: centroid and crowding analysis based on FFI image analysis; False Alarm elimination; False Positive determination; potential photometric binary identification based on the *Gaia* color-magnitude diagram; and removal of ephemeris matches arising from light leakage in the TESS telescope. Centroid-crowding analysis and ephemeris match removal are automated analysis procedures adopted from M20 and Coughlin et al. (2014), respectively. False Alarms (FAs) are cases where, despite a high probability from the Random Forest (RF) classifier, no convincing periodicity is present. False Positives (FPs) are cases here a periodicity is clearly present but is not convincingly attributable to a planetary transit; typically these are blended eclipsing binaries. FA elimination, FP determination, and potential photometric binary identification are performed by independent human vetters. Objects with conflicting dispositions from human vetters are analyzed collaboratively until a final disposition is agreed upon.

The distribution of the reasons light curves are rejected during vetting is shown in Figure 1. The biggest reduction came from the centroid-crowding analysis (§2.1); this effectively excluded candidates near the Galactic Plane. Most of the visual vetting steps (FA elimination, FP determination, and potential photometric binary identification) removed

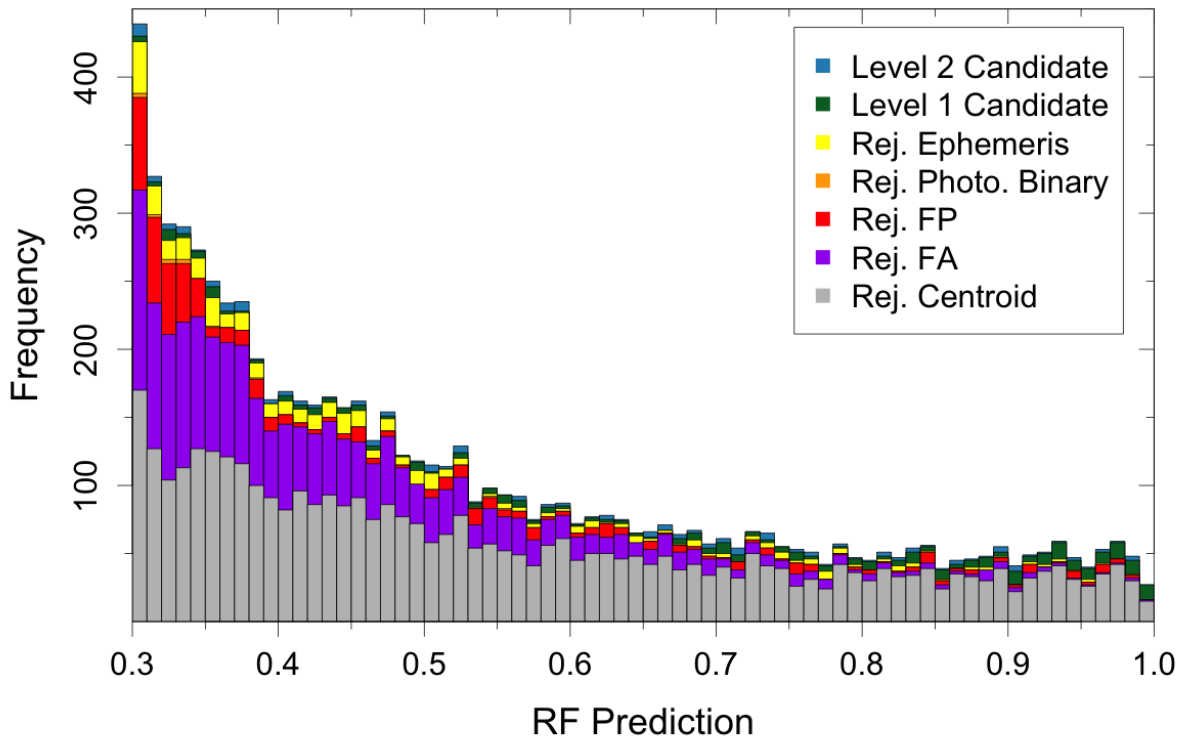


**Figure 1.** Number of light curves rejected for each step in the vetting process as a function of Random Forest prediction value. Level 1 objects satisfied all vetting criteria, while Level 2 objects passed a vetting test only marginally. FP = False Positives, FA = False Alarm.

higher fraction of the DTARPS Analysis List sources with RF prediction values near the 0.30 threshold chosen in Paper I. This is expected; light curves with very high RF probability are more likely to be True Positives than those near the threshold.

Vetting is conducted by the authors using visual examination of graphical and scalar properties. During the vetting process, DTARPS are sorted into two categories referred to as Level 1 candidates and Level 2 candidates. Level 1 candidates are the strongest exoplanet candidates for which no concerns were raised during the vetting process. All evidence is consistent with a true transiting planet. Level 2 candidates are exoplanet candidates that passed the vetting process, but passed one or more vetting test marginally. Any objects for which significant concerns were raised during the vetting process were rejected. We chose to be very conservative in our vetting in order to present a list of transiting exoplanet candidates with the highest possible purity.

### 2.1. Centroid Motion and Crowding Metrics

Unlike the DTARPS analysis in Paper I based on TESS light curves, these initial vetting steps are based on analysis of the TESS images. The procedure is only outlined here; details are provided in §11 of M20. Centroid and crowding metrics for estimating FP probabilities also appear in other transit analysis software packages such as *vespa* (Morton et al. 2016), *robovetter* (Thompson et al. 2018), and *TRICERATOPS* (Giacalone et al. 2021).

Centroid motion analysis measures the motion of the center of light in an aperture applied to the TESS FFIs during the proposed transit event. If the center of light moves substantially from a target during a transit event, it indicates that the transit event detected is most likely due to a blended eclipsing binary whose transit depth is being diluted by the target star making it appear like a planetary transit. Centroid analysis is especially necessary for TESS because its large  $21''$  pixels increase the likelihood of blended background eclipsing binaries, particularly in the crowded Galactic Plane.

In the procedure of M20, flux-weighted centroid in each FFI are calculated in four circular apertures centered on the DTARPS analysis list objects. Orbital parameters from the best TCF periodogram peak are used to identify

the in-transit and out-of-transit times for centroid measurements. Smoothing splines are fitted to the out-of-transit centroid measurements to correct for low-frequency variations in the centroid motion. Principal Components Analysis is applied to the in-transit centroid measurements to identify a bi-variate Gaussian distribution of the centroid for each aperture. The transit event is considered to be associated with the target star if the target had the smallest multivariate (Mahalanobis) distance of all *Gaia* objects within  $3'$  of the target in at least three of the four apertures.

In addition to centroid wobble, M20 calculates two probabilities that the transit signal is associated with the target star based on the crowding around the target (equation 19, M20) and the distribution of the centroid distributions for all four apertures (equation 22). We adopt the same probability cutoffs as M20 and rejected objects from the DTARPS analysis list for which the probability density was less than 30% or the probability that the centroid distribution is associated with the target is less than 50%.

Only 27% of the objects in the DTARPS Analysis List survive this centroid motion and crowding analysis (Figure 1). In particular, nearly all candidates near the Galactic Plane are excluded. As these are probabilistic metrics that do not reflect measured properties of the stars themselves, in §3 below we relax these stringent exclusion criteria for a portion of Galactic longitudes to capture some DTARPS candidates at low Galactic latitudes.

### 2.2. False Alarm Elimination

The DIAmante light curve, TCF periodogram, phase-folded ARIMA residuals, and phase-folded ARIMAX residuals are examined for evidence of a periodic signal. The phase-folded light curves are folded using the TCF peak parameters for period, phase, and duration. The goal is to remove objects from the 7,377 cases with unconvincing periodicities that passed the RF classifier threshold based on 37 features. The FA label is assigned where the periodic signal in the phase-folded light curves or the DIAmante light curve is either unconvincing or entirely absent. FAs are also recognized by their noisy TCF periodograms with no strong isolated peaks, as illustrated in Figure 2. Some FAs arise when sharp features not removed by the ARIMA fit, such as stellar flares or instrumental features (Paper I, §2.5), align to produce a spurious peak in the periodogram. FAs often have marginal TCF periodogram peak signal-to-noise ratios,  $SNR \simeq 12 - 17$ .

FAs are expected to be present with any automated classification procedure that seeks to identify smaller planets. Of the 7,377 stars in the DTARPS Analysis List, 1,006 (66%) that passed centroid and crowding analysis (§2.1) were labeled as FAs.

### 2.3. False Positive Identification

The phase-folded light curve and the TCF periodogram are carefully scrutinized for indicators that the transit signal may come from an eclipsing binary or other variable star rather than a planetary transit. We recall that the RF classifier is trained *against* simulated eclipsing binaries as well as *towards* simulated transiting planets (Paper I, §4.2) so many blended eclipsing binary light curves likely receive low RF probabilities and do not enter the DTARPS Analysis List.

First, an object is labeled FP if the transit depth from the best TCF periodogram peak orbital parameters indicated a ‘planet’ with a radius larger than  $20 R_{\oplus}$ . An example is shown in the top left panel of Figure 3. We set this limit low because of the known tendency for the TCF periodogram peak to underestimate the planet radius (Paper I, §8.1). Hou & Wei (2022) placed an upper limit on the radius of hot Jupiters at  $2.2 R_J$  or  $\sim 25 R_{\oplus}$ , due to tidal heating.

Second, differences in even- *vs.* odd-transits are examined. Measures of even-odd differences are included in the RF classifier but might not dominate other positive measures; the light curve might then exceed the  $P_{RF} = 0.300$  threshold. DIAmante and ARIMAX residual light curves are phase-folded using the double harmonic of the period from the orbital parameters from the TCF periodogram peak. The depths of the even and odd transits are visually compared (Figure 3, top right). Different even and odd transit depths indicate that the signal is strong evidence for an eclipsing binary system whose stars have different luminosities. Due to the paucity of points during transits for TESS single sector light curves, this vetting step is often not sensitive to small differences in stellar luminosities. Only objects whose even and odd transit depths differ by more than the spread of the out-of-transit flux values around the median of the light curve are labeled FPs.

Third, the DIAmante and ARIMAX residual phase-folded light curves are examined for a strong secondary transit. If present, the depth of the secondary transit is compared with the theoretical secondary transit depth given by

$$\delta_2 = \delta_1 \times \sqrt{\frac{R_{\star}}{2} \times \left( \frac{4\pi^2}{GM_{\star}P^2} \right)^{1/3} \times (1 - A_b)^{1/4}} \quad (1)$$

where  $\delta_2$  is the theoretical secondary transit depth,  $\delta_1$  is the primary transit depth (measured from the folded light curve),  $R_*$  is the stellar host radius from the TIC (in  $R_\odot$ ),  $G$  is Newton's gravitational constant,  $M_*$  is the stellar host mass from the TIC (in  $M_\odot$ ),  $P$  is the period of the primary transit depth (in days), and  $A_b$  is the albedo of the planet. If the observed secondary transit depth is deeper than the theoretical secondary eclipse depth with an albedo of 0.5, than the object is labeled FP. An example is shown in the bottom left panel of Figure 3. The position of the secondary transit in phase is also considered. Objects with secondary transits that did not occur half-way between primary transit were labeled as FPs as a possible indicator of an eccentric eclipsing binary system.

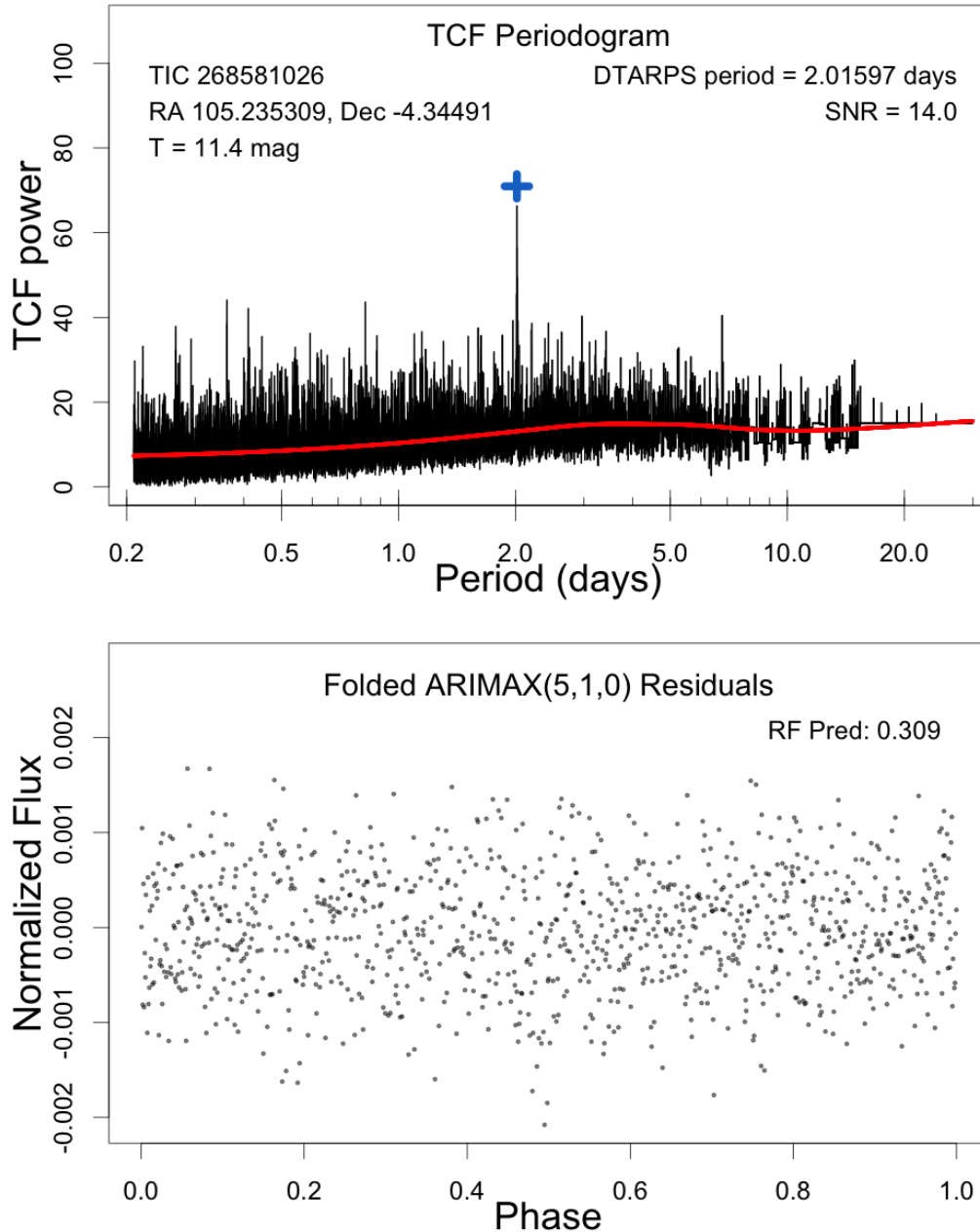


**Figure 2.** Example of a False Alarm light curve. The top panel shows the Transit Comb Filter periodogram with highest-SNR period marked. The bottom panel shows no evident transit in the folded light curve after autoregressive noise is removed. This case had a low TCF signal-to-noise ratio and a Random Forest prediction value only marginally above the threshold of 0.30.

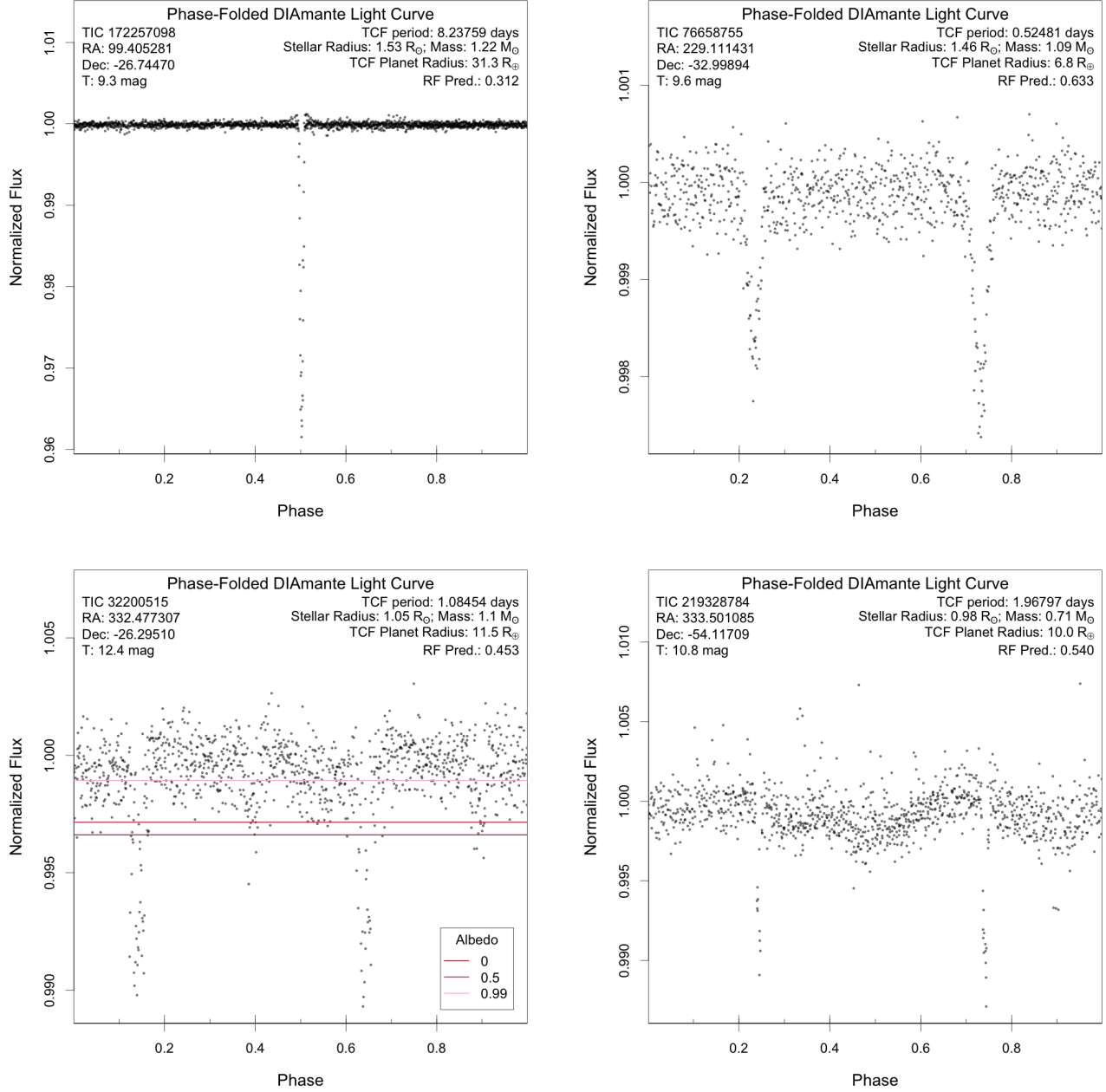


**Figure 3.** Examples of False Positive light curves. These are the light curves from the DIAMante survey prior to ARPS analysis, folded with the TCF peak period. *Top left:* The depth of the transit from the best TCF periodogram peak is too deep. *Top right:* The even and odd transits have different depths. *Bottom left:* The secondary transit is too deep. *Bottom right:* Photometric curvature is present in the phase-folded light curve.

Fourth, residual curvature present in the DIAMante and ARIMAX residual phase-folded light curves (Figure 3 bottom right) may indicate the object is a mutually illuminating and/or tidally distorted binary. Many examples are found in the ensemble of *Kepler* and TESS light curves (Prša et al. 2011, 2022). These objects are removed as likely FPs.

From the list of objects that passed the centroid-motion analysis and False Alarm vetting stages, 333 are labeled as False Positives. Most, but not all, of these light curves have Random Forest probabilities close to the 0.30 threshold (Figure 1).

#### 2.4. Photometric Binary Identification

Photometric properties of the host star for the DTARPS Analysis List is also vetted based on the *Gaia* photometric catalog. The DIAMante data set included subgiants and dwarf FGKM stars identified from color-magnitude cuts (M20). We additionally remove objects potentially involving equal-mass photometric binary stars as they may possibly be eclipsing. Potential photometric binaries were identified by comparing the position of the star on a *Gaia* color-magnitude diagram (Gaia Collaboration et al. 2018), and on a plot of the stellar TIC radius as a function of the TIC effective temperature (Stassun et al. 2019), to a random sample of stars from the full DIAMante data set. Objects whose stars were brighter than the bulk majority of the DIAMante stars with the same *Gaia* color, or stars whose TIC stellar radius was larger than the bulk majority of the DIAMante stars with the same TIC effective temperature, were rejected as possible FPs.

Sixteen DTARPS Analysis List objects that passed centroid-motion analysis, False Alarm elimination and False Positive Determination are rejected using this criterion.

#### 2.5. Ephemeris Match Removal

Ephemeris contamination arises in several ways: nearby bright stars contribute to the measured flux for an object; multiple reflections on telescope optical planes give stray light contamination from more distant very bright stars; and cross-talk and column bleed can occur in the CCD detector array (Coughlin et al. 2014). In an exoplanet search, ephemeris contamination causes multiple sources to exhibit photometric transit signals with the same period and transit epoch.

We identify and remove ephemeris contamination from our candidate list following the procedure developed by Coughlin et al. (2014). Sources from the full DIAMante data set within a distance,  $d_{max}$  of the remaining DTARPS list objects were paired for ephemeris analysis where

$$d_{max} = 12.5'' \times ps_T \times \sqrt{10^6 \times 10^{-0.4 \times m_T} + 1}, \quad (2)$$

$ps_T$  is the 21'' pixel scale of TESS, and  $m_T$  is the TESS T magnitude of the DTARPS Candidates. For each of the paired sources we calculated a modified version of  $\sigma_P$  and  $\sigma_T$  from Coughlin et al. For each pair of sources A and B,

$$\sigma_P = \sqrt{2} \cdot \operatorname{erfcinv} \left( \left| \frac{P_A - P_B}{P_A} \right| \right) \quad (3)$$

and

$$\sigma_T = \sqrt{2} \cdot \operatorname{erfcinv} \left( \left| \frac{T_A - T_B}{P_A} - \operatorname{round} \left( \frac{T_A - T_B}{P_A} \right) \right| \right) \quad (4)$$

where  $P_A$  and  $P_B$  are the periods of source A and B respectively,  $T_A$  and  $T_B$  are the epoch first transit for source A and B respectively, and  $\operatorname{erfcinv}()$  refers to the inverse complementary error function. We focus on ephemeris problems with a source A period to source B period ratio of 1:1, 2:1, or 1:2 by calculating  $\sigma_P$  and  $\sigma_T$  for each of the paired sources for each permutation of source A and B with a period ratio of 1:1, 2:1 and 1:2.

Figure 4 shows the scatter plot of all values for  $\sigma_P$  and  $\sigma_T$  from the source pairs of the DTARPS Analysis List objects and objects from the full DIAMante data set. The minimum value for  $\sigma$  is 0.674 and is equivalent to the worst match between the two sources (Coughlin et al. 2014). The phase from the TCF periodogram peak for a DTARPS Analysis List object is given in integer time steps which constrains the  $\sigma_T$  values into stratified values. The red shaded region in Figure 4 shows the limits we apply to  $\sigma_T$  and  $\sigma_P$  values. The limit for  $\sigma_P$  corresponds to a match within 0.5% between the periods of the two sources (or between the period of one source and the double or half period of another source).

Of the remaining DTARPS objects, 170 lie in the shaded region and were rejected as being likely contaminated by ephemeris matching.

### 3. DTARPS CANDIDATES CATALOG

Of the 7,377 DTARPS Analysis List objects that exceeded the Random Forest classifier threshold in Paper I, the 462 cases that pass the vetting tests in §2 are listed in Table 1. These are designated DTARPS Candidates and represent the principal result of this paper. Notes on individual objects are presented in Appendix A.

The table has 26 columns giving the DTARPS Candidate catalog number and disposition from the DTARPS vetting process (Levels 1 and 2); designations and disposition from other studies (TOI list, cTOI list, M20 or NASA

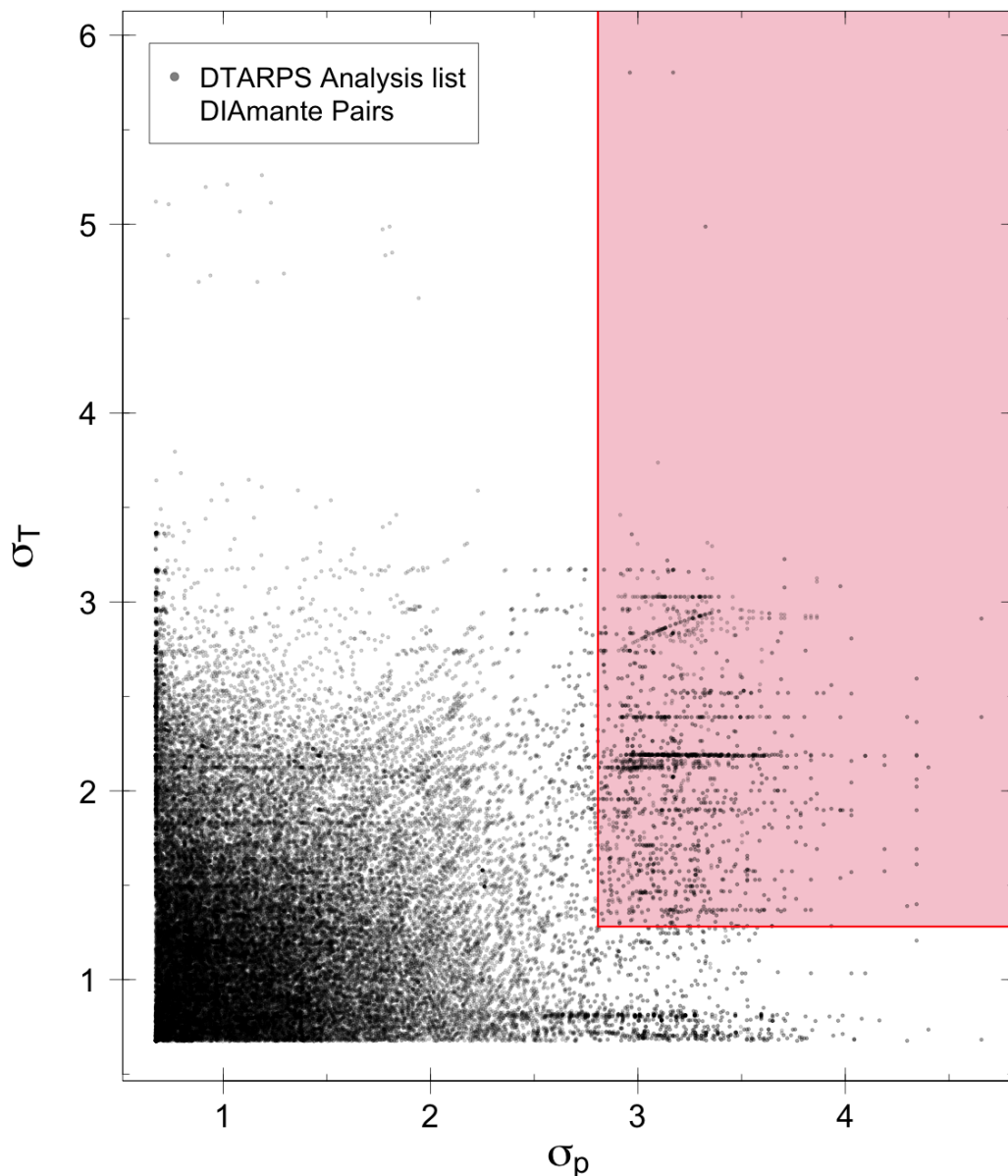


**Figure 4.** Plot of  $\sigma_P$  and  $\sigma_T$  for matches between the 7,377 DTARPS Analysis List objects and the full DIAmante data set of  $\sim 1$  million stars. The red shaded region represents the pairs of points removed as likely ephemeris matches.

Exoplanet Archive); information about the host star from the *Gaia* catalog; information about the DIAmante light curve and ARPS processing; the best TCF period, depth, planet radius and other orbital information; the RF classifier probability; and an indicator of notes based on previous research in Appendix A.

For the first five DTARPS Candidates shown here, the NASA Exoplanet Archive currently labels two as ‘Ambiguous Planetary Candidate’, one as a spectroscopically ‘Confirmed Planet’, and one as a TOI ‘Planetary Candidate’. The appearance of unconfirmed cases in the DTARPS Candidate catalog provides additional evidence they are true planets. DTARPS 5 is newly reported here, but the Appendix A note tells of a possible blended variable star contaminant; further investigation is needed.

A Figure Set of six plots on one page is available for each DTARPS Candidate. The top panels give the DIAmante extracted and preprocessed light curve and autocorrelation function. Annotations give the DTARPS and TIC

identifiers, noise level (IQR = InterQuartile Range), and the probability of the Ljung-Box test that the time series is uncorrelated (Paper I, §2.4). The middle panel shows the TCF periodogram where the best TCF period (highest signal-to-noise ratio after subtraction of the smooth LOESS curve shown in red) is marked with a blue cross (Paper I, §3.2). Annotations give TCF results (best period, depth, and SNR of the peak) and stellar metadata (celestial location,  $T$  magnitude, mass and radius from the TIC) (v8, [Stassun et al. 2019](#)). The bottom panels show the light curve folded modulo the best period at three stages: the DIAMante light curve shown in the top panel; the ARIMA residuals (where a transit signal appears as a double spike); and the ARIMAX residuals (where a transit signal appears as a box-shaped dip; Paper I, §2.2).

Two cases representing smaller planets newly reported here are illustrated in Figure 5, together with scalar values from Table 1 and information from Appendix A, can be described as follows:

**DTARPS 22:** This is CD -25°8457, a bright  $T=9.1$  mag K3 star at distance  $d = 52$  pc. The single-sector DIAMante light curve shows autocorrelated variations with amplitude  $\sim 0.2\%$  likely arising from magnetic activity (top panels). These are removed by a ARIMA(2,1,2) model revealing a signal with  $\text{SNR}=35$  at  $P=0.94401$  days in the TCF periodogram (middle panel). The folded light curve shows a transit-like dip with depth  $0.14\%$  corresponding to a sub-Neptune with radius  $3.0 R_{\oplus}$  (lower panels).

**DTARPS 273:** This is a  $T=12.0$  mag M0 star at distance  $d = 83$  pc that [Kaltenegger et al. \(2019\)](#) places in the *TESS Habitable Zone Star Catalog*. Lying near the southern ecliptic pole, it has several sectors of TESS observation giving a greater ability to reveal small planets than with stars covered by a single sector. The DIAMante light curve shows little variability. The TCF periodogram has a strong peak with  $\text{SNR}=151$  at period  $P=0.369165$  day with several harmonics visible. The folded light curve shows a transit-like dip with depth  $0.12\%$  corresponding to a sub-Neptune with radius  $2.1 R_{\oplus}$ . The periodogram shows a possible peak around  $0.55$  day that is not an alias of the principal spectral peak; this might represent a second planet.

**Table 1.** DTARPS Candidates Catalog

Designations						Star						
DTARPS	Disp	TIC	TOI	NEA	DIAM	R.A.	Dec	T	$T_{eff}$	$R_{\star}$	$M_{\star}$	Dist
(1)	(2)	(3)	(4)	(5)	(6)	(7)	(8)	(9)	(10)	(11)	(12)	(13)
1	1	17361	3127	APC	T	219.33632	-24.95848	11.3	5775	1.26	1.03	309
2	1	1003831	564	CP	T	130.29516	-16.03628	10.7	5550	1.12	0.98	200
3	1	1449640	446	APC	F	75.17161	-35.20261	11.9	6411	1.67	1.29	674
4	1	1525480	2402	PC	T	156.52780	-17.26265	12.3	5519	0.97	0.97	345
5	1	1599403	...	...	F	131.11166	-2.47356	11.7	6508	1.26	1.33	453

NOTE—The full table of 462 DTARPS planet candidates is available in the electronic version of the paper in file DTARPS.MRT. Column definitions:

- (1) DTARPS: Sequence number of DTARPS planet candidates
- (2) Disp: DTARPS disposition based on vetting procedures. 1 = very high confidence. 2 = high confidence
- (3) TIC: TESS Input Catalog identifier
- (4) TOI: TESS Object of Interest (accessed February 2022)
- (5) NEA Disp: NASA Exoplanet Archive (NEA) Disposition. APC = Ambiguous Planet Candidate. CP = Confirmed Planet. FP = False Positive. KP = Known Planet. ... = previously unidentified by NEA (accessed January 2022)
- (6) DIAM: DIAMante planet candidate ([Montalto et al. 2020](#))
- (7-8) R.A., Dec = Right Ascension and Declination (J2000) from Gaia DR2 catalog
- (9) T = TESS band magnitude
- (10-13):  $T_{eff}$ ,  $R_{\star}$ ,  $M_{\star}$ , Dist = Stellar effective temperature (K), radius ( $R_{\odot}$ ), mass ( $M_{\odot}$ ), and distance (pc) from Gaia DR2 catalog

Lightcurve			ARIMA		TCF
$N_{lc}$	$IQR_{lc}$	$P_{LB,lc}$	$IQR_{AR}$	$P_{LB,AR}$	SNR
(14)	(15)	(16)	(17)	(18)	(19)
849	0.0009	-6.0	0.0012	-0.1	83
610	0.0005	-6.0	0.0006	-0.6	34
1147	0.0011	-6.0	0.0015	0.0	52
1079	0.0014	-6.0	0.0016	-0.2	66
590	0.0009	-6.0	0.0010	-0.1	29

NOTE—Column definitions:

(14)  $N_{lc}$ : Number of measurements in TESS FFI lightcurve

(15)  $IQR_{lc}$ : InterQuartile Range of normalized lightcurve fluxes

(16)  $P_{LB,lc}$ : Log probability of autocorrelation in lightcurve from the Ljung-Box test. Values above -2 are consistent with white noise while values below -4 are not.

(17)  $IQR_{AR}$ : InterQuartile Range of ARIMA residuals

(18)  $P_{LB,AR}$ : Log probability of autocorrelation of ARIMA residuals from the Ljung-Box test

(19) SNR: Signal-to-noise of peak power in Transit Comb Filter periodogram

Planet properties					Classifier	Notes
Period	Depth	$R_{pl}$	$T_0$	b	$P_{RF}$	
(20)	(21)	(22)	(23)	(24)	(25)	(26)
3.60667±0.00038	0.0111±0.0014	16.1±2.6	1600.570±0.001	0.9±0.0	0.94	T
1.65092±0.00047	0.0034±0.0009	8.9±2.1	1518.205±0.003	0.9±0.0	0.76	T
3.50173±0.00023	0.0165±0.0002	22.1±1.3	1440.432±0.001	0.6±0.1	0.47	T
5.50845±0.00121	0.0082±0.0003	8.6±0.6	1548.866±0.002	0.4±0.2	1.00	T
1.26251	0.0018	5.9	1473.641	...	0.67	T

NOTE— Period, Depth, Planet Radius and  $T_0$  are from the ARPS analysis if their associated errors are missing. Otherwise they are from the best-fit 'Exoplanet' model. Column definitions:

(20) Period of transit (day)

(21) Depth of transit (fraction of normalized flux)

(22) Planet radius (in Earth radii)

(23) Time of first transit (day)

(24) Impact parameter (fraction of stellar radius)

(25)  $P_{RF}$ : Probability of planet classification from Random Forest classifier

(26) Notes on individual objects appear in Appendix A.

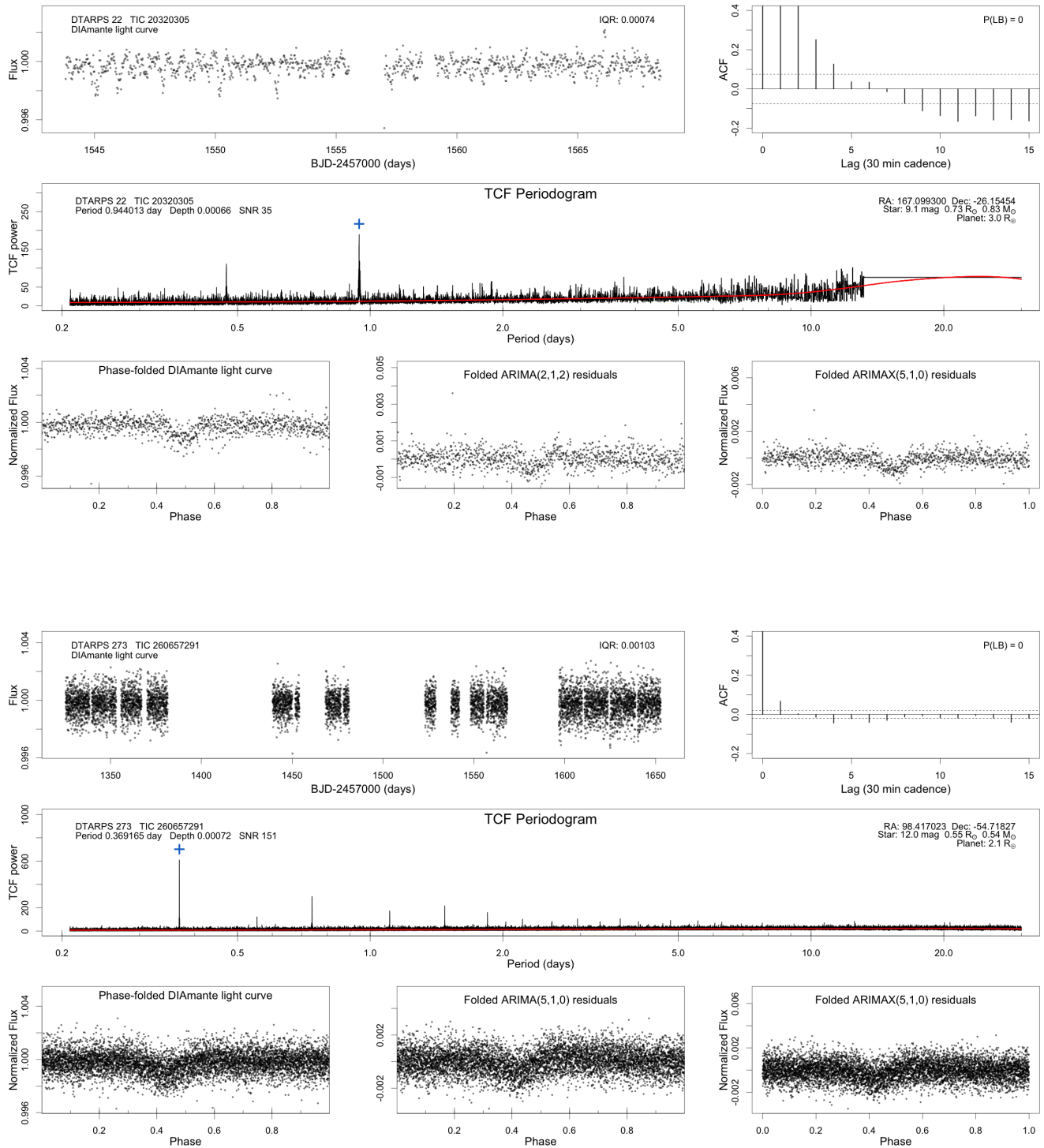


**Figure 5.** Figure Set graphics for two newly reported DTARPS Candidates with small radii: DTARPS 22 and 273. See text for descriptions. The complete Figure Set for 462 DTARPS Candidates is available in the electronic version of the paper.

#### 4. REFINING CANDIDATE PROPERTIES

The ARPS methodology (Caceres et al. 2019b) is designed for sensitive transit detection, not for accurate characterization of transit properties. It is therefore unsurprising that the properties emerging from ARPS, such as planet radius and orbital period, suffer biases and/or inaccuracies. Paper I (§8.1) showed that the transit depth obtained from the TCF algorithm tends to underestimate the planetary radius for injected planets. This is due to the combined effects of ARIMA model overfitting the stellar variations and the TCF underfitting the double-spike pattern. It was also noted during the vetting process that, in some cases, an inaccurate TCF period causes a slight drift in phase from the earlier to later transits. This section describes our efforts to ameliorate these problems. Table 1 incorporates the improved period and radius values.

##### 4.1. Improved Radius with *exoplanet* Fits

Limb darkening transit models (Mandel & Agol 2002) are fitted to the DIAMante light curve for each of the DTARPS Candidates using the *exoplanet* package (Foreman-Mackey et al. 2021) based on Bayesian inference, Gaussian Processes regression, and the PyMC3 algorithm (Salvatier et al. 2016). The *starry* (Luger et al. 2019; Agol et al. 2020) package was applied to create the analytic limb darkening transit models. The light curve models were averaged into 30-minute bins with an oversampling factor of 15 for each of the bins.

The free parameters for these transit models are: the period of the candidate transit ( $P$ ), the epoch of the first transit ( $T_0$ ), the transit depth ( $\delta$ ), the impact parameter ( $b$ ), the stellar mass ( $M_\star$ ), the stellar radius ( $R_\star$ ), and the quadratic limb-darkening coefficients ( $u_0, u_1$ ). Assumed prior distributions are given in Table 2. We use a narrow distribution for the orbital period and epoch of first transit because these are strongly constrained by the TCF and Random Forest classifier. But as TCF transit depths tended to be underestimated, a wider prior is used for depth. Priors for the stellar mass and radius parameters are based on the tabulated errors from the TIC (Stassun et al. 2019) with additional wide bounds. A wide uniform prior is assumed for the impact parameter. Prior distributions for the quadratic limb-darkening coefficients are adopted from Kipping (2013).

The posteriors were sampled with the No U-Turns step method (Homan & Gelman 2014) with PyMC3 using two chains with 2,000 tuning steps and 1,000 draws each. The target acceptance rate was set to 0.99. The posterior for the planet radius was drawn directly from the *starry* transit model for each candidate. Median and standard deviation posterior values are calculated from the 2,000 samples for each parameter. The transit model using the posterior parameters was plotted over the DTARPS candidate light curve and manually inspected.

Well-fitting transit model solutions were obtained for 53% of the DTARPS Candidates. The failures can be attributed to the sparse nature of TESS single-sector data where, in many cases, only a few observations are available to define the transit shape.

##### 4.2. Improved Period and Radius by Visual Inspection

When *exoplanet* failed to find a good transit model fit, the transit period and depth associated with the best TCF periodogram peak are adjusted visually to best fit the candidate transit signal. These DTARPS Candidates are identified in Table 1 by the absence of errors for the transit parameters.

The period of the candidate transit was adjusted if a drift in the transit midpoint was seen over multiple transits. Due to the sparse nature of the light curves (with time steps of 30 minutes or 0.021 days), the period could not be visually adjusted with high precision. These adjusted periods have estimated errors of  $\pm 0.001$  day or  $\sim 1$  minute. TCF

**Table 2.** Assumed Priors for *exoplanet* Fits

Parameter	Description	Prior Distribution
$P$	Orbital period (days)	$\mathcal{U}(P_{\text{TCF}}-0.5, P_{\text{TCF}}+0.5)$
$T_0$	Epoch of first transit (BJD - 2457000)	$\mathcal{N}(T_0, \text{TCF}, 1)$
$\delta$	Transit depth	$\log\mathcal{N}(\delta_{\text{TCF}}, 2)$
$b$	Impact parameter	$\mathcal{U}(0,1)$
$M_\star$	Stellar mass ( $M_\odot$ )	Bounded $\mathcal{N}(M_\star, \epsilon_{M_\star}, 0, 3)$
$R_\star$	Stellar radius ( $R_\odot$ )	Bounded $\mathcal{N}(R_\star, \epsilon_{R_\star}, 0, 3)$
$u_0, u_1$	Quadratic limb-darkening coefficients	Adopted from Kipping (2013)

transit depths were visually adjusted so the depth matched the median of the light curve points during the transit event in the folded light curve. The error for the manual adjustment of the candidate transit depth is approximately estimated to be  $\pm 0.02\%$ .

#### 4.3. Reliability and Accuracy of Planet Properties

In Paper I (§8.1), we found that the TCF periodogram tended to identify spuriously short periods for shallow injected transits and tended to underestimate the radius for deep injected transits. The latter effect is understood: the ARIMA model incorporates some of transit dip and thus the signal in the ARIMA residuals indicate a smaller planet. The former effect is not understood. We now examine whether these problems are alleviated by the corrections described here.

Figure 6 compares the DTARPS periods with those reported for previously identified Confirmed Planets, M20 candidates, unconfirmed Planet Candidates, and planetary injections that were recovered by DTARPS from Paper I (§8.1). Each plot shows stars that were accepted and rejected by our vetting procedure.

The results are excellent. All (100%) of the Confirmed Planets in the DTARPS Candidates list have a DTARPS fitted period that matches the reported period in the NASA Exoplanet Archive or TOI list over the range  $1 < P < 20$  days with a standard deviation of 0.0016 day or 2.3 minutes (top left panel Figure 6). There is no case of DTARPS preferring a 1/2- or 2-times harmonic. Similarly, 98% of the DTARPS Candidates in the candidate lists of M20 and other surveys agree. Most discrepant cases have DTARPS periods equal to 1/2 of the reported period; it is generally not known which is correct. One discrepant period is present: TIC 64071894 has a DTARPS  $P = 0.45917$  day while TOI 458.01 has a reported period  $P = 17.52883$  day. These may be different planets within the same system.

It is gratifying that the erroneous short periods obtained when the DTARPS analysis is applied to planetary injections (Paper I, §8.1) were not found when true Confirmed Planets were examined. We note from Figure 6 (upper left) that our vetting was somewhat too stringent, as it rejected some Confirmed Planets even though ARPS found the correct period.

Figure 7 and Table 3 show a similar comparison between planet radii obtained by DTARPS and other surveys. The astrophysical `exoplanet` or manually corrected radii are used (§4.1-4.2) except in the lower right panel where the underestimation of large radii is evident. Error bars from the `exoplanet` astrophysical fits are plotted when available. The agreement between DTARPS and published radii is good over the range  $2 < R < 20 R_{\oplus}$  with 70 – 80% of radii agreeing within  $\pm 15\%$ . The underestimation of radii seen in Paper I with the injections is not apparent in the comparison to NASA and TOI Confirmed Planets. The radius agreement is worse for objects that were rejected by DTARPS vetting (open points in Figure 7), but this has no impact on the quality of the DTARPS Candidate catalog.

**Table 3.** Differences between Published and DTARPS Planet Radii for Confirmed Planets

Population	< 85%	100% <sup>a</sup>	> 115%	N
	(1)	(2)	(3)	(4)
Super-Earth (< 1.8 $R_{\oplus}$ )	67%	33%	...	3
Sub-Neptune (1.8 to 4 $R_{\oplus}$ )	7%	78%	15%	27
Super-Neptune (4 to 8 $R_{\oplus}$ )	12%	72%	21%	58
Jovian (>8 $R_{\oplus}$ )	9%	87%	15%	183

<sup>a</sup>Objects whose DTARPS radius error bars fall within 15% of the reported radii.

NOTE—Columns 1 – 3 give the percent of the Confirmed Planets and previously identified planet candidates whose DTARPS fitted radius are in the stated range of agreement. Column 4 gives the number of DTARPS planets with Confirmed Planet counterparts in each radius stratum.

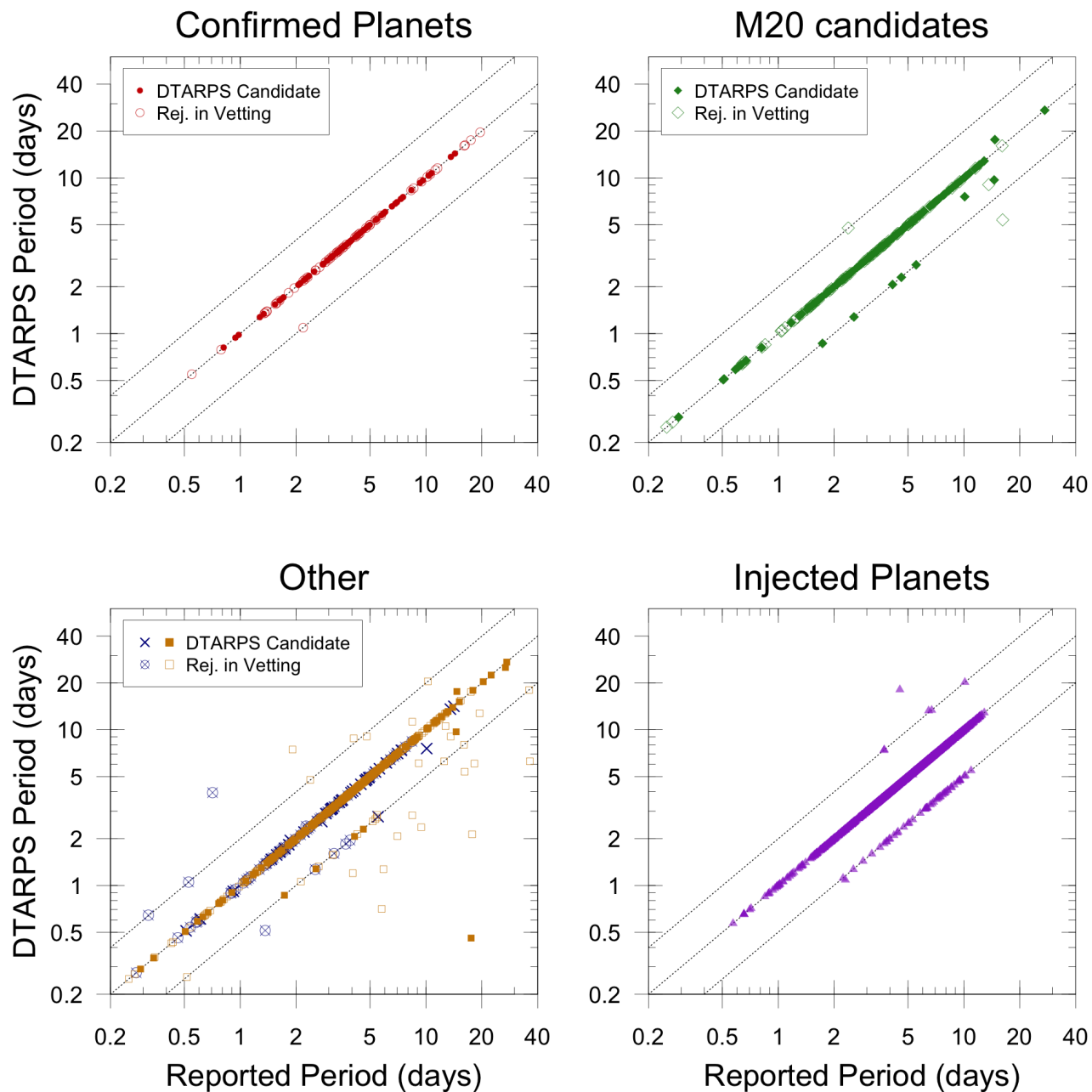


**Figure 6.** Comparison between the refined DTARPS period and the reported periods for different groups of objects: NASA/TOI Confirmed Planets (upper left); M20 candidates (upper right); candidates from other surveys (lower left); and our synthetic injected planets (Paper I). The bottom left panel contains both planet candidates (gold squares) and previously identified False Positives (blue x's). Open symbols represent objects rejected by vetting. The dashed lines indicate the 2:1, 1:1, and 1:2 ratios between the reported and DTARPS period.

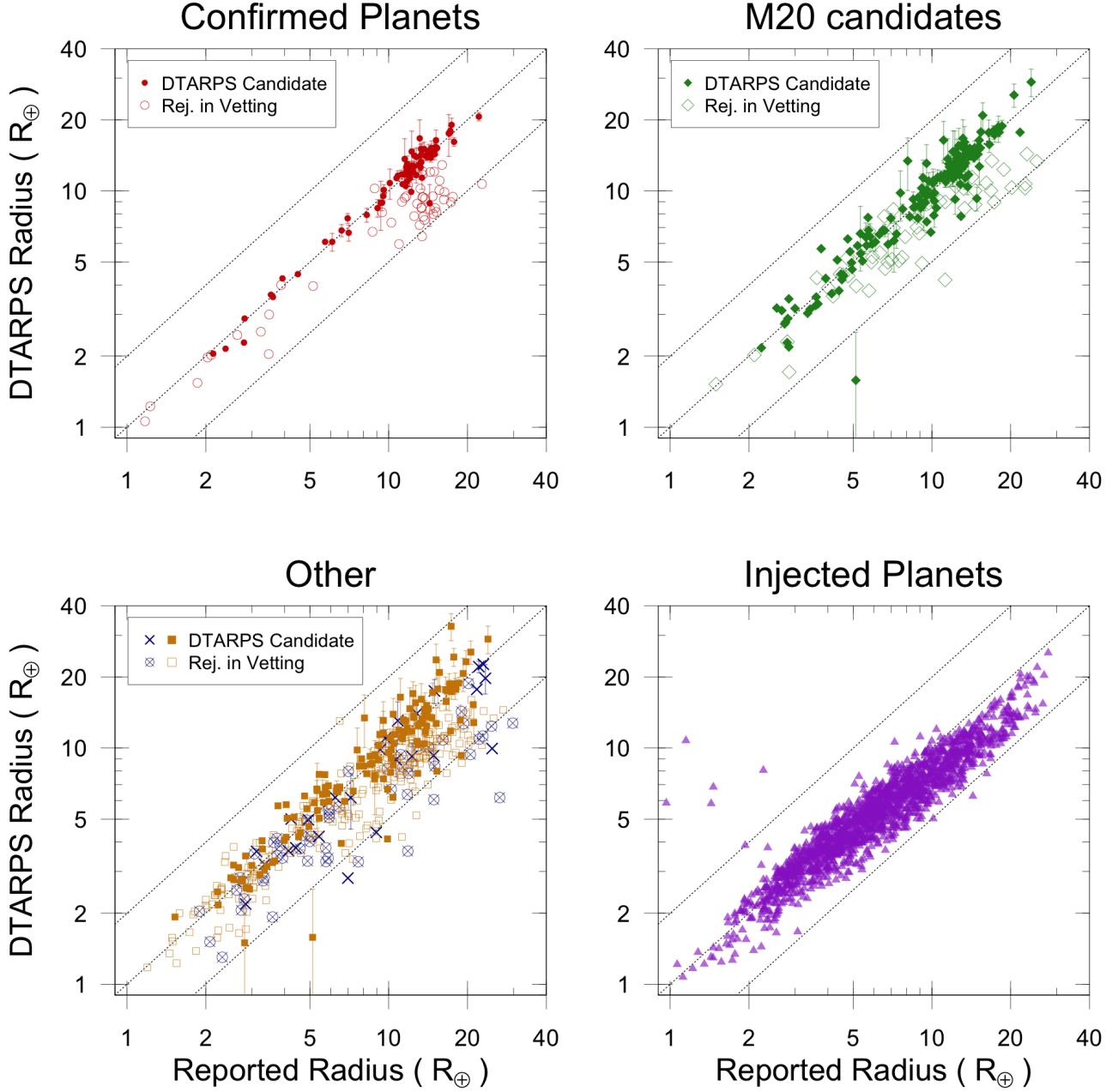


**Figure 7.** Comparison between the refined DTARPS radius and the reported radii for different groups of objects with reported radii and the planetary injections from the positive training set of the RF classifier. The bottom left panel contains both planet candidates (in gold squares) and previously identified False Positives (in blue x's). The bottom right panel is from Paper I. The open points are plotted by the radius from their TCF periodogram peak. The dashed lines indicate the 2:1, 1:1, and 1:2 ratios between the reported radius and the DTARPS radius.

## 5. FLAGGING POTENTIAL PROBLEMS

The analysis in this section is used to identify potential problems in DTARPS Candidates but does not remove objects in the candidate list. The DTARPS disposition of any Level 1 candidate flagged here is changed to Level 2.

### 5.1. Blending and Dilution in the ZTF survey

The Zwicky Transient Facility (ZTF; Bellm et al. 2019; Masci et al. 2019) conducts a wide-field survey that scans the northern hemisphere sky every  $\sim 2$  days from the Palomar Observatory in the  $g$  and  $r$  optical bands with median depths of 20.8 mag and 20.6 mag, respectively. Despite the wide field of view of the telescope ( $47 \text{ deg}^2$ ), ZTF is able to achieve a  $2''0$  full-width-half-maximum point spread function in images. The project releases both photometric measurements and light curves for sources to aid in the identification and characterization of astrophysical transients. ZTF light curves are examined here for eclipsing binaries near DTARPS Candidates that would be blended in the  $21''$  TESS pixel and the photometric ZTF catalog is searched for nearby bright stars that would dilute a true transit signal. Only  $\sim 1/4$  of DTARPS Candidates are covered by the ZTF survey due to their southern declinations. Our study used the ZTF DR9 catalog hosted by the NASA/IPAC Infrared Science Archive.

We examine ZTF light curves from stars within  $15''$  around each DTARPS candidate within the ZTF coverage area to identify potential blended eclipsing binaries. Nearby stars with  $> 50$  observations and  $r < 18$  were considered as potential contaminants. Fifty-eight DTARPS Candidates had blended sources with light curve data that fit these parameters. If a contaminant light curve had a  $\chi^2$  value greater than 1.5, indicating that the light curve was not well fit with a constant magnitude stellar model, then the light curve was examined for evidence of periodic dips. Six DTARPS Candidates (10% of the accessible sample) with nearby objects were found to have variable contaminants and were assigned Level 2 dispositions. Details are provided in Appendix A.

Another  $15''$  search around each DTARPS candidate is performed to identify nearby bright stars that may dilute the depth of a true transit signal. Out of 94 candidates with ZTF observations, 18 had a nearby star with a  $r < 16$  that may cause transit dilution and thus had their disposition set to Level 2. Details appear in Appendix A. Most of the identified possible dilution contaminants are faint (e.g., a 15 magnitude star near an 11–12 magnitude candidate), and only  $\sim 5$  of the possible sources of dilution are likely to substantially affect our depth measurements. Overall, about 5% of DTARPS Candidates may have blended field stars that diluted the DTARPS candidate star by 20-80% in the TESS pixel, reducing the inferred planet radius by 10-30%. In such cases, a Neptune with tabulated radius of  $7 R_{\oplus}$  might actually have radius 8-9  $R_{\oplus}$ . Individual cases are described in Appendix A.

### 5.2. Gaia Radial Velocity Constraints

*Gaia* DR2 includes radial velocities (RVs) with goodness-of-fit measures of the astrometric solution for 7,224,631 sources (Gaia Collaboration et al. 2016, 2018). These quantities can be used to flag candidates with suspected stellar companions, although the relation between the astrometry measurements, RV measurements, and the candidate transit signal is unknown. Therefore if a candidate's *Gaia* DR2 astrometric solution has poor fitting parameters or if the standard deviation of the RV measurement is too large, the disposition of the DTARPS Candidate is set to Level 2 indicating a possible stellar companion.

Evans (2018) found that an astrometric excess noise significance of 5 and an astrometric goodness-of-fit in the along-scan direction of 20 separated planetary systems with confirmed binaries from planetary systems orbiting confirmed single stars. Thirty-nine DTARPS Candidates had either a significance of astrometric excess noise or an astrometric goodness-of-fit in the along-scan direction value greater than these limits (Figure 8, left panel).

Additional thresholds for flagging DTARPS Candidates based on *Gaia* RV measurements were adopted from M20. The standard deviation of the RV measurements,

$$\sigma_{V_R^t} = \sqrt{\frac{2N}{\pi} (\epsilon_{V_R}^2 - 0.11^2)}, \quad (5)$$

was obtained by inverting equation 1 in Katz et al. (2019) where  $\epsilon_{V_R}$  is the reported error of the RV and  $N$  is the number of radial velocity measurements. The  $5\sigma$  boundary (red line) shown in the right panel of Figure 8 was calculated from a fit to RV standard deviation measurements for known planet hosts based on the *Gaia*  $G$  magnitude. Fifty-three DTARPS Candidates have a RV standard deviation in excess of this  $5\sigma$  criterion. Seven of these stars exceeded both thresholds for a poor astrometric solution and RV standard deviation. Dispositions were changed from Level 1 to Level 2 if necessary.

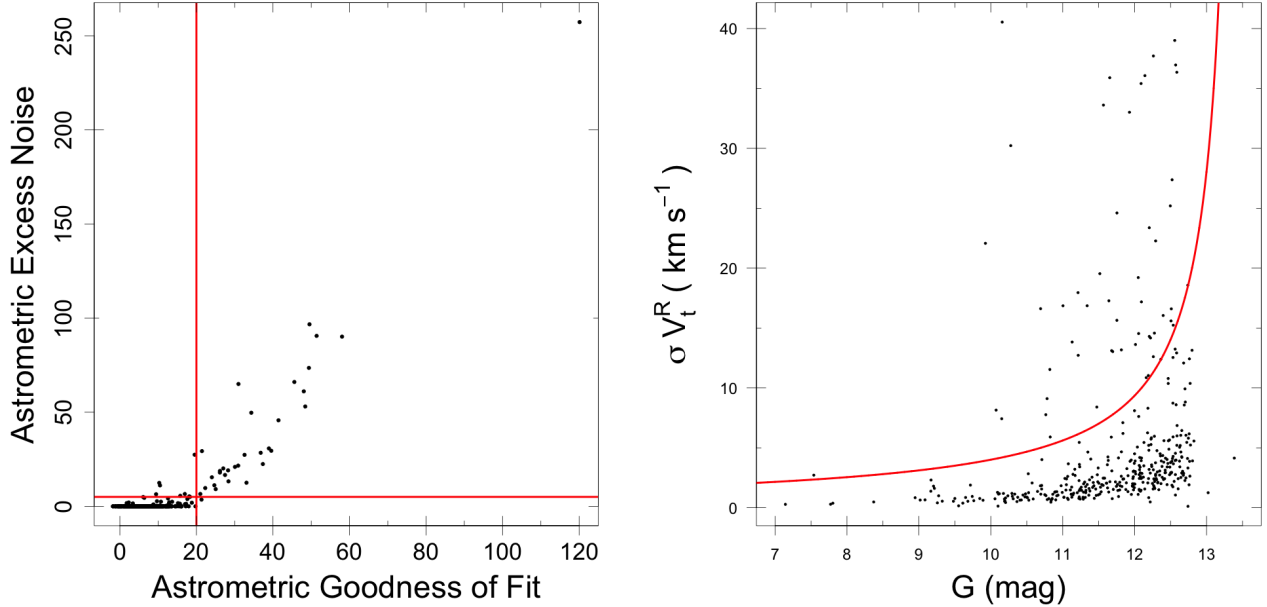


**Figure 8.** Astrometric analysis of DTARPS Candidates from *Gaia* DR2 observations. The red lines in each plot show the upper boundary for a Level 1 candidate. The red boundaries are from [Evans \(2018\)](#). (Left) Significance of the astrometric excess noise and astrometric goodness-of-fit in the along-scan direction for DTARPS Candidates. (Right) Standard deviation of the radial velocity measurements. The red boundary is from [Montalto et al. \(2020\)](#).

### 5.3. Upper Planetary Radii Limit

The radii of the candidates were re-examined after many DTARPS Candidates radii had been fitted with parametric orbital models (§4). Recall that during the vetting process, we had removed DTARPS Analysis List objects with radii greater than  $20 R_{\oplus}$  (§2.3). The disposition of any DTARPS candidate with a corrected planetary radius greater than  $28 R_{\oplus}$  ( $2.5 R_J$ ) was set to Level 2. Seven DTARPS Candidates have a planetary radius above this threshold.

## 6. EVALUATION OF CENTROID-CROWDING ANALYSIS

The centroid analysis applied to the 7,377 DTARPS Analysis List objects at the beginning of our vetting procedure measures possible spatial jitter of light during the photometric transit is combined with a crowding analysis measuring the density of brighter *Gaia* DR2 stars in the immediate vicinity (§2.1, M20). These criteria were perhaps too restrictive since 73% of the stars were removed, including most objects in the Galactic Plane. Centroid-crowding analysis also was responsible for most of the rejections of Confirmed Planets. These problems may arise because the centroid-crowding bias combines the flux-weighted centroid in four apertures in the TESS FFI image; this may not be effective in crowded fields.

In order to evaluate these restrictions on the DTARPS Candidate sample, we processed a sample of  $\sim 1,800$  DTARPS Analysis List objects through every stage of the vetting process except centroid-crowding analysis. This sample has Galactic longitudes from  $193 - 236$  and latitudes mostly within  $\pm 15^\circ$  of the Galactic Plane. The result was an additional 310 DTARPS Candidates that we call the *DTARPS Galactic Plane list*. The sky distribution of these additional DTARPS Candidates is shown in Figure 10; most lie close to the Galactic Plane where the crowding criterion was violated. These objects are listed in Table 2 using nearly the same format as Table 1.

Two cases representing smaller planets newly reported here are illustrated in Figure 9, together with scalar values from Table 4 and information from Appendix A, can be described as follows:

**DTARPS-GP019519368 = TOI-494:** This is a  $T=10.1$  mag K1 star at a distance of 90 pc with TOI designation ‘Planetary Candidate’. It has period  $P = 1.7005$  day, transit depth 0.04% and corresponding planet radius  $1.7 R_{\oplus}$ ; a super-Earth. These parameters agree with the TOI values. The Random Forest probability is high at  $P_{RF} = 0.51$ . The Galactic coordinates are  $(l, b) = (229, 16)$ .

**Table 4.** DTARPS Galactic Plane List

Designations				Star						
TIC	TOI	NEA	DIAM	R.A.	Dec	T	$T_{eff}$	$R_{\star}$	$M_{\star}$	Dist
(1)	(2)	(3)	(4)	(5)	(6)	(7)	(8)	(9)	(10)	(11)
883943	...	...	F	127.02816	-17.49844	10.6	5976	1.18	1.10	232
1129033	398	KP	F	37.15511	-7.06066	9.6	5605	0.93	0.99	105
1605476	...	...	F	131.26395	-4.11884	11.6	6056	1.05	1.13	329
4616346	...	PC	F	101.95155	-22.12333	11.6	5845	1.21	1.05	350
4784880	...	...	F	109.66720	-20.88884	11.0	5725	0.91	1.02	198

NOTE—The full table of 310 DTARPS\_GP objects is available in the electronic version of the paper in file DTARPS\_GP.MRT. Column definitions are the same as for Table 1 except the first two columns are absent. Notes on individual objects appear in Appendix B.

Lightcurve			ARIMA		TCF
$N_{lc}$	$IQR_{lc}$	$P_{LB,lc}$	$IQR_{AR}$	$P_{LB,AR}$	SNR
(12)	(13)	(14)	(15)	(16)	(17)
610	0.0006	-6.0	0.0007	-0.2	29
799	0.0004	-6.0	0.0007	-0.1	65
590	0.0010	-6.0	0.0015	-0.1	56
1962	0.0009	-2.8	0.0010	-0.3	62
1023	0.0009	-5.2	0.0008	-5.3	63

Planet properties					Classifier	Notes
Period	Depth	$R_{pl}$	$T_0$	b	$P_{RF}$	
(18)	(19)	(20)	(21)	(22)	(23)	(24)
1.47000	0.0038	8.0	1468.454	...	0.66	F
$1.36000 \pm 0.00005$	$0.0203 \pm 0.0003$	$13.7 \pm 0.5$	$1413.705 \pm 0.000$	$0.2 \pm 0.1$	0.52	T
$0.42100 \pm 0.00004$	$0.0058 \pm 0.0002$	$7.3 \pm 0.4$	$1517.578 \pm 0.001$	$0.1 \pm 0.1$	0.72	F
0.69047	0.0010	4.6	1468.891	...	0.38	T
2.53600	0.0015	3.8	1520.183	...	0.8	F

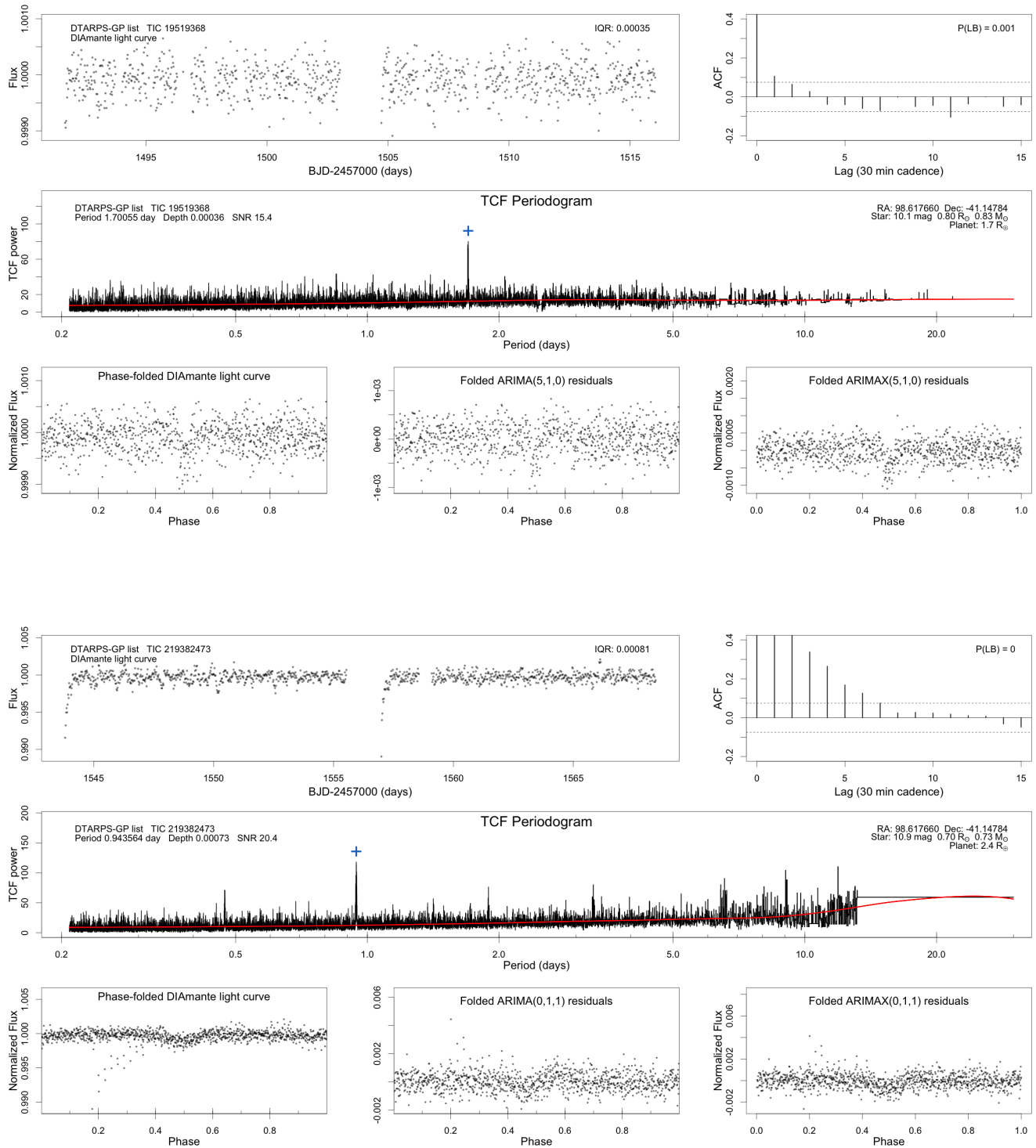


**Figure 9.** Figure Set graphics for two newly reported DTARPS Galactic Plane objects with small planetary radii: DTARPS-GP019519368 and DTARPS-GP219382473. See text for descriptions. The complete Figure Set for 310 DTARPS\_GP stars is available in the electronic version of the paper.

**DTARPS-GP219382473:** This is a newly reported possible transiting planet orbiting a  $T=10.9$  mag K4 star at  $d=96$  pc. It has period  $P = 0.9436$  day, transit depth 0.1% and corresponding planet radius  $2.4 R_{\oplus}$ . The Random Forest probability  $P_{RF} = 0.32$  is only slightly above the 0.30 threshold. The Galactic coordinates are  $(l, b) = (279, 35)$ .

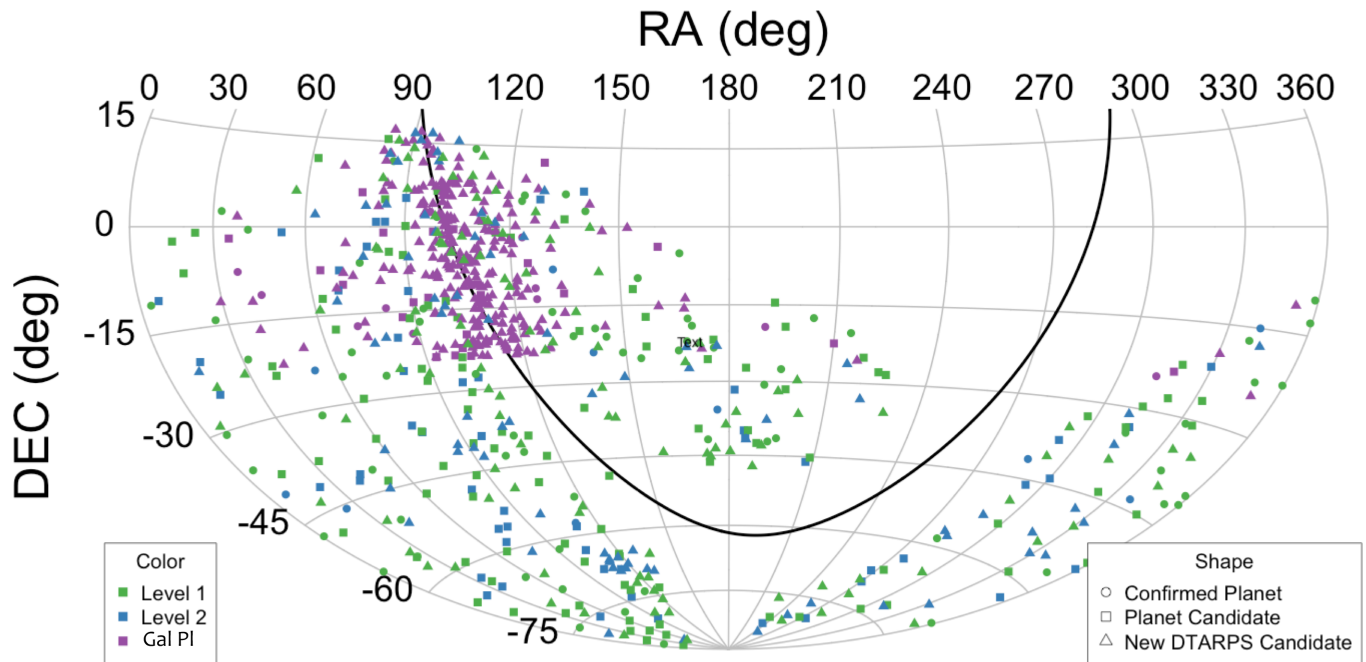


**Figure 10.** Spatial distribution of DTARPS Candidates (Tables 1 and 2). Objects are differentiated by DTARPS disposition (DTARPS Level 1 and 2, DTARPS\_GP) and status with respect to previous surveys (previously known Confirmed Planet, previously known Planet Candidates, and new DTARPS Candidates). The black curve indicates the approximate plane of the galaxy.

The breakdown of the vetting labels for the  $\sim 1,800$  Galactic Plane sample was 53% False Alarms, 18% False Positives, 0.2% possible photometric binaries, 1.5% ephemeris match rejections, and 27% planetary candidates. These proportions are very similar to the vetting label breakdown of the DTARPS Candidates after centroid-crowding analysis (§2.2-2.5).

The 310 DTARPS Galactic Plane objects were also analyzed for ZTF imaging, *Gaia* dynamical constraints, and large planetary radii (§5). The ZTF analysis identified 10 stars with possible blended contamination from nearby variable ZTF light curves out of 140 candidates with light curves available; 34 objects may be affected by possible dilution from a nearby star with  $r < 16$  out of 176 candidates. Details appear in Appendix B. The *Gaia* dynamical constraints found 20 DTARPS Galactic Plane objects with poor astrometric fits and 17 candidates with a RV standard deviation greater than the  $5\sigma$  threshold. Twelve have planetary radii greater than  $28 R_{\oplus}$ . These flags appear with similar rates as with DTARPS Candidates (§5).

It thus appears that applying centroid-crowding criteria significantly reduced the number of planetary candidates in our DTARPS vetting procedure while exhibiting no reduction in sensitivity to Confirmed Planets and little increase in the False Positives or other worrisome properties. Paper III reports that early results from reconnaissance spectroscopy DTARPS Galactic Plane objects appear to have the same low fraction of variable radial velocities as DTARPS candidates. (This result, however, is based on a very small sample.) We find no indication that DTARPS Galactic Plane are drawn from a different population than DTARPS Candidates. At present, it appears that the 310 Galactic Plane objects in Table 4 are promising for further study including spectroscopic follow-up.

This experiment on part of the Galactic Plane suggests that the centroid-crowding vetting step designed by M20 is too strict. Removing it entirely would add  $\sim 1,500$  candidates to our TESS southern hemisphere survey, increasing the fraction of candidates in the 7,377 DTARPS Analysis List from 6.3% to  $\sim 27\%$ . The overall sensitivity for this enlarged DTARPS Candidate catalog would be  $\sim 71\%$  for Confirmed Planets and  $\sim 42\%$  for the planet candidates with specificity  $\sim 37\%$ . The number of DTARPS discoveries in a combined sample would be similar to the pre-flight

prediction of [Barclay et al. \(2018\)](#) discussed in Paper I (§1). However, searching for periodic centroid wobbling in TESS images is clearly advantageous for removal of contaminating eclipsing binaries (Appendix C.3). We therefore suggest that future efforts be made to design a vetting step of intermediate severity that admits more likely candidates in the Galactic Plane region.

## 7. SUMMARY

In Paper I, the AutoRegressive Planet Search methodology was uniformly applied to  $\sim 1$  million TESS Year 1 light curves. This processing had four major steps: removal of trends and instrumental artifacts; removal of best-fit ARIMA models to give nearly-Gaussian white noise residuals; detection of transit-shaped periodic signals with the Transit Comb Filter in ARIMA residuals; and application of an optimized Random Forest classifier applied to 37 scalar features for each star. The classifier was trained towards injected planetary signals and against a combination of random light curves and injected eclipsing binary signals. A threshold to the RF probability was then applied to give the DTARPS Analysis List of 7,377 promising cases for transiting planets.

This procedure has advantages of uniformity and objectivity. Once various analysis parameters and thresholds were chosen, the  $\sim 1$  million stars are processed in identical fashion without human judgment. The DTARPS Analysis List can thus be viewed as well-defined and ‘complete’; for instance, allowing completeness heat maps as a function of period and radius (Paper I, Figure 17). But the DTARPS Analysis List has limited utility for identifying individual exoplanets for further study because it is dominated by contaminants. Thus, a vetting program is needed to cull problematic cases and provide a smaller list of highly probable exoplanet candidates. In the parlance of statistical classification, the DTARPS Analysis List produced in Paper I optimizes *recall* while the DTARPS Candidate Catalog emerging here seeks to optimize *precision* by reducing False Alarms and False Positives through vetting procedures.

Our vetting procedure described in §2 reduces the list 7,377 promising cases nearly 10-fold, giving lists of 772 stars likely to be hosting short-period exoplanets: 462 in the spatially complete DTARPS Candidate catalog (Table 1) and 310 in the spatially incomplete DTARPS Galactic Plane List (Table 4). But the vetting necessarily sacrifices the high standard of uniformity and objectivity achieved with the DTARPS Analysis List. The vetting procedures are based on human evaluations of graphical data, and in the case of centroid motion and crowding metrics, application of thresholds that have major effects on the final sample.

In the DTARPS Candidate catalog, we segregate the more subjective judgments by ‘DTARPS disposition’ flag. Level 1 dispositions are cases where the object satisfies all tests for a planetary transit and there is no evidence for an alternative classification. Level 2 dispositions are cases where we believe the evidence for a planetary transit is convincing, but there is some marginal vetting confirmation. The DTARPS Galactic Plane objects have additional uncertainty as they were not subject to the centroid-crowding analysis. The evidence suggests that the Galactic Plane objects have similar recall and precision rates as the DTARPS Candidates, but there are reasons to believe that they may include more False Positive eclipsing binaries.

Once the DTARPS Candidates catalog membership is established, we make efforts to improve estimates of the inferred planet properties – orbital period and planet radius – during the vetting process. These efforts appear to be very successful: Figures 6 and 7 show that the DTARPS properties are accurate.

The DTARPS Candidates catalog (Table 1) and DTARPS Galactic Plane list (Table 4) are ready for spectroscopic follow-up to remove remaining False Positives, measure other planetary properties, and further investigate the planetary systems. Paper III examines various astronomical properties of these samples, discussing exoplanet types such as the hot Neptune population, Ultra Short Period planets, planets orbiting low-mass stars, and candidates for atmospheric characterization by transmission spectroscopy. The results are informed by preliminary results of reconnaissance spectroscopy of a small portion of the DTARPS Candidate sample. Paper III also returns to the completeness heat maps introduced in Paper I showing that the DTARPS planet occurrence rates are compatible with those obtained with the *Kepler* mission.

The ARPS project is supported at Penn State by NASA grant 80NSSC17K0122 and NSF grant AST-1614690.

The DTARPS project benefits from the vibrant community of Penn State’s Center for Exoplanets and Habitable Worlds that is supported by the Pennsylvania State University, the Eberly College of Science, and the Pennsylvania Space Grant Consortium. This study is also a product of the Center for Astrostatistics supported by the Eberly College of Science. We appreciate comments on the manuscript by members of these Centers – Ian Czekala, Rebekah Dawson, Hyungsuk Tak, Jason Wright – as well as Joel Hartman (Princeton). E.J.M. thanks Jiayin Dong (Penn State) for help executing the `exoplanet` software.

This paper includes data collected by the TESS mission. Funding for the TESS mission is provided by the NASA Explorer Program. This work has made use of data from the European Space Agency (ESA) mission *Gaia* (<https://www.cosmos.esa.int/gaia>), processed by the *Gaia* Data Processing and Analysis Consortium (DPAC, <https://www.cosmos.esa.int/web/gaia/dpac/consortium>). Funding for the DPAC has been provided by national institutions, in particular the institutions participating in the *Gaia* Multilateral Agreement. This research has made use of the NASA Exoplanet Archive, which is operated by the California Institute of Technology, under contract with the National Aeronautics and Space Administration under the Exoplanet Exploration Program. It also made use of the SIMBAD database, operated at CDS, Strasbourg, France. The ZTF analysis is based on observations obtained with the Samuel Oschin Telescope 48-inch and the 60-inch Telescope at the Palomar Observatory as part of the Zwicky Transient Facility project. ZTF is supported by the National Science Foundation under Grant No. AST-2034437 and a collaboration including Caltech, IPAC, the Weizmann Institute for Science, the Oskar Klein Center at Stockholm University, the University of Maryland, Deutsches Elektronen-Synchrotron and Humboldt University, the TANGO Consortium of Taiwan, the University of Wisconsin at Milwaukee, Trinity College Dublin, Lawrence Livermore National Laboratories, and IN2P3, France. This research made use of `exoplanet` and its dependencies (Foreman-Mackey et al. 2021).

*Facility:* TESS, NASA Exoplanet Archive, *Gaia*

*Software:* R core (R Core Team 2020): *forecast* (Hyndman & Athanasopoulos 2021); Python: *Jupyter* (Kluyver et al. 2016), *ArviZ* (Kumar et al. 2019), *Astropy* (Astropy Collaboration et al. 2013, 2018), *celerite* (Foreman-Mackey et al. 2017; Foreman-Mackey 2018), *exoplanet* (Foreman-Mackey et al. 2021), *NumPy* (van der Walt et al. 2011; Harris et al. 2020), *Matplotlib* (Hunter 2007; Droettboom et al. 2016), *PyMC3* (Salvatier et al. 2016), *starry* (Luger et al. 2019), *Theano* (The Theano Development Team et al. 2016)

## REFERENCES

- Affer, L., Micela, G., Favata, F., & Flaccomio, E. 2012, *MNRAS*, 424, 11, doi: [10.1111/j.1365-2966.2012.20802.x](https://doi.org/10.1111/j.1365-2966.2012.20802.x)
- Agol, E., Luger, R., & Foreman-Mackey, D. 2020, *AJ*, 159, 123, doi: [10.3847/1538-3881/ab4fee](https://doi.org/10.3847/1538-3881/ab4fee)
- Andrews, J. J., Chanamé, J., & Agüeros, M. A. 2017, *MNRAS*, 472, 675, doi: [10.1093/mnras/stx2000](https://doi.org/10.1093/mnras/stx2000)
- Armstrong, D. J., Günther, M. N., McCormac, J., et al. 2018, *MNRAS*, 478, 4225, doi: [10.1093/mnras/sty1313](https://doi.org/10.1093/mnras/sty1313)
- Astropy Collaboration, Robitaille, T. P., Tollerud, E. J., et al. 2013, *A&A*, 558, A33, doi: [10.1051/0004-6361/201322068](https://doi.org/10.1051/0004-6361/201322068)
- Astropy Collaboration, Price-Whelan, A. M., Sipőcz, B. M., et al. 2018, *AJ*, 156, 123, doi: [10.3847/1538-3881/aabc4f](https://doi.org/10.3847/1538-3881/aabc4f)
- Barclay, T., Pepper, J., & Quintana, E. V. 2018, *ApJS*, 239, 2, doi: [10.3847/1538-4365/aae3e9](https://doi.org/10.3847/1538-4365/aae3e9)
- Batalha, N. M., Rowe, J. F., Gilliland, R. L., et al. 2010, *ApJL*, 713, L103, doi: [10.1088/2041-8205/713/2/L103](https://doi.org/10.1088/2041-8205/713/2/L103)
- Bellm, E. C., Kulkarni, S. R., Graham, M. J., et al. 2019, *PASP*, 131, 018002, doi: [10.1088/1538-3873/aaecbe](https://doi.org/10.1088/1538-3873/aaecbe)
- Cacciapuoti, L., Kostov, V. B., Kuchner, M., et al. 2022, *MNRAS*, 513, 102, doi: [10.1093/mnras/stac652](https://doi.org/10.1093/mnras/stac652)
- Caceres, G. A., Feigelson, E. D., Jogesh Babu, G., et al. 2019a, *AJ*, 158, 58, doi: [10.3847/1538-3881/ab26ba](https://doi.org/10.3847/1538-3881/ab26ba)
- . 2019b, *AJ*, 158, 57, doi: [10.3847/1538-3881/ab26b8](https://doi.org/10.3847/1538-3881/ab26b8)
- Chen, G., Pallé, E., Welbanks, L., et al. 2018, *A&A*, 616, A145, doi: [10.1051/0004-6361/201833033](https://doi.org/10.1051/0004-6361/201833033)
- Collins, K. A., Collins, K. I., Pepper, J., et al. 2018, *AJ*, 156, 234, doi: [10.3847/1538-3881/aae582](https://doi.org/10.3847/1538-3881/aae582)
- Coughlin, J. L., Thompson, S. E., Bryson, S. T., et al. 2014, *The Astronomical Journal*, 147, 119, doi: [10.1088/0004-6256/147/5/119](https://doi.org/10.1088/0004-6256/147/5/119)
- Coughlin, J. L., Mullally, F., Thompson, S. E., et al. 2016, *ApJS*, 224, 12, doi: [10.3847/0067-0049/224/1/12](https://doi.org/10.3847/0067-0049/224/1/12)
- Dong, J., Huang, C. X., Dawson, R. I., et al. 2021, *ApJS*, 255, 6, doi: [10.3847/1538-4365/abf73c](https://doi.org/10.3847/1538-4365/abf73c)
- Dressing, C. D., Hardegree-Ullman, K., Schlieder, J. E., et al. 2019, *AJ*, 158, 87, doi: [10.3847/1538-3881/ab2895](https://doi.org/10.3847/1538-3881/ab2895)

- Droettboom, M., Hunter, J., Caswell, T. A., et al. 2016, *matplotlib: matplotlib v1.5.1*, doi: [10.5281/zenodo.44579](https://doi.org/10.5281/zenodo.44579)
- Dvash, E., Peleg, Y., Zucker, S., & Giryes, R. 2022, *AJ*, 163, 237, doi: [10.3847/1538-3881/ac5ea2](https://doi.org/10.3847/1538-3881/ac5ea2)
- Eisner, N. L., Barragán, O., Lintott, C., et al. 2021, *MNRAS*, 501, 4669, doi: [10.1093/mnras/staa3739](https://doi.org/10.1093/mnras/staa3739)
- Evans, D. F. 2018, *Research Notes of the American Astronomical Society*, 2, 20, doi: [10.3847/2515-5172/aac173](https://doi.org/10.3847/2515-5172/aac173)
- Feinstein, A. D., Montet, B. T., Foreman-Mackey, D., et al. 2019, *PASP*, 131, 094502, doi: [10.1088/1538-3873/ab291c](https://doi.org/10.1088/1538-3873/ab291c)
- Foreman-Mackey, D. 2018, *Research Notes of the American Astronomical Society*, 2, 31, doi: [10.3847/2515-5172/aaaf6c](https://doi.org/10.3847/2515-5172/aaaf6c)
- Foreman-Mackey, D., Agol, E., Ambikasaran, S., & Angus, R. 2017, *AJ*, 154, 220, doi: [10.3847/1538-3881/aa9332](https://doi.org/10.3847/1538-3881/aa9332)
- Foreman-Mackey, D., Luger, R., Agol, E., et al. 2021, *The Journal of Open Source Software*, 6, 3285, doi: [10.21105/joss.03285](https://doi.org/10.21105/joss.03285)
- Gaia Collaboration, Prusti, T., de Bruijne, J. H. J., et al. 2016, *A&A*, 595, A1, doi: [10.1051/0004-6361/201629272](https://doi.org/10.1051/0004-6361/201629272)
- Gaia Collaboration, Brown, A. G. A., Vallenari, A., et al. 2018, *A&A*, 616, A1, doi: [10.1051/0004-6361/201833051](https://doi.org/10.1051/0004-6361/201833051)
- Giacalone, S., Dressing, C. D., Jensen, E. L. N., et al. 2021, *AJ*, 161, 24, doi: [10.3847/1538-3881/abc6af](https://doi.org/10.3847/1538-3881/abc6af)
- Grievés, N., Ge, J., Thomas, N., et al. 2018, *MNRAS*, 481, 3244, doi: [10.1093/mnras/sty2431](https://doi.org/10.1093/mnras/sty2431)
- Guenther, E. W., Gandolfi, D., Sebastian, D., et al. 2012, *A&A*, 543, A125, doi: [10.1051/0004-6361/201219121](https://doi.org/10.1051/0004-6361/201219121)
- Guerrero, N. M., Seager, S., Huang, C. X., et al. 2021, *ApJS*, 254, 39, doi: [10.3847/1538-4365/abefe1](https://doi.org/10.3847/1538-4365/abefe1)
- Harris, C. R., Millman, K. J., van der Walt, S. J., et al. 2020, *Nature*, 585, 357, doi: [10.1038/s41586-020-2649-2](https://doi.org/10.1038/s41586-020-2649-2)
- Homan, M. D., & Gelman, A. 2014, *J. Mach. Learn. Res.*, 15, 1593–1623
- Hou, Q., & Wei, X. 2022, *MNRAS*, 511, 3133, doi: [10.1093/mnras/stac169](https://doi.org/10.1093/mnras/stac169)
- Hunter, J. D. 2007, *Computing in Science and Engineering*, 9, 90, doi: [10.1109/MCSE.2007.55](https://doi.org/10.1109/MCSE.2007.55)
- Hyndman, R., & Athanasopoulos, G. 2021, *Forecasting: principles and practice (OTexts)*. <https://otexts.com/fpp3/>
- Jenkins, J. M., Caldwell, D. A., Chandrasekaran, H., et al. 2010, *ApJL*, 713, L87, doi: [10.1088/2041-8205/713/2/L87](https://doi.org/10.1088/2041-8205/713/2/L87)
- Jenkins, J. S., Díaz, M. R., Kurtovic, N. T., et al. 2020, *Nature Astronomy*, 4, 1148, doi: [10.1038/s41550-020-1142-z](https://doi.org/10.1038/s41550-020-1142-z)
- Kaltenegger, L., Pepper, J., Stassun, K., & Oelkers, R. 2019, *ApJL*, 874, L8, doi: [10.3847/2041-8213/ab0e8d](https://doi.org/10.3847/2041-8213/ab0e8d)
- Katz, D., Sartoretti, P., Cropper, M., et al. 2019, *A&A*, 622, A205, doi: [10.1051/0004-6361/201833273](https://doi.org/10.1051/0004-6361/201833273)
- Kipping, D. M. 2013, *MNRAS*, 435, 2152, doi: [10.1093/mnras/stt1435](https://doi.org/10.1093/mnras/stt1435)
- Kiraga, M. 2012, *AcA*, 62, 67. <https://arxiv.org/abs/1204.3825>
- Kluyver, T., Ragan-Kelley, B., Pérez, F., et al. 2016, in *Positioning and Power in Academic Publishing: Players, Agents and Agendas*, ed. F. Loizides & B. Schmidt (IOS Press), 87–90. <https://eprints.soton.ac.uk/403913/>
- Kostov, V. B., Mullally, S. E., Quintana, E. V., et al. 2019, *AJ*, 157, 124, doi: [10.3847/1538-3881/ab0110](https://doi.org/10.3847/1538-3881/ab0110)
- Kostov, V. B., Kuchner, M. J., Cacciapuoti, L., et al. 2022, *PASP*, 134, 044401, doi: [10.1088/1538-3873/ac5de0](https://doi.org/10.1088/1538-3873/ac5de0)
- Kruse, E., Agol, E., Luger, R., & Foreman-Mackey, D. 2019, *ApJS*, 244, 11, doi: [10.3847/1538-4365/ab346b](https://doi.org/10.3847/1538-4365/ab346b)
- Kumar, R., Carroll, C., Hartikainen, A., & Martin, O. 2019, *Journal of Open Source Software*, 4, 1143, doi: [10.21105/joss.01143](https://doi.org/10.21105/joss.01143)
- Kunimoto, M., Winn, J., Ricker, G. R., & Vanderspek, R. K. 2022, *AJ*, 163, 290, doi: [10.3847/1538-3881/ac68e3](https://doi.org/10.3847/1538-3881/ac68e3)
- Lendl, M., Anderson, D. R., Bonfanti, A., et al. 2019, *MNRAS*, 482, 301, doi: [10.1093/mnras/sty2667](https://doi.org/10.1093/mnras/sty2667)
- Luger, R., Agol, E., Foreman-Mackey, D., et al. 2019, *AJ*, 157, 64, doi: [10.3847/1538-3881/aae8e5](https://doi.org/10.3847/1538-3881/aae8e5)
- Magliano, C., Covone, G., Dobal, R., et al. 2023, *MNRAS*, 519, 1562, doi: [10.1093/mnras/stac3404](https://doi.org/10.1093/mnras/stac3404)
- Mandel, K., & Agol, E. 2002, *ApJL*, 580, L171, doi: [10.1086/345520](https://doi.org/10.1086/345520)
- Mantovan, G., Montalto, M., Piotto, G., et al. 2022, *MNRAS*, 516, 4432, doi: [10.1093/mnras/stac2451](https://doi.org/10.1093/mnras/stac2451)
- Masci, F. J., Laher, R. R., Rusholme, B., et al. 2019, *PASP*, 131, 018003, doi: [10.1088/1538-3873/aae8ac](https://doi.org/10.1088/1538-3873/aae8ac)
- Mayo, A. W., Vanderburg, A., Latham, D. W., et al. 2018, *AJ*, 155, 136, doi: [10.3847/1538-3881/aaadff](https://doi.org/10.3847/1538-3881/aaadff)
- McCauliff, S. D., Jenkins, J. M., Catanzarite, J., et al. 2015, *ApJ*, 806, 6, doi: [10.1088/0004-637X/806/1/6](https://doi.org/10.1088/0004-637X/806/1/6)
- Melton, E. J., Feigelson, E. D., Montalto, M., et al. 2022a, Submitted to *Astronomical Journal*
- . 2022b, Submitted to *Astronomical Journal*
- Mireles, I., Shporer, A., Grievés, N., et al. 2020, *AJ*, 160, 133, doi: [10.3847/1538-3881/aba526](https://doi.org/10.3847/1538-3881/aba526)
- Montalto, M., Borsato, L., Granata, V., et al. 2020, *MNRAS*, 498, 1726, doi: [10.1093/mnras/staa2438](https://doi.org/10.1093/mnras/staa2438)
- Morton, T. D., Bryson, S. T., Coughlin, J. L., et al. 2016, *ApJ*, 822, 86, doi: [10.3847/0004-637X/822/2/86](https://doi.org/10.3847/0004-637X/822/2/86)
- Neveu-VanMalle, M., Queloz, D., Anderson, D. R., et al. 2014, *A&A*, 572, A49, doi: [10.1051/0004-6361/201424744](https://doi.org/10.1051/0004-6361/201424744)
- Ofman, L., Averbuch, A., Shlisselberg, A., et al. 2022, *NewA*, 91, 101693, doi: [10.1016/j.newast.2021.101693](https://doi.org/10.1016/j.newast.2021.101693)

- Olmschenk, G., Ishitani Silva, S., Rau, G., et al. 2021, *AJ*, 161, 273, doi: [10.3847/1538-3881/abf4c6](https://doi.org/10.3847/1538-3881/abf4c6)
- Palle, E., Chen, G., Prieto-Arranz, J., et al. 2017, *A&A*, 602, L15, doi: [10.1051/0004-6361/201731018](https://doi.org/10.1051/0004-6361/201731018)
- Prša, A., Batalha, N., Slawson, R. W., et al. 2011, *AJ*, 141, 83, doi: [10.1088/0004-6256/141/3/83](https://doi.org/10.1088/0004-6256/141/3/83)
- Prša, A., Kochoska, A., Conroy, K. E., et al. 2022, *ApJS*, 258, 16, doi: [10.3847/1538-4365/ac324a](https://doi.org/10.3847/1538-4365/ac324a)
- R Core Team. 2020, *R: A Language and Environment for Statistical Computing*, R Foundation for Statistical Computing, Vienna, Austria.  
<https://www.R-project.org/>
- Rao, S., Mahabal, A., Rao, N., & Raghavendra, C. 2021, *MNRAS*, 502, 2845, doi: [10.1093/mnras/stab203](https://doi.org/10.1093/mnras/stab203)
- Salvatier, J., Wiecki, T. V., & Fonnesbeck, C. 2016, *PeerJ Computer Science*, 2, e55
- Schanche, N., Collier Cameron, A., Almenara, J. M., et al. 2019, *MNRAS*, 488, 4905, doi: [10.1093/mnras/stz2064](https://doi.org/10.1093/mnras/stz2064)
- Shallue, C. J., & Vanderburg, A. 2018, *AJ*, 155, 94, doi: [10.3847/1538-3881/aa9e09](https://doi.org/10.3847/1538-3881/aa9e09)
- Skaf, N., Bieger, M. F., Edwards, B., et al. 2020, *AJ*, 160, 109, doi: [10.3847/1538-3881/ab94a3](https://doi.org/10.3847/1538-3881/ab94a3)
- Stassun, K. G., Oelkers, R. J., Paegert, M., et al. 2019, *AJ*, 158, 138, doi: [10.3847/1538-3881/ab3467](https://doi.org/10.3847/1538-3881/ab3467)
- Teske, J. K., Khanal, S., & Ramírez, I. 2016, *ApJ*, 819, 19, doi: [10.3847/0004-637X/819/1/19](https://doi.org/10.3847/0004-637X/819/1/19)
- The Theano Development Team, Al-Rfou, R., Alain, G., et al. 2016, arXiv e-prints, arXiv:1605.02688.  
<https://arxiv.org/abs/1605.02688>
- Thompson, S. E., Coughlin, J. L., Hoffman, K., et al. 2018, *ApJS*, 235, 38, doi: [10.3847/1538-4365/aab4f9](https://doi.org/10.3847/1538-4365/aab4f9)
- Triaud, A. H. M. J., Martin, D. V., Ségransan, D., et al. 2017, *A&A*, 608, A129, doi: [10.1051/0004-6361/201730993](https://doi.org/10.1051/0004-6361/201730993)
- Tu, Z.-L., Yang, M., Zhang, Z. J., & Wang, F. Y. 2020, *ApJ*, 890, 46, doi: [10.3847/1538-4357/ab6606](https://doi.org/10.3847/1538-4357/ab6606)
- van Altena, W. F., Lee, J. T., & Hoffleit, D. 1995, *VizieR Online Data Catalog*, I/174
- van der Walt, S., Colbert, S. C., & Varoquaux, G. 2011, *Computing in Science Engineering*, 13, 22, doi: [10.1109/MCSE.2011.37](https://doi.org/10.1109/MCSE.2011.37)
- von Boetticher, A., Triaud, A. H. M. J., Queloz, D., et al. 2019, *A&A*, 625, A150, doi: [10.1051/0004-6361/201834539](https://doi.org/10.1051/0004-6361/201834539)
- Yu, L., Vanderburg, A., Huang, C., et al. 2019, *AJ*, 158, 25, doi: [10.3847/1538-3881/ab21d6](https://doi.org/10.3847/1538-3881/ab21d6)
- Zink, J. K., Hardegree-Ullman, K. K., Christiansen, J. L., et al. 2021, *AJ*, 162, 259, doi: [10.3847/1538-3881/ac2309](https://doi.org/10.3847/1538-3881/ac2309)

## APPENDIX

## A. NOTES ON DTARPS CANDIDATES

Sources:

CTOI: Community TESS Objects of Interest

Montalto et al. (2020): DIAMante project

NEA/TOI: NASA Exoplanet Archive and TESS Objects of Interest (accessed February 2022)

SIMBAD: SIMBAD Astronomical Databased, CDS, Strasbourg FR

SPOC: TESS Science Processing Operations Center, NASA-Ames (Jon Jenkins, private communication, November 2022)

DTARPS 1 = TIC 17361 = TOI-3127 = CTOI 17361.01. Disposition 'Ambiguous Planetary Candidate' with period  $P = 3.6071013$ , transit depth 0.97% and planet radius  $13 R_{\oplus}$ . [NEA/TOI] Planetary candidate from DIAMante analysis (Montalto et al. 2020). [CTOI]

DTARPS 2 = TIC 1003831 = TOI-564. Spectroscopically 'Confirmed Planet' with period  $P = 1.6511$  d, mass  $M = 460 M_{\oplus}$  and radius  $R = 1.0 R_J$  orbiting a F6 IV-V star. [NEA/TOI]

DTARPS 3 = TIC 1449640 = TOI-446. Disposition 'Ambiguous Planetary Candidate' with period  $P = 3.5018023$ , transit depth 1.94% and planet radius  $13 R_{\oplus}$ . [NEA/TOI]

DTARPS 4 = TIC 1525480 = TOI-2402 = CTOI 1525480.01. Disposition 'Planetary Candidate' with period  $P = 5.5094951$ , transit depth 1.61% and planet radius  $22 R_{\oplus}$ . [NEA/TOI] DIAMante survey and CTIO entry (Montalto et al. 2020). [CTOI]

DTARPS 5 = TIC 1599403. ZTF 414209300031141 star  $6''$  from TIC star at  $r=16.0$  mag with multiple dips to 16.2. Possible blended contaminant.

DTARPS 9 = TIC 9033144 = TOI-367. Disposition 'False Positive' with period  $P = 4.71502$ , transit depth 0.47% and equivalent planet radius  $18 R_{\oplus}$ . [NEA/TOI]

DTARPS 10 = TIC 9725627 = TOI-239. Disposition 'Known Planet' with period  $P = 4.1567815$ , transit depth 0.47% and planet radius  $10 R_{\oplus}$ . [NEA/TOI]

DTARPS 11 = TIC 11356662 = CTOI 1356662.01. Planetary candidate from DIAMante analysis with period  $P = 3.24887$  d, transit depth 0.77 mmag and planet radius  $2.8 R_{\oplus}$  (Montalto et al. 2020). [NEA/CTOI] Very deep V-shaped transits, likely EB. [SPOC]

DTARPS 12 = TIC 11762560. ZTF 409204100025935 star  $6''$  from TIC star at  $r=15.9$  and  $g=17.0$  with 0.3 mag dips. Possible blended contaminant.

DTARPS 13 = TIC 13021029 = WASP 61 = TOI-439. Spectroscopically 'Confirmed Planet' with period  $P = 3.8559$  d, mass  $M = 654 M_{\oplus}$  and radius  $R = 1.24 R_J$ . [NEA/TOI]

DTARPS 14 = TIC 13349647 = WASP 36 = TOI-567. Spectroscopically 'Confirmed Planet' with period  $P = 1.5373653$  d, mass  $M = 730 M_{\oplus}$  and radius  $R = 1.3 R_J$ . [NEA/TOI]

DTARPS 15 = TIC 14091633 = TOI-447. Disposition 'Ambiguous Planetary Candidate' with period  $P = 55292743$ , transit depth 1.79% and planet radius  $23 R_{\oplus}$ . [NEA/TOI] Very deep V-shaped transits, likely EB. [SPOC]

DTARPS 16 = TIC 14091704 = TOI-445. Disposition 'Planetary Candidate' with period  $P = 0.7649571$ , transit depth 0.19% and planet radius  $13 R_{\oplus}$ . Planetary candidate with period  $P = 0.764880$  d, transit depth = 0.19% and width 1.5 h, triage probability 99.5% and vetting probability 49% from deep learning analysis (Yu et al. 2019).[NEA/TOI]

DTARPS 18 = TIC 16490297 = 1SWASP J074724.19+122830.3. Double-line spectroscopic eclipsing binary with period  $P = 2.751483$  d, transit depth 2.3% and width 3% (Schanche et al. 2019). False Positive in the SuperWASP and DIAMante surveys (Montalto et al. 2020). [SIMBAD]

DTARPS 21 = TIC 20178111 = TOI-467. Disposition 'False Positive' with period  $P = 1.734422$ , transit depth 0.12% and planet radius  $4 R_{\oplus}$ . [NEA/TOI] Planetary candidate with period  $P = 1.734102$  d, transit depth = 0.23% and width 2.2 h, triage probability 99.4% and vetting probability 41% from deep learning analysis (Yu et al. 2019).

DTARPS 22 = TIC 20320305 = CD-25 8473. Bright K3 V star at distance  $d = 52$  pc. [SIMBAD] Blended eclipsing binary  $20''$  offset from target. [SPOC]

DTARPS 27 = TIC 22221375 = HD 86226 = TOI-652. Spectroscopically 'Confirmed Planet' HD 86226 c with period  $P = 3.98442$  d, mass  $M = 7.25 M_{\oplus}$  and radius  $R = 0.193 R_J$  orbiting a G1 V star. HD 86226 b has period  $P = 1695$  d.. [NEA/TOI]

DTARPS 28 = TIC 22529346 = WASP-121 = TOI-495. Spectroscopically 'Confirmed Planet' with period  $P = 1.2749255$  d, mass  $M = 375 M_{\oplus}$  and radius  $R = 1.865 R_J$  orbiting a F6 V star. [NEA/TOI]

DTARPS 30 = TIC 22767596. Transit depth differs in two TESS sectors.

DTARPS 32 = TIC 24695044 = TOI-2195 = CTOI 24695044.01. Disposition 'Planetary Candidate' with period  $P = 4.165693$  d, transit depth 0.77% and planet radius  $9 R_{\oplus}$ . [NEA/TOI] Planetary candidate from DIAMante analysis (Montalto et al. 2020). [CTOI]

DTARPS 33 = TIC 25155310 = WASP-126 = TOI-114. Spectroscopically 'Confirmed Planet' with period  $P = 3.2888$  d, mass  $M = 89 M_{\oplus}$  and radius  $R = 0.96 R_J$  orbiting a G2 star. WASP-126 c has period  $P = 7.63$  d. [NEA/TOI] Planetary candidate with period  $P = 3.288961$  d, transit depth = 0.70% and width 3.7 h, triage probability 99.6% and vetting probability 89% from deep learning analysis (Yu et al. 2019).

DTARPS 34 = TIC 26264354 = CTOI 26264354.01. Planetary candidate from DIAMante analysis with period  $P = 3.24887$  d, transit depth 0.77 mmag and planet radius  $2.8 R_{\oplus}$  (Montalto et al. 2020). [CTOI]

DTARPS 35 = TIC 29430403 = CTOI 29430403.01. Planetary candidate from DIAMante analysis with period  $P = 1.87756$  d, transit depth 16.2 mmag and planet radius  $13 R_{\oplus}$  (Montalto et al. 2020). [CTOI]

DTARPS 37 = TIC 31142436 = CTOI 31142436.01 Planetary candidate from DIAMante analysis with period  $P = 5.2714$  d, transit depth 1.4 mmag and planet radius  $3.0 R_{\oplus}$  (Montalto et al. 2020). [CTOI] Planetary candidate with period  $P = 5.271984$  d, transit depth = 0.11% and width 4.1 h, triage probability 45% and vetting probability 25% from deep learning analysis (Yu et al. 2019).

DTARPS 38 = TIC 32925763 = TOI-2352 = CTOI 32925763.01. Disposition 'Planetary Candidate' with period  $P = 10.7846$  d, transit depth 1.7 mmag and planet radius  $8 R_{\oplus}$ . [NEA/TOI] Planetary candidate from DIAMante analysis (Montalto et al. 2020). [CTOI]

DTARPS 39 = TIC 32949757 = WASP-160A. The planet is a transiting hot Saturn with period  $P = 3.7684952$  d, mass  $M_p = 0.3 M_J$  and radius  $R_p = 1.1 R_J$  orbiting component K0 V WASP-160B of a near equal-mass visual binary with separation  $29''$  (Lendl et al. 2019). Planetary candidate with period  $P = 3.767558$  d, transit depth = 1.1% and width 2.9 h, triage probability 94% and vetting probability 85% from deep learning analysis (Yu et al. 2019). [SIMBAD]

DTARPS 40 = TIC 33692729 = TOI-469. Disposition 'Planetary Candidate' with period  $P = 13.6308024$  d, transit depth 0.12% and planet radius  $3.5 R_{\oplus}$ . [NEA/TOI]

DTARPS 41 = TIC 34196883 = UCAC4 380-013011. Planetary candidate with period  $P = 1.617181$  d, transit depth = 0.8% and width 3.5 h, triage probability 99% and vetting probability 36% from deep learning analysis (Yu et al. 2019). [SIMBAD]

DTARPS 42 = TIC 35703676. Possible dilution of transit depth by ZTF 399310100000336 with  $i=15.0$  lying  $8''$  from the DTARPS candidate.

DTARPS 43 = TIC 35857242 = WASP-138 = TOI-400. Spectroscopically 'Confirmed Planet' with period  $P = 3.634433$  d, mass  $M = 388 M_{\oplus}$  and radius  $R = 1.09 R_J$ . [NEA/TOI]

DTARPS 46 = TIC 36734222 = WASP-43 = TOI-656. Spectroscopically 'Confirmed Planet' with period  $P = 0.81347437$  d, mass  $M = 651 M_{\oplus}$  and radius  $R = 1.036 R_J$  orbiting a K7 V star. [NEA/TOI]

DTARPS 47 = TIC 37718056 = WASP-158 = TOI-1908. Spectroscopically 'Confirmed Planet' with period  $P = 3.656333$  d, mass  $M = 886 M_{\oplus}$  and radius  $R = 1.07 R_J$  orbiting a F6 V star. [NEA/TOI]

DTARPS 48 = TIC 38129218 = CTOI 38129218.01. Planetary candidate from DIAMante analysis with period  $P = 2.40172$  d, transit depth 3.2 mmag and planet radius  $10 R_{\oplus}$  (Montalto et al. 2020). [CTOI]

DTARPS 49 = TIC 38696105 = TOI-281. Disposition 'Planetary Candidate' with period  $P = 5.5764964$  d, transit depth 0.07% and planet radius  $4 R_{\oplus}$ . [NEA/TOI] Planetary candidate with period  $P = 5.577113$  d, transit depth = 0.06% and width 2.4 h, triage probability 72% and vetting probability 69% from deep learning analysis (Yu et al. 2019).

DTARPS 52 = TIC 39018923 = TOI-2216. Disposition 'Planetary Candidate' with period  $P = 5.68083$  d, transit depth 0.21% and planet radius  $6 R_{\oplus}$ . [NEA/TOI]

DTARPS 53 = TIC 39414571 = TOI-2364 = CTOI 39414571.01 . Disposition 'Planetary Candidate' with period  $P = 4.0197444$  d, transit depth 0.97% and planet radius  $10 R_{\oplus}$ . [NEA/TOI] Planetary candidate from DIAMante analysis (Montalto et al. 2020). [CTOI]

DTARPS 54 = TIC 40083958 = TOI-851. Disposition 'Planetary Candidate' with period  $P = 1.7018884$  d.

DTARPS 55 = TIC 41995709 = TOI-4192. Disposition 'Planetary Candidate' with period  $P = 4.2300182$  d, transit depth 0.35% and planet radius  $17 R_{\oplus}$ . [NEA/TOI]

DTARPS 56 = TIC 43647325 = WASP-35 = TOI-423. Spectroscopically 'Confirmed Planet' with period  $P = 3.161575$  d, mass  $M = 228 M_{\oplus}$  and radius  $R = 1.32 R_J$ . [NEA/TOI] ZTF 407204300018522 variable star  $12''$  from the TIC star at  $r=16.4-16.5$  with flares to 16.2. Possible dilution of transit depth by ZTF 355114200027081 with  $g=15.8$  lying  $4''$  from the DTARPS candidate.

DTARPS 57 = TIC 44737596 = HATS-75 = TOI-552. Spectroscopically 'Confirmed Planet' with period  $P = 2.7886556$  d, mass  $M = 156 M_{\oplus}$  and radius  $R = 0.88 R_J$ . [NEA/TOI]

DTARPS 58 = TIC 46096489 = WASP-16 = TOI-818. Disposition 'Known Planet' with period  $P = 3.118536$  d, transit depth 1.22% and planet radius  $12 R_{\oplus}$ . [NEA/TOI] Spectroscopically 'Confirmed Planet' with period  $P = 3.1186068$  d, mass  $M = 288 M_{\oplus}$  and radius  $R = 1.22 R_J$ . [NEA/TOI]

DTARPS 61 = TIC 49079670 = TOI-641. Disposition 'Planetary Candidate' with period  $P = 1.8934942$  d, transit depth 0.08% and planet radius  $3.2 R_{\oplus}$ . [NEA/TOI] Planetary candidate with period  $P = 1.891807$  d, transit depth = 0.08% and width 1.4 h, triage probability 89% and vetting probability 81% from deep learning analysis (Yu et al. 2019).

DTARPS 62 = TIC 50309953 = TOI-1109 = CTOI 50309953.01. Disposition 'False Positive' with period  $P = 7.04083$  d, transit depth 0.16% and equivalent planet radius  $8 R_{\oplus}$ . [NEA/TOI] Planet candidate with period 7.04 d, transit depth 1.1 mmag and planet radius  $5 R_{\oplus}$  (Lipponen). [CTOI]

DTARPS 63 = TIC 50528326. Possible dilution of transit depth by ZTF 1401216300006538 with  $r=13.1$  lying  $10''$  from the DTARPS candidate.

DTARPS 64 = TIC 52216463 = HD 102197. Spectral type F8 V. [SIMBAD]

DTARPS 65 = TIC 52369802. Possible dilution of transit depth by ZTF 1557204200008320 with  $r=16.0$  lying  $12''$  and by ZTF 1557204200008312 with  $r=15.6$  lying  $14''$  from the DTARPS candidate.

DTARPS 66 = TIC 52449797 = CTOI 52449797.01. Planetary candidate from DIAMante analysis with period  $P = 2.44958$  d, transit depth 0.9 mmag and planet radius  $2.8 R_{\oplus}$  (Montalto et al. 2020) [CTOI] TCF periodogram shows additional peaks suggesting possible multiplanet system.

DTARPS 69 = TIC 53189332 = WASP'106 = TOI-660. Spectroscopically 'Confirmed Planet' with period  $P = 9.28971$  d, mass  $M = 541 M_{\oplus}$  and radius  $R = 1.02 R_J$  orbiting an F9 star. [NEA/TOI]

DTARPS 71 = TIC 53750200 = HATS-41 = TOI-1914. Spectroscopically 'Confirmed Planet' with period  $P = 4.193649$  d, mass  $M = 3082 M_{\oplus}$  and radius  $R = 1.33 R_J$ . [NEA/TOI]

DTARPS 72= TIC 54064834 = UCAC4 312-015385. Planetary candidate with period  $P = 6.057196$  d, transit depth = 0.3% and width 2.5 h, triage probability 92% and vetting probability 77% from deep learning analysis (Yu et al. 2019). [SIMBAD]

DTARPS 74 = TIC 55999432 = BD -07°859 = ASAS J043811-0726.3 = 1RXS J043811.1-072621. Photometric variable due to rotationally modulated starspots with amplitude 0.1 mag with  $T = 2.1$  d rotational period (Kiraga 2012). X-ray source in the ROSAT Bright Survey. The star appears in a study on super-flares (SIMBAD not yet ingested) (Tu et al. 2020). [SIMBAD]

DTARPS 75 = TIC 59280552. Possible dilution of transit depth by ZTF 511209400013617 with  $r=14.8$  lying  $11''$  from the DTARPS candidate.

DTARPS 77 = TIC 61117473 = TOI-3122. Disposition 'Planetary Candidate' with period  $P = 6.182444$  d, transit depth 1.04% and planet radius  $14 R_{\oplus}$ . [NEA/TOI]

DTARPS 79 = TIC 61404104 = TYC 5950-1237-1. Planetary candidate with period  $P = 4.116773$  d, transit depth = 0.13% and width 3.6 h, triage probability 98% and vetting probability 73% from deep learning analysis (Yu et al. 2019). [SIMBAD]

DTARPS 81 = TIC 61980227 = TOI-2316. Disposition 'Ambiguous Planetary Candidate' with period  $P = 3.0958985$  d, transit depth 1.04% and planet radius  $19 R_{\oplus}$ . [NEA/TOI]

DTARPS 84 = TIC 64070344 = CTOI 64070344.01. Planetary candidate from DIAMante analysis with period  $P = 2.73716$  d, transit depth 8.3 mmag and planet radius  $14 R_{\oplus}$  (Montalto et al. 2020). [CTOI]

DTARPS 85 = TIC 64071894 = TOI-458. Disposition 'Planetary Candidate' with period  $P = 17.5288347$  d, transit depth 0.11% and planet radius  $2.9 R_{\oplus}$ . [NEA/TOI]

DTARPS 88 = TIC 67196573 = TOI-2499 = CTOI 67196573.01. Disposition 'Planetary Candidate' with period  $P = 2.5574812$  d, transit depth 0.19% and planet radius  $18 R_{\oplus}$ . [NEA/TOI] Planetary candidate with period  $P = 2.556024$  d, transit depth = 0.33% and width 1.1 h, triage probability 69% and vetting probability 73% from deep learning analysis (Yu et al. 2019).

DTARPS 89 = TIC 68007716 = TOI-2587. Disposition 'Planetary Candidate' with period  $P = 5.4566563$  d, transit depth 0.42% and planet radius  $11 R_{\oplus}$ . [NEA/TOI] Possible dilution of transit depth by ZTF 412210100031240 with  $r=13.6$  lying  $9''$  from the DTARPS candidate.

DTARPS 90 = TIC 70914192 = TOI-427. Disposition 'Ambiguous Planetary Candidate' with period  $P = 0.6090253$  d, transit depth 0.42% and planet radius  $11 R_{\oplus}$ . [NEA/TOI]

DTARPS 93 = TIC 72985822 = TOI-754. Disposition 'Planetary Candidate' with period  $P = 3.8642753$  d, transit depth 0.73% and planet radius  $14 R_{\oplus}$ . [NEA/TOI]

DTARPS 94 = TIC 73038411 = TOI-978. Disposition 'Planetary Candidate' with period  $P = 13.1659202$  d, transit depth 0.51% and planet radius  $11 R_{\oplus}$ . [NEA/TOI] Planetary candidate with period  $P = 15.854$  d and planet radius  $12 R_{\oplus}$  found in warm Jupiter survey (Dong et al. 2021). [SIMBAD]

DTARPS 102 = TIC 88571421 = TYC 6439-1132-1 = EBLM J0315-24. Single-line spectroscopic binary, eclipsing binary with low mass companion with orbital period  $P = 3.190524$  d with 5% eccentricity (Triaud et al. 2017). The F5 primary has mass  $M = 1.3 M_{\odot}$  and radius  $R = 1.3 R_{\odot}$ . The secondary has mass  $M = 0.24 M_{\odot}$ . [SIMBAD]

DTARPS 103 = TIC 89020549 = TOI-132. Spectroscopically 'Confirmed Planet' with period  $P = 2.1097019$  d, mass  $M = 22 M_{\oplus}$  and radius  $R = 0.305 R_J$  orbiting a G8 V star.. [NEA/TOI]

DTARPS 104 = TIC 92350408 = CTOI 92350408.01. Planetary candidate from DIAMante analysis with period  $P = 2.95639$  d, transit depth 13.2 mmag and planet radius  $24 R_{\oplus}$  (Montalto et al. 2020). [CTOI] Likely False Positive due to large radius. [SPOC]

DTARPS 105 = TIC 92352621 = CD -34°14724B = WASP-94B. Spectroscopically confirmed hot Jupiters orbiting each component of a wide binary system with separation  $15''$  (Neveu-VanMalle et al. 2014). The planet around F8 star WASP-94A has a retrograde orbit with period  $P=3.95019$  d, mass  $M=0.45 M_J$  and radius  $R = 1.7 R_J$ . The planet around F9 star WASP-94B has period  $P = 2.00839$  d, mass  $M = 196 M_{\oplus}$ . The host stars have slightly different metallicities (Teske et al. 2016). [SIMBAD]

DTARPS 106 = TIC 92359850 = TOI-387. Disposition 'False Positive' with period  $P = 4.155$  d. [NEA/TOI]

DTARPS 107 = TIC 92880568 = TOI-958. Disposition 'Ambiguous Planetary Candidate' with period  $P = 0.5875044$  d, transit depth 0.17% and planet radius  $14 R_{\oplus}$ . [NEA/TOI] Planetary candidate with period  $P = 0.588447$  d, transit depth = 0.35% and width 1.4 h, triage probability 99.3% and vetting probability 14% from deep learning analysis (Yu et al. 2019).

DTARPS 111 = TIC 97409519 = WASP-124 = TOI-113. Spectroscopically 'Confirmed Planet' with period  $P = 3.37265$  d, mass  $M = 190 M_{\oplus}$  and radius  $R = 1.24 R_J$  orbiting a F9 star. [NEA/TOI]

DTARPS 112 = TIC 97479438. Possible dilution of transit depth by ZTF 562202100006601 with  $r=15.6$  lying  $10''$  from the DTARPS candidate.

DTARPS 113 = TIC 97861072. Possible dilution of transit depth by ZTF 1557205400032288 with  $r=15.5$  lying  $8''$  from the DTARPS candidate.

DTARPS 115 = TIC 98494121 = TOI-2240. Disposition 'False Positive' with period  $P = 3.06555$  d, transit depth 0.29% and equivalent planet radius  $5 R_{\oplus}$ . [NEA/TOI]

DTARPS 116 = TIC 100100827 = WASP-18 = TOI-185. Spectroscopically 'Confirmed Planet' WASP-18b has period  $P = 0.941452$  d with mass  $M = 3300 M_{\oplus}$  and radius  $R = 1.1 R_J$ . A second planet WASP-18c has period  $P = 2.1558$  d. [NEA/TOI] Transit depth differs in two TESS sectors.

DTARPS 117 = TIC 100589632 = TOI-2342 = CTOI 100589632.01. Disposition 'False Positive' with period  $P = 3.9471567$  d, transit depth 0.19% and equivalent planet radius  $4 R_{\oplus}$ . [NEA/TOI] Planetary candidate from DIAMante analysis (Montalto et al. 2020). [CTOI] Planetary candidate with period  $P = 3.946770$  d, transit depth = 0.18% and width 1.8 h, triage probability 80% and vetting probability 69% from deep learning analysis (Yu et al. 2019).

DTARPS 118 = TIC 101395259 = TOI-623. Disposition 'False Positive' with period  $P = 15.51486$  d, transit depth 0.62% and equivalent planet radius  $13 R_{\oplus}$ . [NEA/TOI]

DTARPS 121 = TIC 102192004 = WASP-174 = TOI-1919. Spectroscopically 'Confirmed Planet' with period  $P = 4.2337$  d, mass  $M = 413 M_{\oplus}$  and radius  $R = 1.3 R_J$  orbiting an F6 star. [NEA/TOI]

DTARPS 126 = TIC 114749636 = WASP-147 = TOI-306. Spectroscopically 'Confirmed Planet' with period  $P = 4.60273$  d, mass  $M = 87 M_{\oplus}$  and radius  $R = 1.1 R_J$  orbiting a G4 star. [NEA/TOI]

DTARPS 128 = TIC 115693377 = TYC 7528-481-1 = EBLM J0027-41. Single-line spectroscopic binary, eclipsing binary with low mass companion with orbital period  $P = 4.9279889$  d with 2% eccentricity (Triaud et al. 2017). The F8 primary has mass  $M = 1.2 M_{\odot}$  and radius  $R = 1.2 R_{\odot}$ . The secondary has mass  $M = 0.53 M_{\odot}$ . False Positive in the KELT survey (Collins et al. 2018). [SIMBAD]

DTARPS 129 = TIC 116156517 = WASP-190 = TOI-338. Spectroscopically 'Confirmed Planet' with period  $P = 5.367753$  d, mass  $M = 318 M_{\oplus}$  and radius  $R = 1.15 R_J$  orbiting an F6 IV-V star. [NEA/TOI]

DTARPS 130 = TIC 117772549 = CTOI 117772549.01. Planetary candidate from DIAMante analysis with period  $P = 7.87854$  d, transit depth 0.5 mmag and planet radius  $5 R_{\oplus}$  (Montalto et al. 2020). [CTOI]

DTARPS 132 = TIC 118956453 = WASP-170 = TOI-1925. Spectroscopically 'Confirmed Planet' with period  $P = 2.34478022$  d, mass  $M = 508 M_{\oplus}$  and radius  $R = 1.096 R_J$  orbiting an F6 IV-V star. [NEA/TOI]

DTARPS 133 = TIC 119292328 = TOI-512. Disposition 'Planetary Candidate' with two planets. TOI-512.01 has period  $P = 7.1887332$  d, transit depth 0.03% and planet radius  $1.5 R_{\oplus}$ . [NEA/TOI] TOI 512.02 has period  $P = 20.2749388$  m, transit depth 0.04% and planet radius  $1.7 R_{\oplus}$ . [NEA/TOI]

DTARPS 135 = TIC 120247528 = TOI-1071. Disposition 'Known Planet' with period  $P = 3.553814$  d, transit depth 1.00% and planet radius  $12 R_{\oplus}$ . [NEA/TOI]

DTARPS 136 = TIC 120610833 = WASP-45 = TOI-229. Spectroscopically 'Confirmed Planet' with period  $P = 3.12609$  d, mass  $M = 320 M_{\oplus}$  and radius  $R = 1.15 R_J$  orbiting an F6 IV-V star. [NEA/TOI]

DTARPS 137 = TIC 122870280. Possible dilution of transit depth by ZTF 1457201200003550 with  $r=13.1$  lying  $10''$  from the DTARPS candidate.

DTARPS 140 = TIC 124206468 = TOI-2357 = CTOI 124206468.01. Disposition 'Planetary Candidate' with period  $P = 7.0955$  d, transit depth 0.54% and planet radius  $12 R_{\oplus}$ . [NEA/TOI] Planetary candidate from DIAMante analysis (Montalto et al. 2020). [CTOI]

DTARPS 142 = TIC 128790976 = TOI-1124. Disposition 'Ambiguous Planetary Candidate' with period  $P = 3.51874$  d, transit depth 0.58% and planet radius  $21 R_{\oplus}$ . [NEA/TOI]

DTARPS 143 = TIC 134537478 = KELT-14 = TOI-501. Disposition 'Known Planet' with period  $P = 1.7100535$  d, transit depth 1.27% and planet radius  $17 R_{\oplus}$ . [NEA/TOI] Spectroscopically 'Confirmed Planet' with period  $P = 1.7100567$  d, mass  $M = 400 M_{\oplus}$  and radius  $R = 1.7 R_J$  orbiting a G4 star. [NEA/TOI]

DTARPS 145 = TIC 135050395 = CTOI 135050395.01. Planetary candidate from DIAMante analysis with period  $P = 6.76012$  d, transit depth 23.1 mmag and planet radius  $13 R_{\oplus}$  (Montalto et al. 2020). [CTOI]

DTARPS 146 = TIC 135145585 = CTOI 135145585.01. Planetary candidate from DIAMante analysis with period  $P = 1.51001$  d, transit depth 4.5 mmag and planet radius  $8 R_{\oplus}$  (Montalto et al. 2020). [CTOI]

DTARPS 148 = TIC 135243705 = CTOI 135243705.01. Planetary candidate from DIAMante analysis with period  $P = 2.65883$  d, transit depth 9.5 mmag and planet radius  $12 R_{\oplus}$  (Montalto et al. 2020). [CTOI] Blended eclipsing binary in nearby 14 mag star. [SPOC]

DTARPS 149 = TIC 138727432 = TOI-853. Disposition 'Planetary Candidate' with period  $P = 6.8646554$  d, transit depth 0.51% and planet radius  $17 R_{\oplus}$ . [NEA/TOI]

DTARPS 150 = TIC 139285832 = TOI-332. Disposition 'Planetary Candidate' with period  $P = 0.77685$  d, transit depth 0.08% and planet radius  $3.2 R_{\oplus}$ . [NEA/TOI]

DTARPS 151 = TIC 139733308 = HATS-5 = TOI-452. Spectroscopically 'Confirmed Planet' with period  $P = 4.763387$  d, mass  $M = 75 M_{\oplus}$  and radius  $R = 0.912 R_J$  orbiting a G star. [NEA/TOI]

DTARPS 154 = TIC 140691463 = TOI-157. Spectroscopically 'Confirmed Planet' with period  $P = 2.0845435$  d, mass  $M = 375 M_{\oplus}$  and radius  $R = 1.286 R_J$  orbiting a G9 IV star. [NEA/TOI] TCF preferred period is  $P = 2.08450$  d. Planetary candidate with period  $P = 2.084444$  d, transit depth = 1.29% and width 2.3 h, triage probability 99.2% and vetting probability 60% from deep learning analysis (Yu et al. 2019).

DTARPS 155 = TIC 142305141 = CTOI 142305141.01. Planetary candidate from DIAMante analysis with period  $P = 1.96047$  d, transit depth 51.0 mmag and planet radius  $14 R_{\oplus}$  (Montalto et al. 2020). [CTOI]

DTARPS 156 = TIC 142378043 = TOI-1997. Disposition 'Planetary Candidate' with period  $P = 1.8363262$  d, transit depth 0.08% and planet radius  $5 R_{\oplus}$ . [NEA/TOI]

DTARPS 159 = TIC 143257768 = CTOI 143257768.01. Planetary candidate from DIAMante analysis with Period 1.66241 d, transit depth 12.8 mmag and planet radius 18  $R_{\oplus}$  (Montalto et al. 2020). [CTOI]

DTARPS 162 = TIC 144164538 = CTOI 144164538.01. Planetary candidate from DIAMante analysis with period  $P = 3.12849$  d, transit depth 3.1 mmag and planet radius 1  $R_{\oplus}$  (Montalto et al. 2020). [CTOI]

DTARPS 163 = TIC 144426921 = TYC 7779-146-1. Double-lined spectroscopic binary with period  $P = 3.105131$  d and transit depth = 22 mmag in the KELT False Positive catalog (Collins et al. 2018). False Positives in DIAMante survey Montalto et al. (2020). [SIMBAD]

DTARPS 164 = TIC 144700903 = TOI-532. Spectroscopically 'Confirmed Planet' with period  $P = 2.3266508$  d, mass  $M = 62 M_{\oplus}$  and radius  $R = 0.519 R_J$ . [NEA/TOI]

DTARPS 166 = TIC 145750719 = HATS-60 = TOI-303. Spectroscopically 'Confirmed Planet' with period  $P = 10.695264$  d, mass  $M = 13.8 M_{\oplus}$  and radius  $R = 0.27 R_J$ . [NEA/TOI]

DTARPS 168 = TOI 146467675 = TOI-955. Disposition 'False Positive' with period  $P = 1.63715$  d, transit depth 0.08% and equivalent planet radius 5  $R_{\oplus}$ . [NEA/TOI]

DTARPS 169 = TIC 147115277 = HD 204019 [SIMBAD]

DTARPS 170 = TIC 147203645 = TOI-166. Disposition 'Planetary Candidate' with period  $P = 5.0613599$  d, transit depth 0.54% and planet radius 10  $R_{\oplus}$ . [NEA/TOI]

DTARPS 171 = TIC 150098860 = TOI-220. Spectroscopically 'Confirmed Planet' with period  $P = 3.12609$  d, mass  $M = 320 M_{\oplus}$  and radius  $R = 1.15 R_J$  orbiting an F6 IV-V star. [NEA/TOI] Planetary candidate with period  $P = 10.692789$  d, transit depth = 0.06% and width 2.5 h, triage probability 88% and vetting probability 80% from deep learning analysis (Yu et al. 2019).

DTARPS 172 = TIC 150430484 = TOI-859. Disposition 'Planetary Candidate' with period  $P = 51543182$  d, transit depth 0.24% and planet radius 10  $R_{\oplus}$ . [NEA/TOI]

DTARPS 173 = TIC 150437346 = TOI-2220. Disposition 'Planetary Candidate' with period  $P = 1.3926509$  d, transit depth 0.72% and planet radius 17  $R_{\oplus}$ . [NEA/TOI] Planetary candidate with period  $P = 1.392659$  d, transit depth = 0.71% and width 2.1 h, triage probability 99.3% and vetting probability 38% from deep learning analysis (Yu et al. 2019).

DTARPS 174 = TIC 152147232 = TOI-759. Disposition 'Ambiguous Planetary Candidate' with period  $P = 4.213316$  d, transit depth 0.72% and planet radius 13  $R_{\oplus}$ . [NEA/TOI]

DTARPS 175 = TIC 152226055 = CTOI 152226055.01. Planetary candidate from DIAMante analysis with period  $P = 1.43115$  d, transit depth 3.5 mmag and planet radius 5  $R_{\oplus}$  (Montalto et al. 2020). [CTOI] Blended eclipsing binary in 13 mag star 18'' from target. [SPOC]

DTARPS 179 = TIC 156075294 = TOI-299. Disposition 'Planetary Candidate' with period  $P = 57216199$  d, transit depth 0.54% and planet radius 9  $R_{\oplus}$ . [NEA/TOI]

DTARPS 181 = TIC 156947629 = CTOI 156947629.01. Planetary candidate from DIAMante analysis with period  $P = 5.25347$  d, transit depth 2.1 mmag and planet radius 6  $R_{\oplus}$  (Montalto et al. 2020). [CTOI]

DTARPS 183 = TIC 157230659 = NGTS-12. Spectroscopically 'Confirmed Planet' with period  $P = 7.532806$  d, mass  $M = 66 M_{\oplus}$  and radius  $R = 1.048 R_J$  orbiting a G star. [NEA/TOI]

DTARPS 184 = TIC 159951311 = WASP-139 = TOI-265. Spectroscopically 'Confirmed Planet' with period  $P = 5.924262$  d, mass  $M = 37 M_{\oplus}$  and radius  $R = 0.8 R_J$  orbiting a K0 star. [NEA/TOI]

DTARPS 185 = TIC 160148385 = WASP-96 = TOI-247. Spectroscopically 'Confirmed Planet' with period  $P = 3.4252602$  d, mass  $M = 155 M_{\oplus}$  and radius  $R = 1.2 R_J$  orbiting a G8 star. [NEA/TOI]

DTARPS 190 = TIC 166836920 = WASP-99 = TOI-267. Confirmed planet with period  $P = 5.75251$  d, mass  $M = 883 M_{\oplus}$  and radius  $R = 1.1 R_J$  orbiting a F8 star. [NEA/TOI]

DTARPS 191 = TIC 167792080 = CTOI 167792080.01. Planetary candidate with period  $P = 3.253503$  d, transit depth 6.0 mmag and radius 15  $R_{\oplus}$  vetted with DAVE (Galgano) [CTOI] Eclipsing binary in 15 mag star 32'' from target. [SPOC]

DTARPS 192 = TIC 168281028 = HATS-38 = CTOI 168281028.01. Confirmed planet with period  $P = 4.375021$  d, mass  $M = 23 M_{\oplus}$  and radius  $R = 0.6 R_J$ . [NEA/TOI] Planetary candidate from DIAMante analysis with period  $P = 4.37416$  d, transit depth 3.5 mmag and planet radius 6  $R_{\oplus}$  (Montalto et al. 2020). [CTOI]

DTARPS 193 = TIC 170102285 = WASP-23 = TOI-477. Confirmed planet with period  $P = 2.94443$  d, mass  $M = 279 M_{\oplus}$  and radius  $R = 0.96 R_J$ . [NEA/TOI] Planetary candidate with period  $P = 2.941959$  d, transit depth

= 2.03% and width 2.6 h, triage probability 98% and vetting probability 84% from deep learning analysis (Yu et al. 2019).

DTARPS 194 = TIC 172193428 = TOI-502. Disposition 'Planetary Candidate' with period  $P = 2.9412694$  d, transit depth 0.24% and planet radius  $9 R_{\oplus}$ . [NEA/TOI] Planetary candidate with period  $P = 2.939634$  d, transit depth = 0.19% and width 1.2 h, triage probability 89% and vetting probability 80% from deep learning analysis (Yu et al. 2019).

DTARPS 195 = TIC 172409594 = TYC 6512-2125-1. Planetary candidate with period  $P = 0.341709$  d, transit depth = 0.23% and width 1.3 h, triage probability 92% and vetting probability 18% from deep learning analysis (Yu et al. 2019). [SIMBAD]

DTARPS 196 = TIC 173640199 = TOI-618. Disposition 'Planetary Candidate' with period  $P = 4.4352884$  d, transit depth 0.28% and planet radius  $8 R_{\oplus}$ . [NEA/TOI]

DTARPS 197 = TIC 176685457 = NGTS-9 = TOI-1935. Confirmed planet with period  $P = 4.43527$  d, mass  $M = 921 M_{\oplus}$  and radius  $R = 1.07 R_J$  orbiting a F8 star. [NEA/TOI]

DTARPS 199 = TIC 177079323 = TOI-2353 = CTOI 177079323.01. Disposition 'Planetary Candidate' with period  $P = 5.7518756$  d, transit depth 0.08% and planet radius  $6 R_{\oplus}$ . [NEA/TOI] Planetary candidate from DIAMante analysis (Montalto et al. 2020). [CTOI]

DTARPS 200 = TIC 177162886 = TOI-899. Disposition 'Planetary Candidate' with period  $P = 12.8461782$  d, transit depth 0.89% and planet radius  $12 R_{\oplus}$ . [NEA/TOI]

DTARPS 202 = TIC 177350401 = CTOI 177350401.01. DIAMante planet candidate with period  $P = 12.07461$  d, transit depth 4.3 mmag, planet radius  $9 R_{\oplus}$  (Montalto et al. 2020). [CTOI] Blended eclipsing binary in 14 map star  $16''$  from target. [SPOC]

DTARPS 205 = TIC 179033846 = TOI-2675 = CTOI 179033846.01. Disposition 'Planetary Candidate' with period  $P = 1.476869$  d, transit depth 0.27% and planet radius  $13 R_{\oplus}$ . [NEA/TOI] Planetary candidate from DIAMante analysis (Montalto et al. 2020). [CTOI]

DTARPS 206 = TIC 180145006 = TOI-312. Disposition 'Ambiguous Planetary Candidate' with period  $P = 3.5413787$  d, transit depth 0.48% and planet radius  $10 R_{\oplus}$ . [NEA/TOI]

DTARPS 207 = TIC 180991313 = TOI-2330 = CTOI 180991313.01. Disposition 'Known Planet' with period  $P = 2.2088214$  d, transit depth 0.78% and planet radius  $12 R_{\oplus}$ . [NEA/TOI] Planetary candidate from DIAMante analysis (Montalto et al. 2020). [CTOI]

DTARPS 208 = TIC 183120439 = TOI-169. Confirmed planet with period  $P = 2.2554477$  d, mass  $M = 251 M_{\oplus}$  and radius  $R = 1.086 R_J$  orbiting a G1 V star. [NEA/TOI]

DTARPS 209 = TIC 183537452 = WASP-29 = TOI-192. Spectroscopically 'Confirmed Planet' with period  $P = 3.92273$  d, mass  $M = 73 M_{\oplus}$  and radius  $R = 0.77 R_J$ . [NEA/TOI]

DTARPS 210 = TIC 184240683 = WASP-5 = TOI-250. Spectroscopically 'Confirmed Planet' with period  $P = 1.68243142$  d, mass  $M = 498 M_{\oplus}$  and radius  $R = 1.167 R_J$ . [NEA/TOI]

DTARPS 211 = TIC 186936449 = TOI-2665 = CTOI 186936449.01. Disposition 'Planetary Candidate' with period  $P = 2.8456575$  d, transit depth 0.23% and planet radius  $7 R_{\oplus}$ . [NEA/TOI] Planetary Candidate from convolutional neural network analysis (Olmschenk et al. 2021). [CTOI]

DTARPS 212 = TIC 188570092 = HATS-72 = TOI-294. Spectroscopically 'Confirmed Planet' with period  $P = 7.32829$  d, mass  $M = 40 M_{\oplus}$  and radius  $R = 0.722 R_J$ . [NEA/TOI]

DTARPS 213 = TIC 200324182 = CTOI 200324182.01. DIAMante planet candidate with period  $P = 1.29699$  d, transit depth 1.9 mmag, planet radius  $6 R_{\oplus}$  (Montalto et al. 2020). [CTOI] Planetary candidate with period  $P = 1.297000$  d, transit depth = 0.19% and width 1.5 h, triage probability 99.1% and vetting probability 72% from deep learning analysis (Yu et al. 2019).

DTARPS 214 = TIC 201177276 = TOI-2379 = CTOI 201177276.01. Disposition 'Planetary Candidate' with period  $P = 5.4694164$  d, transit depth 3.19% and planet radius  $11 R_{\oplus}$ . [NEA/TOI] Planetary candidate from DIAMante analysis (Montalto et al. 2020). [CTOI]

DTARPS 215 = TIC 201248411 = HIP 65 A = TOI-129. Spectroscopically 'Confirmed Planet' with period  $P = 0.9809734$  d, mass  $M = 1021 M_{\oplus}$  and radius  $2.03 R_J$ . [NEA/TOI]

DTARPS 216 = TIC 201899356 = CTOI 201899356.01. DIAMante planet candidate with period  $P = 3.10853$  d, transit depth 11.1 mmag, planet radius  $14 R_{\oplus}$  (Montalto et al. 2020). [CTOI]

DTARPS 217 = TIC 204376737 = WASP-6 = TOI-231. Spectroscopically 'Confirmed Planet' with period  $P = 3.36100239$  d, mass  $M = 153 M_{\oplus}$  and radius  $R = 1.224 R_J$ . [NEA/TOI]

DTARPS 218 = TIC 204671232 = TOI-2361 = CTOI 204671232.01. Disposition 'Planetary Candidate' with period  $P = 8.71546$  d, transit depth 1.20% and planet radius  $12 R_{\oplus}$ . [NEA/TOI] Planetary candidate from DIAMante analysis (Montalto et al. 2020). [CTOI]

DTARPS 220 = TIC 209459275 = TOI-559. Spectroscopically 'Confirmed Planet' with period  $P = 6.9839095$  d, mass  $M = 1910 M_{\oplus}$  and radius  $R = 1.091 R_J$  orbiting a G V star. [NEA/TOI]

DTARPS 223 = TIC 219205407 = TOI-946. Disposition 'False Positive' with period  $P = 6.1253092$  d, transit depth 3.94% and planet radius  $22 R_{\oplus}$ . [NEA/TOI] Planetary candidate with period  $P = 6.125959$  d, transit depth = 3.41% and width 1.8 h, triage probability 98% and vetting probability 18% from deep learning analysis (Yu et al. 2019).

DTARPS 224 = TIC 219396153 = CTOI 219396153.01. DIAMante planet candidate with period  $P = 10.24172$  d, transit depth 10.2 mmag, planet radius  $5 R_{\oplus}$  (Montalto et al. 2020). [CTOI]

DTARPS 225 = TIC 219421728 = CTOI 219421728.01. DIAMante planet candidate with period  $P = 0.67113$  d, transit depth 4.2 mmag, planet radius  $10 R_{\oplus}$  (Montalto et al. 2020). [CTOI] Planetary candidate with period  $P = 0.671078$  d, transit depth = 0.40% and width 1.7 h, triage probability 99.6% and vetting probability 29% from deep learning analysis (Yu et al. 2019).

DTARPS 226 = TIC 219698950 = HATS-1 = TOI-766. Disposition 'False Positive' with period  $P = 1.571151$  d, transit depth 0.08% and planet radius  $3.5 R_{\oplus}$ . [NEA/TOI] Spectroscopically 'Confirmed Planet' with period  $P = 3.446459$  d, mass  $M = 589 M_{\oplus}$  and radius  $R = 1.3 R_{\odot}$ . [NEA/TOI]

DTARPS 227 = TIC 219701535 = TOI-2399 = CTOI 219701535.01. Disposition 'Planetary Candidate' with period  $P = 5.4681892$  d, transit depth 0.43% and planet radius  $11 R_{\oplus}$ . [NEA/TOI] Planetary candidate from DIAMante analysis (Montalto et al. 2020). [CTOI]

DTARPS 228 = TIC 219766989 = TOI-2354 = CTOI 219766989.01. Disposition 'False Positive' with period  $P = 0.5198892$  d, transit depth 0.27% and planet radius  $10 R_{\oplus}$ . [NEA/TOI] Planetary candidate from DIAMante analysis (Montalto et al. 2020). [CTOI]

DTARPS 229 = TIC 219924802 = TOI-3282. Disposition 'Ambiguous Planetary Candidate' with period  $P = 2.9478339$  d, transit depth 0.50% and planet radius  $19 R_{\oplus}$ . [NEA/TOI]

DTARPS 230 = TIC 220068921 = TOI-2369 = CTOI 220068921.01. Disposition 'Planetary Candidate' with period  $P = 3.36376$  d, transit depth 0.70% and planet radius  $10 R_{\oplus}$ . [NEA/TOI] Planetary candidate from DIAMante analysis (Montalto et al. 2020). [CTOI]

DTARPS 231 = TIC 220076110 = TOI-2796 = CTOI 220076110.01. Disposition 'Planetary Candidate' with period  $P = 4.808498$  d, transit depth 1.10% and planet radius  $15 R_{\oplus}$ . [NEA/TOI] Planetary candidate from DIAMante analysis (Montalto et al. 2020). [CTOI]

DTARPS 232 = TIC 220144363 = TOI-4199. Disposition 'Planetary Candidate' with period  $P = 4.4466179$  d, transit depth 0.79% and planet radius  $17 R_{\oplus}$ . [NEA/TOI]

DTARPS 233 = TIC 220396259 = TOI-379. Disposition 'False Positive' with period  $P = 0.91677$  d, transit depth 0.03% and equivalent planet radius  $3.1 R_{\oplus}$ . [NEA/TOI]

DTARPS 234 = TIC 220417892 = CTOI 220417892.01 DIAMante planet candidate with period  $P = 7.0339$  d, transit depth 10.7 mag, planet radius  $17 R_{\oplus}$  (Montalto et al. 2020). [CTOI]

DTARPS 235 = TIC 220459826 = TOI-872. Disposition 'Planetary Candidate' with two planets. TOI-872.01 has period  $P = 2.2395609$  d, transit depth 0.11% and planet radius  $2.7 R_{\oplus}$ . TOI-872.02 has  $P = 4.9727684$ , transit depth 0.10% and planet radius  $2.6 R_{\oplus}$ . [NEA/TOI] Planetary candidate with period  $P = 2.239526$  d, transit depth = 0.10% and width 1.3 h, triage probability 55% and vetting probability 63% from deep learning analysis (Yu et al. 2019).

DTARPS 236 = TIC 220518305 = TOI-156. Disposition 'False Positive' with period  $P = 14.152$  d, transit depth 0.38% and planet radius  $11 R_{\oplus}$ . [NEA/TOI]

DTARPS 237 = TIC 220568520 = TYC 8863-203-1. Single line spectroscopic binary with metal-rich primary star and a low-mass stellar companion in an eccentric orbit (Mireles et al. 2020). The primary has mass  $M_{\star} = 1.03 M_{\odot}$  and radius  $R_{\star} = 1.01 R_{\odot}$ . The secondary has orbital period  $P = 18.5577$  d, eccentricity 10%, radius  $R_p = 1.25 R_J$  and mass  $M_p = 107 M_J$ . [SIMBAD]

DTARPS 238 = TIC 229047362 = WASP-25 = TOI-767. Disposition 'Known Planet' with period  $P = 3.764873$  d, transit depth 2.22% and planet radius  $14 R_{\oplus}$ . [NEA/TOI] Spectroscopically 'Confirmed Planet' with period  $P = 3.764827$  d, mass  $M = 190 M_{\oplus}$  and radius  $R = 1.247 R_J$ . [NEA/TOI]

DTARPS 243 = TIC 230980206 = TOI-2649 = CTOI 230980206.01. Disposition 'Planetary Candidate' with period  $P = 3.375591$  d, transit depth 1.16% and planet radius  $13 R_{\oplus}$ . [NEA/TOI] Planetary candidate from convolutional neural network analysis (Olmschenk et al. 2021). [CTOI]

DTARPS 245 = TIC 230982885 = WASP-97 = TOI-195. Spectroscopically 'Confirmed Planet' with period  $P = 2.07276$  d, mass  $M = 432 M_{\oplus}$  and radius  $R = 1.13 R_J$  orbiting a G5 star. [NEA/TOI]

DTARPS 250 = TIC 233964642 = TOI-334. Disposition 'Ambiguous Planetary Candidate' with period  $P = 17.9158854$  d, transit depth 0.89% and planet radius  $21 R_{\oplus}$ . [NEA/TOI]

DTARPS 251 = TIC 234489976 = TOI-2308. Disposition 'Planetary Candidate' with period  $P = 3.8686895$  d, transit depth 0.80% and planet radius  $14 R_{\oplus}$ . [NEA/TOI]

DTARPS 252 = TIC 235015217 = CTOI 235015217.01. DIAMante planet candidate with period  $P = 4.08793$  d, transit depth 4.1 mmag, planet radius  $13 R_{\oplus}$  (Montalto et al. 2020). [CTOI]

DTARPS 254 = TIC 235067594 = CTOI 235067592.01. DIAMante planet candidate with period  $P = 8.29477$  d, transit depth 4.7 mmag, planet radius  $7 R_{\oplus}$  (Montalto et al. 2020). [CTOI] Planetary candidate with period  $P = 8.296909$  d, transit depth = 0.37% and width 3.0 h, triage probability 89% and vetting probability 83% from deep learning analysis (Yu et al. 2019).

DTARPS 256 = TIC 237885040 = TOI-2387. Disposition 'Planetary Candidate' with period  $P = 5.6601098$  d, transit depth 0.84% and planet radius  $12 R_{\oplus}$ . [NEA/TOI]

DTARPS 257 = TIC 238176110 = WASP-91 = TOI-116. Spectroscopically 'Confirmed Planet' with period  $P = 2.798581$  d, mass  $M = 425 M_{\oplus}$  and radius  $R = 1.03 R_J$  orbiting a K3 star. [NEA/TOI]

DTARPS 259 = TIC 243641947 = TOI-3235. Disposition 'Planetary Candidate' with period  $P = 2.5927363$  d, transit depth 7.44% and planet radius  $10 R_{\oplus}$ . [NEA/TOI]

DTARPS 262 = TIC 248075138 = WASP-42 = TOI-769. Spectroscopically 'Confirmed Planet' with period  $P = 4.9816872$  d, mass  $M = 159 M_{\oplus}$  and radius  $R = 1.063 R_J$ . [NEA/TOI]

DTARPS 264 = TIC 249022743 = CTOI 249022743.01. DIAMante planet candidate with period  $P = 2.25601$  d, transit depth 1.2 mmag, planet radius  $4 R_{\oplus}$  (Montalto et al. 2020). [CTOI]

DTARPS 265 = TIC 250386181 = TOI-390. Disposition 'False Positive' with period  $P = 1.470258$  d, transit depth 0.26% and planet radius  $9 R_{\oplus}$ . [NEA/TOI] ZTF 400202200029768 variable star  $5''$  from TIC star with range  $r=15.4-17.4$ . Possible blended contaminant, Possible dilution of transit depth by ZTF 1393210200029826 with  $r=15.6$  lying  $6''$  from the DTARPS candidate.

DTARPS 266 = TIC 251848941 = TOI-178. Confirmed planet with period  $P = 1.914558$  d, mass  $M = 1.5 M_{\oplus}$  and radius  $R = 0.103 R_J$  orbiting a K star. TOI-178 c has period  $P = 3.23845$  d, TOI-178 d has period  $P = 6.5577$  d, TOI-178 e has period  $P = 9.955936$  d, TOI-178 f has period  $P = 15.231915$  d, TOI-178 g has period  $P = 2.07095$  d.. [NEA/TOI]

DTARPS 267 = TIC 254113311 = TOI-1130. Spectroscopically 'Confirmed Planet' TOI-1130 b with period  $P = 4.066499$  d, unknown mass and radius  $R = 0.326 R_J$  orbiting a K7 star. TOI-1130 c has period  $P = 8.350381$  d. [NEA/TOI]

DTARPS 269 = TIC 256158543 = TOI-3329 = CTOI 256158543.01. Disposition 'Planetary Candidate' with period  $P = 5.0648607$  d, transit depth 0.97% and planet radius  $13 R_{\oplus}$ . [NEA/TOI]. Planetary candidate from convolutional neural network analysis (Olmschenk et al. 2021). [CTOI]

DTARPS 270 = TIC 257567854 = WASP-22 = TOI-403. Spectroscopically 'Confirmed Planet' with period  $P = 3.53269$  d, mass  $M = 178 M_{\oplus}$  and radius  $R = 1.12 R_J$  orbiting a G1 V star. [NEA/TOI]

DTARPS 272 = TIC 260043723 = TOI-217. Disposition 'False Positive' with period  $P = 3.13879$  d, transit depth 0.05% and planet radius  $5 R_{\oplus}$ . [NEA/TOI]

DTARPS 273 = TIC 260657291 = UCAC4 177-008238. M0 V star at distance  $d = 83$  pc in TESS Habitable Zone Star Catalog (Kaltenegger et al. 2019). [SIMBAD] Blended eclipsing binary on 17 mag star  $17''$  from target. [SPOC]

DTARPD 274 = TIC 261261490 = CTOI 261261490.01. DIAMante planet candidate with period  $P = 3.539589$  d, transit depth 0.7 mmag, planet radius  $3.8 R_{\oplus}$  (Montalto et al. 2020). [CTOI] Eclipsing binary in 14 mag star  $33''$  from target. [SPOC]

DTARPS 277 = TIC 263003176 = HD 5278 = TOI-130. Spectroscopically 'Confirmed Planet' HD 5278 b with period  $P = 14.339156$  d, mass  $M = 7.8 M_{\oplus}$  and radius  $R = 0.219 R_J$  orbiting a F V star. HD 5278 c has period  $P = 40.87$  d. [NEA/TOI]

DTARPS 285 = TIC 266980320 = HD 219666 = TOI-118. Spectroscopically 'Confirmed Planet' with period  $P = 6.03607$  d, mass  $M = 16.6 M_{\oplus}$  and radius  $R = 0.42 R_J$ . [NEA/TOI]

DTARPS 286 = TIC 268529943 = CTOI 268529943.01. DIAMante planet candidate with period  $P = 4.30059$  d, transit depth 21.6 mmag, planet radius  $19 R_{\oplus}$  (Montalto et al. 2020). [CTOI]

DTARPS 287 = TIC 268644785 = KELT-15 = TOI-505. Spectroscopically 'Confirmed Planet' with period  $P = 3.329441$  d, mass  $M = 289 M_{\oplus}$  and radius  $R = 1.443 R_J$ . [NEA/TOI]

DTARPS 288 = TIC 268766053 = WASP-53 = TOI-272. Spectroscopically 'Confirmed Planet' WASP-53 b with period  $P = 3.3098443$  d, mass  $M = 667 M_{\oplus}$  and radius  $R = 1.07 R_J$ . WASP-53 c has period  $P = 2840$  d. [NEA/TOI]

DTARPS 290 = TIC 269558487 = TOI-855. Disposition 'Planetary Candidate' with period  $P = 1.8301278$  d, transit depth 0.13% and planet radius  $5 R_{\oplus}$ . [NEA/TOI]

DTARPS 291 = TIC 270348758 = TYC 7282-1700-1. Blended eclipsing binary with period  $P = 1.738217$  d and transit depth 28 mmag in KELT False Positive catalog (Collins et al. 2018). [SIMBAD]

DTARPS 292 = TIC 270380593 = WASP-156 = TOI-465. Spectroscopically 'Confirmed Planet' with period  $P = 3.836189$  d, mass  $M = 40.68 M_{\oplus}$  and radius  $R = 0.51 R_J$ . [NEA/TOI]

DTARPS 293 = TIC 270456887 = CTOI 270456887.01. DIAMante planet candidate with period  $P = 2.26843$  d, transit depth 7.8 mmag, planet radius  $15.2 R_{\oplus}$  (Montalto et al. 2020). [CTOI]

DTARPS 294 = TIC 270468559 = HAT-P-42 = TOI-571. Spectroscopically 'Confirmed Planet' with period  $P = 4.641878$  d, mass  $M \sim 300 M_{\oplus}$  and radius  $R = 1.28 R_J$ . [NEA/TOI]

DTARPS 296 = TIC 271269442 = 1SWASP J075926.35+070728.4. False Positive (no radial velocity variations, Schanche et al. (2019)). ZTF 463213400031454 star  $6''$  from TIC star at  $r=17.0$  with dips to 17.3. Possible blended contaminant.

DTARPS 297 = TIC 271893367 = TOI-501. Spectroscopically 'Confirmed Planet' with period  $P = 5.857487$  d, mass  $M = 798 M_{\oplus}$  and radius  $R = 1.255 R_J$  orbiting an F star. [NEA/TOI]

DTARPS 300 = TIC 273695332 = TOI-2223. Disposition 'Planetary Candidate' with period  $P = 6.9320855$  d, transit depth 0.69% and planet radius  $13 R_{\oplus}$ . [NEA/TOI]

DTARPS 302 = TIC 277712294 = TYC 245-630-1 = EBLM J1013+01 = 1SWASP J101350.84+015928.1. Single-line spectroscopic binary, eclipsing binary with low mass companion with orbital period  $P = 2.891182$  day (Schanche et al. 2019). The primary has mass  $M = 1.0 M_{\odot}$ , rotation velocity  $v \sin(i) = 16 \text{ km s}^{-1}$ , metallicity  $[Fe/H] = 0.3$  and age around 5 Gyr (von Boetticher et al. 2019). The secondary has mass  $M = 0.18 M_{\odot}$  and radius  $R = 0.15 R_{\odot}$  producing a transit with depth 4%. The star appears in a study on super-flares (SIMBAD not yet ingested) (Tu et al. 2020). [SIMBAD]

DTARPS 306 = TIC 280614628. ZTF 412214100006023 star  $14''$  from TIC star at  $r=18.0$  with dips to 18.5. Possible blended contaminant. Possible dilution of transit depth by ZTF 412214100006142 with  $r=14.0$  lying  $12''$  from the DTARPS candidate.

DTARPS 307 = TIC 281143479. Possible dilution of transit depth by ZTF 460301200023076 with  $i=15.6$  lying  $10''$  from the DTARPS candidate.

DTARPS 308 = TIC 281408474 = TOI-628. Spectroscopically 'Confirmed Planet' with period  $P = 53.4095675$  d, mass  $M = 2011 M_{\oplus}$  and radius  $R = 1.06 R_J$ . [NEA/TOI]

DTARPS 309 = TIC 282498590 = TOI-2492 = CTOI 282498590.01. Disposition 'Ambiguous Planetary Candidate' with period  $P = 10.1011438$  d, transit depth 1.31% and planet radius  $18 R_{\oplus}$ . [NEA/TOI] Planetary candidate from DIAMante analysis (Montalto et al. 2020). [CTOI]

DTARPS 310 = TIC 282505014 = TYC 4809-264-1 = CoRoT 110769585. Spectral type F7 IV (Guenther et al. 2012). [SIMBAD]

DTARPS 311 = TIC 282576340 = TOI-2494. Disposition 'Planetary Candidate' with two planets. TOI-2494.01 has period  $P = 8.3761316$  d, transit depth 0.90% and planet radius  $10 R_{\oplus}$ . TOI-2494.02 has  $P = 2.4087648$  d, transit depth 0.06% and planet radius  $2.2 R_{\oplus}$ . [NEA/TOI]

DTARPS 312 = TIC 283605976 = TOI-4679. Disposition 'Planetary Candidate' with period  $P = 10.1011438$  d, transit depth 1.31% and planet radius  $18 R_{\oplus}$ . [NEA/TOI]

DTARPS 314 = TIC 286099128 = TOI-3422. Disposition 'Planetary Candidate' with period  $P = 3.7788872$  d, transit depth 1.81% and planet radius  $14 R_{\oplus}$ . [NEA/TOI]

DTARPS 315 = TIC 287328202 = CTOI 287328202.01. DIAMante planet candidate with period  $P = 3.8348$  d, transit depth 1.1 mmag, planet radius  $5.7 R_{\oplus}$  (Montalto et al. 2020). [CTOI]

DTARPS 316 = TIC 287721202 = TOI-3022. Disposition 'Planetary Candidate' with period  $P = 8.990904$  d, transit depth 0.65% and planet radius  $10 R_{\oplus}$ . [NEA/TOI]

DTARPS 318 = TIC 2899889797 = TOI-4178 = CTOI 2899889797.01. Disposition 'Planetary Candidate' with period  $P = 2.2042197$  d, transit depth 0.3% and planet radius  $14 R_{\oplus}$ . [NEA/TOI] Planetary candidate from DIAMante analysis (Montalto et al. 2020). [CTOI]

DTARPS 319 = TIC 290036495 = TOI-2351. Disposition 'Planetary Candidate' with period  $P = 5.2524$  d, transit depth 2.16% and planet radius  $19 R_{\oplus}$ . [NEA/TOI]

DTARPS 321 = TIC 290777444 = CTOI 290777444.01. DIAMante planet candidate with period  $P = 6.10795$  d, transit depth 14.8 mmag, planet radius  $18 R_{\oplus}$  (Montalto et al. 2020). [CTOI] Possible dilution of transit depth by ZTF 461209100035300 with  $r=14.8$  lying  $9''$  and by ZTF 461209100035304 with  $r=15.3$  lying  $11''$  from the DTARPS candidate.

DTARPS 322 = TIC 292777663 = CTOI 292777663.01. DIAMante planet candidate with period  $P = 4.60314$  d, transit depth 1.1 mmag, planet radius  $5 R_{\oplus}$  (Montalto et al. 2020). [CTOI]

DTARPS 324 = TIC 294301883 = WASP-55 = TOI-774. Spectroscopically 'Confirmed Planet' with period  $P = 5.857487$  d, mass  $M = 798 M_{\oplus}$  and radius  $R = 1.255 R_J$  orbiting an F star. [NEA/TOI]

DTARPS 325 = TIC 294691204 = TOI-5018 = CTOI 294691204.01. Disposition 'Planetary Candidate' with period  $P = 6.5859565$  d, transit depth 0.16% and planet radius  $6 R_{\oplus}$ . [NEA/TOI] Planetary candidate from DIAMante analysis (Montalto et al. 2020). [CTOI]

DTARPS 327 = TIC 295176393 = CTOI 295176393.01. DIAMante planet candidate with period  $P = 27.2519$  d, transit depth 5.3 mmag, planet radius  $13 R_{\oplus}$  (Montalto et al. 2020). [CTOI]

DTARPS 328 = TIC 295541511 = TOI-1117. Disposition 'Planetary Candidate' with period  $P = 2.2264788$  d, transit depth 0.06% and planet radius  $= 2.7 R_{\oplus}$ . [NEA/TOI]

DTARPS 329 = TIC 299780329 = TOI-1869 = CTOI 299780329.01. Disposition 'Planetary Candidate' with period  $P = 1.6024044$  d, transit depth 0.14% and planet radius  $6 R_{\oplus}$ . [NEA/TOI] Planetary candidate from eleanor analysis (Feinstein et al. 2019).

DTARPS 330 = TIC 300116105 = CTOI 300116105.01. DIAMante planet candidate with period  $P = 2.07693$  d, transit depth 3.3 mmag, planet radius  $7 R_{\oplus}$  (Montalto et al. 2020). [CTOI] Planetary candidate with period  $P = 2.075595$  d, transit depth  $= 0.31\%$  and width 1.4 h, triage probability 94% and vetting probability 65% from deep learning analysis (Yu et al. 2019).

DTARPS 334 = TIC 300560295 = CTOI 300560295.01. Planetary candidate with period  $P = 10.28889$  d, transit depth 0.42%, planet radius  $18 R_{\oplus}$  (Lipponen). [CTOI] Eccentric eclipsing binary. [SPOC]

DTARPS 335 = TIC 301343785 = TOI-2347 = CTOI 301345785.01. Disposition 'Ambiguous Planetary Candidate' with period  $P = 1.1736318$  d, transit depth 0.15% and planet radius  $8 R_{\oplus}$ . [NEA/TOI] Planetary candidate from DIAMante analysis (Montalto et al. 2020). [CTOI]

DTARPS 336 = TIC 301980693 = CTOI 301980693.01. Planetary candidate with period  $P = 4.782639$  d, transit depth 24.1 mmag, planet radius  $17 R_{\oplus}$  (Lipponen). [CTOI]

DTARPS 338 = TIC 302333151 = TOI-2315 = CTOI 302333151.01. Disposition 'Ambiguous Planetary Candidate' with period  $P = 1.4408228$  d, transit depth 0.45% and planet radius  $10 R_{\oplus}$ . [NEA/TOI] Planetary candidate from DIAMante analysis (Montalto et al. 2020). [CTOI]

DTARPS 339 = TIC 302495337 = CTOI 302495337.01. DIAMante planet candidate with period  $P = 2.24986$  d, transit depth 0.6 mmag, planet radius  $3.7 R_{\oplus}$  (Montalto et al. 2020). [CTOI] Possible dilution of transit depth by ZTF 511216200000551 with  $r=13.8$  lying  $15''$  from the DTARPS candidate.

DTARPS 340 = TIC 302924206 = TOI-2362 = CTOI 302924206.01. Disposition 'Planetary Candidate' with period  $P = 6.9444047$  d, transit depth 0.45% and planet radius  $10 R_{\oplus}$ . [NEA/TOI] Planetary candidate from DIAMante analysis (Montalto et al. 2020). [CTOI]

DTARPS 341 = TIC 306337838 = TOI-2397 = CTOI 306337838.01. Disposition 'Planetary Candidate' with period  $P = 6.00327$  d, transit depth 0.49% and planet radius  $8 R_{\oplus}$ . [NEA/TOI] Planetary candidate from DIAMante analysis (Montalto et al. 2020). [CTOI]

DTARPS 342 = TIC 306362738 = WASP-49 = TOI-479 = CTOI 306362738.01. Spectroscopically 'Confirmed Planet' with period  $P = 2.7817387$  d, mass  $M = 127 M_{\oplus}$  and radius  $R = 1.115 R_J$  orbiting a G6 V star. [NEA/TOI]

DTARPS 350 = TIC 308098254 = WASP-162 = TOI-1906. Spectroscopically 'Confirmed Planet' with period  $P = 9.62468$  d, mass  $M = 1652 M_{\oplus}$  and radius  $R = 1 R_J$  orbiting a K0 star. [NEA/TOI]

DTARPS 354 = TIC 312091232 = CTOI 312091232.01. DIAMante planet candidate with period  $P = 4.34801$  d, transit depth 4.7 mmag, planet radius  $7 R_{\oplus}$  (Montalto et al. 2020). [CTOI] Blended eclipsing binary on 13 mag star  $21''$  from target. [SPOC]

DTARPS 355 = TIC 314865962 = TOI-208. Disposition 'Planetary Candidate' with period  $P = 22.4642328$  d, transit depth 0.06% and planet radius  $2.5 R_{\oplus}$ . [NEA/TOI]

DTARPS 357 = TIC 317548889 = TOI-480. Disposition 'Planetary Candidate' with period  $P = 6.8659582$  d, transit depth 0.03% and planet radius  $2.8 R_{\oplus}$ . [NEA/TOI]

DTARPS 360 = TIC 318756174 = CTOI 318756174.01. Planet candidate with period 3.374443 d, transit depth 13.8 mmag and planet radius  $14 R_{\oplus}$  from convolutional neural network analysis (Olmschenk et al. 2021). [CTOI]

DTARPS 361 = TIC 321011127 = TOI-860. Disposition 'Planetary Candidate' with period  $P = 6.4535152$  d, transit depth 1.12% and planet radius  $20 R_{\oplus}$ . [NEA/TOI]

DTARPS 362 = TIC 322807675 = TOI-2398 = CTOI 322807675.01. Disposition 'Planetary Candidate' with period  $P = 19.4061437$  d, transit depth 1.11% and planet radius  $9 R_{\oplus}$ . [NEA/TOI] Planetary candidate from DIAMante analysis (Montalto et al. 2020). [CTOI]

DTARPS 364 = TIC 325680697 = TOI-414. Disposition 'False Positive' with period = 1.82488 d. [NEA/TOI]

DTARPS 365 = TIC 326092637 = CTOI 326092637.01. DIAMante planet candidate with period  $P = 4.61824$  d, transit depth 13.6 mmag, planet radius  $18 R_{\oplus}$  (Montalto et al. 2020). [CTOI]

DTARPS 366 = TIC 327301957 = TOI-1074. Disposition 'Planetary Candidate' with period  $P = 13.9427597$  d, transit depth 0.14% and planet radius  $2.8 R_{\oplus}$ . [NEA/TOI]

DTARPS 369 = TIC 327952677 = TOI-295. Disposition 'Known Planet' with period  $P = 3.3971091$  d, transit depth 0.99% and planet radius  $14 R_{\oplus}$ . [NEA/TOI]

DTARPS 372 = TIC 332660150 = TOI-938. Disposition 'Planetary Candidate' with period  $P = 8.8073507$  d, transit depth 0.17% and planet radius  $4 R_{\oplus}$ . [NEA/TOI]

DTARPS 373 = TIC 333426440 = TYC 5390-2210-1. Planetary candidate with period  $P = 2.423293$  d, transit depth = 1.6% and width 3.7 h, triage probability 99% and vetting probability 16% from deep learning analysis (Yu et al. 2019). [SIMBAD]

DTARPS 375 = TIC 339672028 = TOI-481. Spectroscopically 'Confirmed Planet' with period  $P = 10.33111$  d, mass  $M = 486 M_{\oplus}$  and radius  $R = 0.99 R_J$  orbiting a G star. [NEA/TOI]

DTARPS 376 = TIC 339733013 = TOI-417. Disposition 'False Positive' with period  $P = 5.62162$  d, transit depth 0.06% and planet radius  $3.4 R_{\oplus}$ . [NEA/TOI]

DTARPS 378 = TIC 341105361. Transit depth differs in two TESS sectors.

DTARPS 379 = TIC 341411516 = CTOI 341411516.01. DIAMante planet candidate with period  $P = 3.10911$  d, transit depth 1.3 mmag, planet radius  $2.7 R_{\oplus}$  (Montalto et al. 2020). [CTOI]

DTARPS 381 = TIC 343936388 = UCAC4 208-011547. Warm Jupiter in TESS FFI images with period  $P = 15.144$  d, radius  $6.4 R_{\oplus}$  and possible high eccentricity  $\simeq 0.5$  orbiting a primary star with radius  $R = 0.86 R_{\odot}$  (Dong et al. 2021). A Transit Timing Variation signal may be present. [SIMBAD]

DTARPS 386 = TIC 350153977 = TOI-908. Disposition 'Planetary Candidate' with period  $P = 3.1837681$  d, transit depth 0.08% and planet radius  $3.1 R_{\oplus}$ . [NEA/TOI]

DTARPS 387 = TIC 350480660 = CTOI 365956062.01 = TYC 8527-329-1 = EBLM J0543-56. Single-line spectroscopic binary, eclipsing binary with low mass companion with orbital period  $P = 4.463860$  d (von Boetticher et al. 2019). The F8 primary has mass  $M = 1.3 M_{\odot}$ , radius  $R = 1.3 R_{\odot}$ , and age  $t = 1$  Gyr. The secondary has mass  $M = 0.16 M_{\odot}$  and radius  $R = 0.19 R_{\odot}$ . [SIMBAD] Planetary candidate vetted with DAVE (Rao et al. 2021). [CTOI]

DTARPS 388 = TIC 355637190 = TOI-293. Disposition 'Ambiguous Planetary Candidate' with period  $P = 0.80546$  d, transit depth 0.31% and planet radius  $9 R_{\oplus}$ . [NEA/TOI]

DTARPS 390 = TIC 365956062 = CTOI 365956062.01. DIAMante planet candidate with period  $P = 1.80765$  d, transit depth 1.2 mmag, planet radius  $5 R_{\oplus}$  (Montalto et al. 2020). [CTOI]

DTARPS 392 = TIC 369376388 = TOI-2486 = CTOI 369376388.01. Disposition 'Planetary Candidate' with period  $P = 1.5411563$  d, transit depth 0.15% and planet radius  $3.7 R_{\oplus}$ . [NEA/TOI] Planetary candidate from DIAMante analysis (Montalto et al. 2020). [CTOI]

DTARPS 394 = TIC 370138999 = TOI-3260 = CTOI 370138999.01. Disposition 'Planetary Candidate' with period  $P = 11.4519176$  d, transit depth 0.26% and planet radius  $8 R_{\oplus}$ . [NEA/TOI] Planetary candidate from DIAMante analysis (Montalto et al. 2020). [CTOI]

DTARPS 395 = TIC 372909372 = CTOI 372909372.01. DIAMante planet candidate with period  $P = 9.01803$  d, transit depth 1.1 mmag, planet radius  $5 R_{\oplus}$  (Montalto et al. 2020). [CTOI]

DTARPS 397 = TIC 382068562 = TOI-924. Disposition 'Planetary Candidate' with period  $P = 12.1273412$  d, transit depth 1.93% and planet radius  $19 R_{\oplus}$ . [NEA/TOI]

DTARPS 398 = TIC 382188882 = TOI-276. Disposition 'False Positive' with period  $P = 4.800523$  d, transit depth 0.54% and equivalent planet radius  $15 R_{\oplus}$ . [NEA/TOI]

DTARPS 400 = TIC 382602147 = TOI-2384 = CTOI 382602147.01. Disposition 'Planetary Candidate' with period  $P = 2.1356844$  d, transit depth 2.88% and planet radius  $11 R_{\oplus}$ . [NEA/TOI] Planetary candidate from DIAMante analysis (Montalto et al. 2020). [CTOI]

DTARPS 401 = TIC 382626661 = TOI-283. Disposition 'Planetary Candidate' with period  $P = 17.6175219$  d, transit depth 0.07% and planet radius  $2.3 R_{\oplus}$ . [NEA/TOI]

DTARPS 402 = TIC 384469512. Transit depth differs in two TESS sectors.

DTARPS 406 = TIC 388104525 = WASP-119 = TOI-112. Spectroscopically 'Confirmed Planet' with period  $P = 2.49979$  d, mass  $M = 391 M_{\oplus}$  and radius  $R = 1.4 R_J$  orbiting a G5 star. [NEA/TOI]

DTARPS 407 = TIC 388198242 = TOI-2224 = CTOI 388198242.01. Disposition 'Planetary Candidate' with period  $P = 0.5055105$  d, transit depth 0.23% and planet radius  $5 R_{\oplus}$ . [NEA/TOI] Planetary candidate from DIAMante analysis (Montalto et al. 2020). [CTOI]

DTARPS 409 = TIC 391949880 = TOI-128. Disposition 'Planetary Candidate' with period  $P = 4.9404681$  d, transit depth 0.03% and planet radius  $2.2 R_{\oplus}$ . [NEA/TOI]

DTARPS 410 = TIC 393940766 = TOI-148. Disposition 'Confirmed Planet' with period  $P = 4.8670689$  d, transit depth 0.49% and planet radius  $8.2 R_{\oplus}$ . [NEA/TOI]

DTARPS 414 = TIC 394698182 = TOI-170. Disposition 'Planetary Candidate' with period  $P = 1.0690773$  d, transit depth 1.16% and planet radius  $14 R_{\oplus}$ . [NEA/TOI]

DTARPS 412 = TIC 394721720 = TOI-4378 = CTOI 394721720.01. Disposition 'Planetary Candidate' with period  $P = 1.0690773$  d, transit depth 0.30% and planet radius  $10 R_{\oplus}$ . [NEA/TOI] Planetary candidate from DAVE vetting (Rao).

DTARPS 414 = TIC 398943781 = WASP-41 = TOI-780. Spectroscopically 'Confirmed Planet' with period  $P = 3052404$  d, mass  $M = 299 M_{\oplus}$  and radius  $R = 1.18 R_J$ . [NEA/TOI]

DTARPS 415 = TIC 401125028 = TOI-2368 = CTOI 401125028.01. Disposition 'Planetary Candidate' with period  $P = 5.1750108$  d, transit depth 2.72% and planet radius  $15 R_{\oplus}$ . [NEA/TOI] Planetary candidate from DIAMante analysis (Montalto et al. 2020). [CTOI]

DTARPS 416 = TIC 402026209 = WASP-4 = TOI-232. Spectroscopically 'Confirmed Planet' with period  $P = 1.3382299$  d, mass  $M = 397 M_{\oplus}$  and radius  $R = 1.341 R_J$  orbiting a G8 star. [NEA/TOI]

DTARPS 420 = TIC 403135192 = TOI-2226. Disposition 'Planetary Candidate' with period  $P = 0.9018226$  d, transit depth 0.08% and planet radius  $4 R_{\oplus}$ . [NEA/TOI]

DTARPS 422 = TIC 404467699 = TOI-857. Disposition 'Known Planet' with period  $P = 3.9080236$  d, transit depth 0.81% and planet radius  $15 R_{\oplus}$ . [NEA/TOI]

DTARPS 423 = TIC 404518509 = HD 21520 = TOI-4320 = CTOI 404518509.01. Disposition 'Planetary Candidate' with two planets. TOI-4320.01 has period  $P = 703.6156148$  d, transit depth 0.06% and planet radius  $2.9 R_{\oplus}$ . TOI-4320.02 has period  $P = 46.4093732$ , transit depth 0.04% and planet radius  $2.2 R_{\oplus}$ . [NEA/TOI] A cool Jupiter with period  $P \sim 27$  d, transit depth 2.6% and planet radius  $R = 2.9 R_{\oplus}$  discovered photometrically in the Planet Hunters TESS survey (Eisner et al. 2021). [SIMBAD]

DTARPS 425 = TIC 407126408 = TOI-913. Disposition 'Planetary Candidate' with period  $P = 11.094122$  d, transit depth 0.11% and planet radius  $2.5 R_{\oplus}$ . [NEA/TOI]

DTARPS 426 = TIC 407127579 = TOI-5064. Disposition 'Planetary Candidate' with period  $P = 3.5108018$  d, transit depth 0.10% and planet radius  $5 R_{\oplus}$ . [NEA/TOI]

DTARPS 428 = TIC 408310006 = WASP-166 = TOI-576. Spectroscopically 'Confirmed Planet' with period  $P = 5.44354$  d, mass  $M = 32 M_{\oplus}$  and radius  $R = 0.63 R_J$  orbiting a F9 star. [NEA/TOI]

DTARPS 431 = TIC 421455387 = TOI-578. Disposition 'Ambiguous Planetary Candidate' with period  $P = 2.50876$  d, transit depth 0.56% and planet radius  $19 R_{\oplus}$ . [NEA/TOI]

DTARPS 432 = TIC 423275733 = WASP-142 = TOI-578. Spectroscopically 'Confirmed Planet' with period  $P = 2.052868$  d, mass  $M = 266 M_{\oplus}$  and radius  $R = 1.53 R_J$  orbiting a F8 star. [NEA/TOI]

DTARPS 433 = TIC 425721385 = TOI-1128. Disposition 'False Positive' with period  $P = 13.5499$  d, transit depth 0.12% and planet radius  $6 R_{\oplus}$ . [NEA/TOI]

DTARPS 434 = TIC 428699140 = TOI-3082. Disposition 'Planetary Candidate' with period  $P = 1.9268755$  d, transit depth 0.24% and planet radius  $3.2 R_{\oplus}$ . [NEA/TOI]

DTARPS 436 = TIC 429304876 = TOI-682. Disposition 'Confirmed Planet' with period  $P = 6.8392339$  d, transit depth 0.12% and planet radius  $3.8 R_{\oplus}$ . [NEA/TOI]

DTARPS 438 = TIC 434477274 = CTOI 434477274.01. DIAMante planet candidate with period  $P = 2.89641$  d, transit depth 6.3 mmag, planet radius  $11 R_{\oplus}$  (Montalto et al. 2020). [CTOI]

DTARPS 441 = TIC 437242640 = WASP-34 = TOI-744. Disposition 'Known Planet' with period  $P = 4.317685$  d, transit depth 1.15% and planet radius  $14 R_{\oplus}$ . [NEA/TOI] Spectroscopically 'Confirmed Planet' with period  $P = 4.3176782$  d, mass  $M = 187 M_{\oplus}$  and radius  $R = 1.22 R_J$ . [NEA/TOI]

DTARPS 445 = TIC 437248515 = WASP-31 = TOI-683. Disposition 'Known Planet' with period  $P = 3.4058883$  d, transit depth 1.65% and planet radius  $16 R_{\oplus}$ . [NEA/TOI] Spectroscopically 'Confirmed Planet' with period  $P = 3.4059096$  d, mass  $M = 151 M_{\oplus}$  and radius  $R = 1.549 R_J$ . [NEA/TOI]

DTARPS 444 = TIC 439366537 = CTOI 439366537.01. DIAMante planet candidate with period  $P = 4.31448$  d, transit depth 1.0 mmag, planet radius  $5 R_{\oplus}$  (Montalto et al. 2020). [CTOI] Blended eclipsing binary in 11 mag star  $22''$  from target. [SPOC]

DTARPS 445 = TIC 440777904 = HAT-P-24 = TOI-511. Spectroscopically 'Confirmed Planet' with period  $P = 3.3552479$  d, mass  $M = 230 M_{\oplus}$  and radius  $R = 1.242 R_J$  orbiting a F8 star. [NEA/TOI]

DTARPS 446 = TIC 440872576 = TOI-3160. Disposition 'Planetary Candidate' with period  $P = 3.9714761$  d, transit depth 0.83% and planet radius  $15 R_{\oplus}$ . [NEA/TOI]

DTARPS 447 = TIC 440957227 = TYC 6760-962-1. Single-line spectroscopic binary with period  $P = 3.418911$  d and transit depth 20 mmag in the KELT False Positive catalog (Collins et al. 2018). [SIMBAD]

DTARPS 448 = TIC 441159680 = TOI-2367 = CTOI 441159680.01. Disposition 'Planetary Candidate' with period  $P = 5.74984$  d, transit depth 1.77% and planet radius  $14 R_{\oplus}$ . [NEA/TOI] Planetary candidate from DIAMante analysis (Montalto et al. 2020). [CTOI]

DTARPS 450 = TIC 443618156 = 1SWASP J111644.43-015207.5 = EBLM J1116-01. Single-line spectroscopic binary, eclipsing binary with low mass companion with orbital period  $P = 7.375828$  d with zero eccentricity (Triado et al. 2017). The G0 primary has mass  $M = 1.2 M_{\odot}$  and radius  $R = 1.3 R_{\odot}$ . The secondary has mass  $M = 0.21 M_{\odot}$ . False Positive in the SuperWASP and DIAMante surveys (Schanche et al. 2019; Montalto et al. 2020). [SIMBAD]

DTARPS 454 = TIC 455096220 = HAT-P-35 = TOI-489. Spectroscopically 'Confirmed Planet' with period  $P = 3.646706$  d, mass  $M = 335 M_{\oplus}$  and radius  $R = 1.332 R_J$ . [NEA/TOI]

DTARPS 455 = TIC 455135327 = HAT-P-30 = TOI-490. Spectroscopically 'Confirmed Planet' with period  $P = 2.810595$  d, mass  $M = 225 M_{\oplus}$  and radius  $R = 1.34 R_J$ . [NEA/TOI]

DTARPS 458 = TIC 469782185 = TOI-1123. Disposition 'Ambiguous Planetary Candidate' with period  $P = 1.20928$  d, transit depth 1.19% and planet radius  $15 R_{\oplus}$ . [NEA/TOI]

DTARPS 459 = TIC 469821652 = TOI-3263. Disposition 'Planetary Candidate' with period  $P = 5.6155837$  d, transit depth 0.27% and planet radius  $8 R_{\oplus}$ . [NEA/TOI]

DTARPS 462 = TIC 738065944 = CTOI 738065944.01. DIAMante planet candidate with period  $P = 7.75543$  d, transit depth 7.7 mmag, planet radius  $10 R_{\oplus}$  (Montalto et al. 2020). [NEA/CTOI]

## B. NOTES ON GALACTIC PLANE LIST

TIC 1129033 = WASP-77 = TOI-398. Spectroscopically 'Confirmed Planet' with period  $P = 1.360030$  d, mass  $M = 560 M_{\oplus}$  and radius  $R = 1.2 R_J$  orbiting a G8 V star. [NEA/TOI]

TIC 4616346 = TYC 5961-487-1. Planetary candidate with period  $P = 0.690059$  d, transit depth = 0.12% and width 1.8 h, triage probability 41% and vetting probability 10% from deep learning analysis (Yu et al. 2019). [SIMBAD]

TIC 10827386 = TOI-2876. Disposition 'Planetary Candidate' with period  $P = 62996307$ , transit depth 0.95% and planet radius  $9 R_{\oplus}$ . [NEA/TOI]

TIC 19519368 = TOI-494. Disposition 'Planetary Candidate' with period  $P = 1.7018884$  d, transit depth 0.05% and planet radius  $1.7 R_{\oplus}$ . [NEA/TOI]

TIC 19937775. Possible dilution of transit depth by ZTF 1407203100035038  $2''$  from the DTARPS candidate with magnitude 15.0.

TIC 21184505 = BD +1246°1868 = EPIC 211424769. Periodic variable discovered in the K2 ecliptic plane survey with  $P = 5.176243$  d from a secondary object with radius  $8 - 25 R_{\oplus}$  orbiting a mass  $M = 1.1 M_{\odot}$  star. Classified as a False Positive due to large radial velocity amplitude by [Mayo et al. \(2018\)](#) but classified as a planet candidate by [Kostov et al. \(2019\)](#). [SIMBAD]

TIC 24773172. Possible dilution of transit depth by anonymous ZTF star  $4''$  from the DTARPS candidate with estimated magnitude 16.

TIC 33521996 = HATS-6 = TOI-468. Spectroscopically 'Confirmed Planet' with period  $P = 3.3452725$  d, mass  $M = 100 M_{\oplus}$  and radius  $R = 0.998 R_J$  orbiting a M1 V star [NEA/TOI]

TIC 34371411 = TYC 5371-981-1 = CTOI 3437411.01. Planet candidate with period 3.882755 d, transit depth 9.7 mmag and planet radius  $15 R_{\oplus}$  from convolutional neural network analysis ([Olmschenk et al. 2021](#)). [CTOI] Planetary candidate with period  $P = 3.881647$  d, transit depth = 0.9% and width 4.5 h, triage probability .99% and vetting probability 82% from deep learning analysis ([Yu et al. 2019](#)). [SIMBAD]

TIC 36209863 = HD 295526 = CoRoT 102856619. Spectral type G4 V ([Guenther et al. 2012](#)). [SIMBAD] Possible dilution of transit depth by anonymous ZTF star with  $g=15$  lying  $2''$  from the DTARPS candidate.

TIC 36559570. Possible dilution of transit depth by ZTF 1455202200016625 with  $r=14.8$  lying  $10''$ , and by ZTF 410209200038811 lying  $13''$  from the DTARPS candidate.

TIC 36916955. Possible dilution of transit depth by ZTF 410104100044112 with  $g=15.6$  lying  $4''$  from the DTARPS candidate.

TIC 37167097 = CTOI 37167097.01. Planet candidate with period 1.98 d and transit depth 0.9 mmag from Lightkurve analysis (Chiarello). [CTOI]

TIC 38696105 = TOI-281. Disposition 'Planetary Candidate' with period  $P = 5.5764964$  d, transit depth 0.07% and planet radius  $4 R_{\oplus}$ . [NEA/TOI] Planetary candidate with period  $P = 5.577113$  d, transit depth = 0.06% and width 2.4 h, triage probability 72% and vetting probability 69% from deep learning analysis ([Yu et al. 2019](#)).

TIC 48176862 = UCAC4 333-014584. Planetary candidate with period  $P = 1.925622$  d, transit depth = 2.0% and width 4.2 h, triage probability 99% and vetting probability 15% from deep learning analysis ([Yu et al. 2019](#)). [SIMBAD]

TIC 50712784 = WASP-161 = TOI-1912. Spectroscopically 'Confirmed Planet' with period  $P = 5.4060425$  d, mass  $M = 791 M_{\oplus}$  and radius  $R = 1.143 R_J$ . [NEA/TOI]

TIC 53588284. ZTF 410202300051074 star  $7''$  from TIC star at  $r=17.3$  mag with dips of 0.3-0.6 mag. Possible blended contaminant.

TIC 56096837 = TOI-2700 = CTOI 56096837.01. Disposition 'Planetary Candidate' with period  $P = 4.6636858$  d, transit depth 1.11% and planet radius  $13 R_{\oplus}$ . [NEA/TOI] Planet candidate from convolutional neural network analysis ([Olmschenk et al. 2021](#)). [CTOI] Possible dilution of transit depth by ZTF 1346213200001469 with  $r=15.8$  lying  $16''$  from the DTARPS candidate.

TIC 61755686. Possible dilution of transit depth by ZTF 1405216400024997 with  $r=13.9$  lying  $9''$  from the DTARPS candidate.

TIC 64573956. Possible dilution of transit depth by ZTF 1405215100024359 with  $r=15.7$  lying  $8''$  from the DTARPS candidate.

TIC 67772767 = TOI-939 = CTOI 67772767.01. Disposition 'Planetary Candidate' with period  $P = 7.6107227$  d, transit depth 0.64% and planet radius  $12 R_{\oplus}$ . [NEA/TOI] Planetary candidate from DIAMANTE analysis ([Montalto et al. 2020](#)). [CTOI]

TIC 79137967. Transit depth differs in two TESS sectors.

TIC 79143083 = TYC 6522-2373-1. Planetary candidate with period  $P = 1.503826$  d, transit depth = 0.32% and width 3.1 h, triage probability 99% and vetting probability 21% from deep learning analysis ([Yu et al. 2019](#)). [SIMBAD]

TIC 79431527 = TOI-2762. Disposition 'Planetary Candidate' with period  $P = 3.9072351$  d, transit depth 1.47% and planet radius  $14 R_{\oplus}$ . [NEA/TOI]

TIC 94239926. The TCF periodogram peak occurs at  $P=3.512516$  d but the true period is more likely the 1/2 harmonic,  $P=1.756$  d. Transits are not perfectly aligned with either period.

TIC 94986319 = TOI-421. Spectroscopically confirmed planet. TOI-421 b has period  $P = 5.19672$  d, mass  $M = 7 M_{\oplus}$  and radius  $R = 0.239 R_J$  orbiting a G9 V star. TOI-421 c has period  $P = 16.06819$  d. [NEA/TOI]

TIC 95057860 = TOI-4201. Disposition 'Planetary Candidate' with period  $P = 3.5809733$  d, transit depth 3.69% and planet radius  $12 R_{\oplus}$ . [NEA/TOI]

TIC 95589845 = TOI-4794 = CTOI 95589845.01. Disposition 'Planetary Candidate' with period  $P = 3.5658043$  d, transit depth 3.69% and planet radius  $12 R_{\oplus}$ . [NEA/TOI] Planet candidate with period 3.565656 d, transit depth 6.3 mmag and planet radius  $15 R_{\oplus}$  from convolutional neural network analysis (Olmschenk et al. 2021). [CTOI]

TIC 99493790 = TOI-162. Disposition 'Ambiguous Planetary Candidate' with period  $P = 7.76686$  d, transit depth 2.44% and planet radius  $17 R_{\oplus}$ . [NEA/TOI]

TIC 117979897 = WASP-141 = TOI-443. Spectroscopically 'Confirmed Planet' with period  $P = 3.310651$  d, mass  $M = 855 M_{\oplus}$  and radius  $R = 1.2 R_J$  orbiting a F9 star. [NEA/TOI]

TIC 122981686. Possible dilution of transit depth by ZTF 413308300032702 with  $i=12.1$  lying  $13''$  from the DTARPS candidate.

TIC 12379043 = TOI-499. Disposition 'Planetary Candidate' with period  $P = 8.533527$  d, transit depth 0.17% and planet radius  $7 R_{\oplus}$ . [NEA/TOI]

TIC 124379043 = TOI-2803. Disposition 'Planetary Candidate' with period  $P = 1.962292$  d, transit depth 2.09% and planet radius  $17 R_{\oplus}$ . [NEA/TOI]

TIC 124498746. Possible dilution of transit depth by ZTF 1404203200050954 with  $r=15.8$  lying  $3''$  from the DTARPS candidate. Transit depth differs in two TESS sectors.

TIC 125018207. Possible dilution of transit depth by anonymous ZTF stars with  $r \simeq 14$  lying  $3''$ , and by ZTF 1404207100022773 with  $r=15.7$  lying  $14''$  from the DTARPS candidate.

TIC 125201129. ZTF 411203300034623 variable star  $8''$  from the TIC star with range  $r=16.6-17.7$  and possible dips. Possible blended contaminants.

TIC 125424836 = TOI-3250. Disposition 'Planetary Candidate' with period  $P = 3.2800191$  d, transit depth 0.84% and planet radius  $17 R_{\oplus}$ . [NEA/TOI]

TIC 143350972 = TOI-440. Disposition 'False Positive' with period  $P = 1.0817$  d, transit depth 0.03% and equivalent planet radius  $2.1 R_{\oplus}$ . [NEA/TOI]

TIC 143525808. Transit depth differs in two TESS sectors.

TIC 168343381. Possible dilution of transit depth by ZTF 1456208400024340 with  $r=14.0$  lying  $8''$  from the DTARPS candidate.

TIC 169226820 = TYC 4916-897-1. Secondary of wide binary with separation  $40''$  (Andrews et al. 2017). The DTARPS signal with  $P = 4.17188$  d and transit depth 0.5% appears to be blending from the G5 primary, BD -  $03^{\circ}2978$ , that has a transiting planet WASP 127b lying in the Neptune desert. It has orbital period  $P = 4.178070$  d, transit depth 1%, sub-Saturn mass ( $M_p = 0.18 M_J$ ), and super-Jupiter radius ( $R_p = 1.37 R_J$ ). The atmosphere has water, clouds, and super-solar abundances of metals (Palle et al. 2017; Chen et al. 2018; Skaf et al. 2020). [SIMBAD]

TIC 170112990. Possible dilution of transit depth by ZTF 361209400014478 with  $r=12.5$  lying  $7''$  from the DTARPS candidate.

TIC 177068644. Possible dilution of transit depth by ZTF 359213200011341 with  $r=13.9$  lying  $11''$  from the DTARPS candidate.

TIC 177722855 = TOI-971. Disposition 'False Positive' with period  $P = 2.3903658$  d, transit depth 0.09% and planet radius  $5 R_{\oplus}$ . [NEA/TOI]

TIC 178162579 = TOI-2842 = CTOI 178162579.01. Disposition 'Planetary Candidate' with period  $P = 3.5514016$  d, transit depth 0.85% and planet radius  $12 R_{\oplus}$ . [NEA/TOI] Planetary candidate from convolutional neural network analysis (Olmschenk et al. 2021). [CTOI]

TIC 178265008. ZTF 411202400042939 variable star  $6''$  from TIC star at  $r \simeq 15.5$  mag with one dip to 15.9, and  $g \simeq 16.3$  with dips to 16.7. Possible blended contaminant.

TIC 178367144 = WASP-180 = TOI-966. Spectroscopically 'Confirmed Planet' with period  $P = 3.409264$  d, mass  $M = 286 M_{\oplus}$  and radius  $R = 1.2 R_J$  orbiting a F7 star. [NEA/TOI]

TIC 178580001. Possible dilution of transit depth by ZTF 411202400042939 with  $r=15.5$  lying  $6''$  from the DTARPS candidate.

TIC 179159972 = TOI-965. Disposition 'False Positive' with period  $P = 1.37101$  d, transit depth 0.16% and planet radius  $5 R_{\oplus}$ . [NEA/TOI]

TIC 180145006 = TOI-312. Disposition 'Ambiguous Planetary Candidate' with period  $P = 3.5413787$  d, transit depth 0.48% and planet radius  $10 R_{\oplus}$ . [NEA/TOI]

TIC 220294417. ZTF 513202300040813 star 9'' from the TIC star variable star at r=14.6 with occasional dips of 0.2 mag. Possible blended contaminant. Possible dilution of transit depth by ZTF 513202300017328 with r=15.6 lying 13'' from the DTARPS candidate.

TIC 229375359. Possible dilution of transit depth by ZTF 1507206200040686 with r=14.4 lying 7'' from the DTARPS candidate.

TIC 231158418. ZTF 461216400044713 star 6'' from TIC star, variable around 17 mag with powerful flares (13.9) and dips (17.5). Possible blended contaminant.

TIC 231387465 = TYC 6539-1365-1 = ASAS J073957-2247.6 = 1RXS J073957.1-224740 . Photometric variable due to rotationally modulated starspots with amplitude 0.03 mag (Kiraga 2012). X-ray source in the ROSAT All Sky Survey. [SIMBAD]

TIC 232395760 = HD 291277 [SIMBAD]

TIC 234091431 = CoRoT 102768606. Rotation period = 72 d (Affer et al. 2012). [SIMBAD]

TIC 234721262. Possible dilution of transit depth by ZTF 1454209200032757 with r=15.3 lying 7'' and by ZTF 1454209200032753 with r=15.5 lying 8'' from the DTARPS candidate.

TIC 234880209 = HD 259137. MARVELS survey shows a G2 V star with mass  $M = 1.0 M_{\odot}$ ,  $R = 0.9 R_{\odot}$  and  $[\text{Fe}/\text{H}] = -0.3$  (Grievess et al. 2018). [SIMBAD]

TIC 235166044. ZTF 461215100039761 star 15'' from TIC star at r=16.2 with dips to 17.4. Possible blended contaminant.

TIC 235183588. Possible dilution of transit depth by ZTF 513201400048716 with r=15.4 lying 5'' from the DTARPS candidate.

TIC 235500384. Possible dilution of transit depth by ZTF 461214100016409 with r=15.2 lying 9'' from the DTARPS candidate.

TIC 235548135. Possible dilution of transit depth by ZTF 514204400005818 with r=16.0 lying 5'' from the DTARPS candidate.

TIC 237566605. Possible dilution of transit depth by ZTF 461303100038845 with r=15.2 lying 12'' from the DTARPS candidate.

TIC 237757429. ZTF 461202400008213 star 12'' from TIC star with r=17.1 and dips to 18.5. Possible blended contaminant.

TIC 265045591. ZTF 464201400031816 star 6'' from TIC star with r=17.1 and frequent dips to 17.4. Possible blended contaminant.

TIC 266009692. ZTF 460207200012300 star 16'' from TIC star with long-term variability around r=15.7 and occasional dips to 16.6. Possible blended contaminant.

TIC 268587594 = HD 6217. Spectral type G2-G3 V. [SIMBAD]

TIC 271098608. Possible dilution of transit depth by ZTF 1510208100027480 with r=13.0 lying 7'' from the DTARPS candidate.

TIC 271374913 = TYC 180-2570-1 = 1SWASP J074943.21+005213.8. Planetary candidate with  $P = 1.267550762$  day, transit depth = 0.64% and width = 0.12 (Schanche et al. 2019). Blended star: TRAPPIST partial transit shows the eclipse is on the fainter star to the north. [SIMBAD]

TIC 279942918. Possible dilution of transit depth by ZTF 412215100007035 with r=14.0 lying 12'' from the DTARPS candidate.

TIC 283303192 = TOI-2741. Disposition 'Planetary Candidate' with period  $P = 6.817089$  d, transit depth 0.24% and planet radius  $6 R_{\oplus}$ . [NEA/TOI] Possible dilution of transit depth by ZTF 411216300042309 with r=15.2 lying 7'' from the DTARPS candidate.

TIC 284859630 = TOI-2716 = CTOI 284859630.01. Disposition 'Planetary Candidate' with period  $P = 7.5420435$  d, transit depth 0.77% and planet radius  $10 R_{\oplus}$ . [NEA/TOI] Planetary candidate from convolutional neural network analysis (Olmschenk et al. 2021). [CTOI]

TIC 286865921 = WASP-83 = TOI-773. Spectroscopically 'Confirmed Planet' with period  $P = 4.4654291$  d, mass  $M = 199 M_{\oplus}$  and radius  $R = 1.335 R_J$ . [NEA/TOI]

TIC 293847411. Possible dilution of transit depth by ZTF 460303100001701 with r=15.2 lying 5'' from the DTARPS candidate.

TIC 296179330 = Ross 56 = Gliese 268.5 = NLTT 17658. High-proper motion K5 star. Long thought to be in the solar neighborhood with  $d \simeq 20 - 35$  pc (van Altena et al. 1995), Gaia measures parallax = 2.3 mas ( $d \simeq 430$  pc). [SIMBAD]

TIC 317022315 = UCAC4 370-009760. Planetary candidate with period  $P = 2.226672$  d, transit depth = 0.45% and width 4.8 h, triage probability 98% and vetting probability 28% from deep learning analysis (Yu et al. 2019). [SIMBAD]

TIC 318282352. Possible dilution of transit depth by ZTF 360211200008757 with  $r=12.6$  lying  $11''$  from the DTARPS candidate.

TIC 318345342. Possible dilution of transit depth by ZTF 462202400034471 with  $r=15.5$  lying  $8''$  from the DTARPS candidate.

TIC 318796593 = TOI=2886. Disposition 'Planetary Candidate' with period  $P = 1.6020002$  d, transit depth 2.15% and planet radius  $19 R_{\oplus}$ . [NEA/TOI]

TIC 318899586. ZTF 360115200036643 variable star 9? from TIC star at  $g \simeq 17.9$  with dips to 18.4. Possible blended contaminant.

TIC 319014919 = TYC 186-2418-1. MARVELS survey shows a G6 V star with mass  $M = 1.0 M_{\odot}$ ,  $R = 1.0 R_{\odot}$  and  $[\text{Fe}/\text{H}] = 0.2$ , thin disk star with high proper motion (Grievus et al. 2018). [SIMBAD]

TIC 332911893 = TOI-4672. Disposition 'Planetary Candidate' with period  $P = 6.6132132$  d, transit depth 1.00% and planet radius  $15 R_{\oplus}$ . [NEA/TOI] Possible dilution of transit depth by ZTF 1457208200043405 with  $r=15.6$  lying  $4''$  from the DTARPS candidate.

TIC 336732616 = HATS-3 = TOI-103. Spectroscopically 'Confirmed Planet' with period  $P = 3.547851$  d, mass  $M = 340 M_{\oplus}$  and radius  $R = 1.381 R_J$  orbiting a F star. [NEA/TOI]

TIC 340889095. Transit depth differs in two TESS sectors.

TIC 348756659 = TOI-4823 = CTOI 348756659.01. Disposition 'Planetary Candidate' with period  $P = 3.7259874$  d, transit depth 1.85% and planet radius  $15 R_{\oplus}$ . [NEA/TOI] Planetary candidate from DIAMante analysis (Montalto et al. 2020). [CTOI]

TIC 382391899 = WASP-50 = TOI-391. Spectroscopically 'Confirmed Planet' with period  $P = 1.9550959$  d, mass  $M = 466 M_{\oplus}$  and radius  $R = 1.153 R_J$ . [NEA/TOI]

TIC 386275406. Possible dilution of transit depth by ZTF 1559201100022341 with  $r=15.7$  lying  $15''$  from the DTARPS candidate.

TIC 409594381 = TOI-4214. Disposition 'Planetary Candidate' with period  $P = 3.491383$  d, transit depth 0.47% and planet radius  $11 R_{\oplus}$ . [NEA/TOI]

TIC 409794137 = TOI-1478. Spectroscopically 'Confirmed Planet' with period  $P = 10.180249$  d, mass  $M = 270 M_{\oplus}$  and radius  $R = 1.06 R_J$ . [NEA/TOI]

TIC 415559926. Possible dilution of transit depth by ZTF 1558212100025586 with  $r=15.6$  lying  $10''$  from the DTARPS candidate.

TIC 427377458 = CTOI 427377458.01. Planetary candidate with period  $P = 2.53$  d, transit depth 0.05 from Lightkurve analysis. [CTOI]

TIC 436243305. Possible dilution of transit depth by ZTF 1505207100007186 with  $r=15.2$  lying  $103''$ , by ZTF 1505207100007178 with  $r=15.0$  lying  $13''$ , and by ZTF 1505207100007124 with  $r=14.8$  lying  $14''$  from the DTARPS candidate.

TIC 438338723 = UCAC4 532-026425 = EPIC 202086968. Eclipsing binary discovered in K2 ecliptic plane survey with period  $P = 3.698$ , transit depth = 3.1% and duration 3.5 h (Kruse et al. 2019). The star is also in a visual binary system with separation  $2''$  (Dressing et al. 2019). [SIMBAD]

TIC 449050247 = TOI-951. Disposition 'False Positive' with period  $P = 2.96845$  d, transit depth 1.70% and planet radius  $20 R_{\oplus}$ . [NEA/TOI]

TIC 449050248. Possible dilution of transit depth by ZTF 1503204200026587 with  $r=15.9$  lying  $5''$  from the DTARPS candidate.

TOI 468958331. Possible dilution of transit depth by ZTF 462216100010590 with  $r=13.6$  lying  $11''$  from the DTARPS candidate.

### C. CATALOG COMPARISON WITH OTHER SURVEYS

Paper I (§10 and Appendix) compared the performance of the DTARPS analysis and classifier to previous studies including the Confirmed Planets from the NASA Exoplanet Archive, the TESS Objects of Interest (TOI) list, community TOI (cTOI) list, DIAMante candidate list (M20), and a variety of additional surveys. Here, we provide a similar analysis for the DTARPS Candidate catalog after vetting procedures are applied. We do not consider the DTARPS Galactic Plane list here because coverage of low Galactic latitudes in other surveys is uneven.

For individual DTARPS Candidates, cross-listings to external surveys are given in Appendix A. DTARPS Candidates recover 44 objects from WASP and NGTS, 13 from HATS, 2 from KELT, and 1 from TESS PlanetHunters. Cross-listings include 13 from the HD/BD/CD catalogs of bright stars and 16 from the Tycho catalog. The cross-listings also reveals a very small fraction ( $\sim 1\%$ ) of known False Positives: five DTARPS Candidates are in the Low Mass Extreme Binary catalog (Triaud et al. 2017; von Boetticher et al. 2019), and one is a spectroscopic binary discovered in the K2 survey (Kruse et al. 2019). In addition, two are magnetically active X-ray emitting stars in the 1RXS catalog, and one is erroneously listed as a solar neighborhood star in the Gliese catalog.

We now turn to the relationships between our DTARPS Candidate catalog and other planet searches treated as an ensemble.

#### C.1. DIAMante Candidates

The comparison with the DIAMante candidate exoplanets is important because the M20 and DTARPS studies are based on the same DIAMante data set though with different analysis methodology. The DTARPS Analysis List of 7,377 promising stars includes 213 M20 candidates (Paper I, §10.1). Of these, 158 (74%) are DTARPS Candidates in Table 1. These include 56 Confirmed Planets on the NASA Exoplanet Archive, 91 planet candidates (46 of which had been promoted to the TOI list from the cTOI list), and 11 False Positives.

The 55 M20 objects rejected by DTARPS vetting include 7 Confirmed Planets on the NASA Exoplanet Archive, 44 planetary candidates (20 of which had been promoted to the TOI list from the cTOI list), and 4 FPs from the TOI list. Of the 7 rejected Confirmed Planets, 2 are considered False Alarms (i.e. insufficient evidence for periodicity in the light curve), 1 as a potential photometric binary, and 4 as ephemeris matches. The 44 planetary candidates not confirmed by DTARPS include 6 that failed centroid-crowding analysis, 15 False Alarms, 11 with even/odd transit differences, 6 with curvature in the light curve, 3 as possible photometric equal-mass binaries, and 3 for ephemeris matching.

#### C.2. NASA Exoplanet Archive Confirmed Planets

The Confirmed Planets from the NASA Exoplanet Archive and TOI lists represent the most reliable collection of transiting systems for analyzing the performance of the DTARPS method. All the targets have been spectroscopically confirmed from previous transit surveys so the astrophysical False Positive should be negligible.

The DTARPS Analysis List includes 130 Confirmed Planets in the NASA Exoplanet Archive and TOI lists (Paper I, §10.2-10.3), 82 are listed in Table 1 indicating a 62% sensitivity rate. Thirty-seven Confirmed Planets were rejected by centroid-crowding analysis, 5 as False Alarms, 2 as potential photometric binary stellar hosts, and 4 for ephemeris matching.

Most of the Confirmed Planets that were rejected did not pass centroid-crowding analysis (§2.1) suggesting that these criteria may have been too strict (§6). Most centroid-crowding rejections (25 of 37) had been discovered by ground-based surveys with much smaller pixel scales than the TESS cameras making it easier to verify the source of the transit signal in crowded fields. Of the remaining 12 Confirmed planets rejected by centroid-crowding analysis, 1 was discovered in the K2 survey and the 11 were from two-minute cadence TESS targets. If we exclude the Confirmed Planets rejected by centroid-crowding analysis or ephemeris matching in the sensitivity measurement, DTARPS has 87% sensitivity towards Confirmed Planets using visual vetting tests.

Figure 11 shows the vetting sensitivity (left) and the vetting rejections (right) for the Confirmed Planets list. The DTARPS method is more sensitive to hot and warm Jovian planets ( $R_p > 8 R_\oplus$ ) with 64% recovered than to super-Neptunes, Neptunes, or super-Earths ( $R_p < 8 R_\oplus$ ) with 52% recovered. DTARPS does a poor job for any planets with longer periods ( $P \gtrsim 12$  day). In Figure 11-right, the vetting rejections have been split into two categories depending on whether the Confirmed Planet failed due to vetting restrictions based on the TESS instrumentation (centroid-crowding analysis affected by the large pixel size or ephemeris matching affected by telescope optics) or vetting restrictions due to the light curve (visual vetting tests). The vetting rejections from TESS instrumentation tend to exclude larger

Jovian planets while the vetting rejections from visual vetting were biased against super-Earths and sub-Neptunes. The visual vetting bias is easily explained by weak transit signal strength in single-sector TESS observations. The centroid-crowding bias is discussed in (§6).

### C.3. Previously Known False Positives

The list of previously identified False Positives combines objects from the TOI list, cTOI list, Affer et al. (2012), Collins et al. (2018), Dressing et al. (2019), Eisner et al. (2021), Feinstein et al. (2019), Kostov et al. (2019), Kruse et al. (2019), Mayo et al. (2018), Olmschenk et al. (2021), Schanche et al. (2019), Tu et al. (2020), von Boetticher et al. (2019), and Yu et al. (2019). The Random Forest classifier was effective in rejecting known False Positives, accepting 113 of 513 FPs in the full  $\sim 1$  million star sample. The DTARPS vetting procedure was able to remove another 78 False Positives, leaving only 35 among the 462 DTARPS Candidates. The rejected False Positives include 48 removed by centroid-crowding analysis, 5 by ephemeris matches, and 25 by visual vetting.

The False Positive list sources are heterogeneous with a wide range of information available. For the 35 False Positives in the DTARPS Candidate catalog, 17 are designated eclipsing binary systems, 5 as low-mass eclipsing binary system, 2 as blended eclipsing binary systems, 2 as single-line spectroscopic eclipsing binary systems, and 1 as a double-line spectroscopic eclipsing binary system (Appendix A).

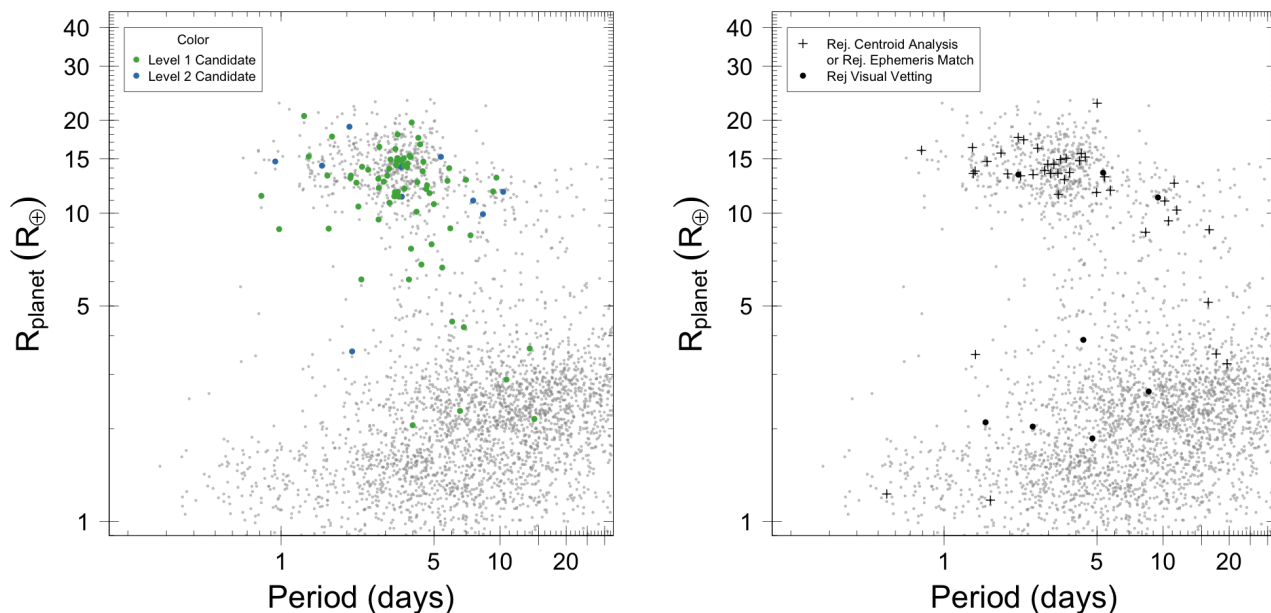


**Figure 11.** Radius-Period plots for Confirmed Planets in the DTARPS Analysis List (Paper I) that passed DTARPS vetting (left panel) and that were rejected by DTARPS vetting (right panel). All Confirmed Planets on the NASA Exoplanet Archive, mostly from the *Kepler* survey, are plotted as small gray dots. The DTARPS candidate points are colored by DTARPS disposition (left panel). In the right panel, planets rejected by the DTARPS vetting process are plotted as pluses if the planet was rejected by either centroid-crowding analysis or ephemeris matching, or are plotted as circles if the planet was rejected by the visual vetting process.